Declassified and Approved For Release 2013/03/04 : CIA-RDP10-02196R000300010004-7

Russian Original Vol. 53, No. 4, October, 1982

April, 1983

DS-Sec 657

File

SATEAZ 53(4) 655-746 (1982)

SOVIET ATOMIC ENERGY

АТОМНАЯ ЭНЕРГИЯ
(ATOMNAYA ÉNERGIYA)

TRANSLATED FROM RUSSIAN

CONSULTANTS BUREAU, NEW YORK

Declassified and Approved For Release 2013/03/04 : CIA-RDP10-02196R000300010004-7

Declassified and Approved For Release 2013/03/04 : CIA-RDP10-02196R000300010004-7

SOVIET ATOMIC ENERGY

Soviet Atomic Energy is abstracted or indexed in *Chemical Abstracts, Chemical Titles, Pollution Abstracts, Science Research Abstracts, Parts A and B, Safety Science Abstracts Journal, Current Contents, Energy Research Abstracts,* and *Engineering Index.*

Mailed in the USA by Publications Expediting, Inc., 200 Meacham Avenue, Elmont, NY 11003.

POSTMASTER: Send address changes to *Soviet Atomic Energy,* Plenum Publishing Corporation, 233 Spring Street, New York, NY 10013.

Soviet Atomic Energy is a translation of *Atomnaya Énergiya,* a publication of the Academy of Sciences of the USSR.

An agreement with the Copyright Agency of the USSR (VAAP) makes available both advance copies of the Russian journal and original glossy photographs and artwork. This serves to decrease the necessary time lag between publication of the original and publication of the translation and helps to improve the quality of the latter. The translation began with the first issue of the Russian journal.

Editorial Board of *Atomnaya Énergiya:*

Editor: O. D. Kazachkovskii

Associate Editors: N. A. Vlasov and N. N. Ponomarev-Stepnoi

Secretary: A. J. Artemov

I. N. Golovin
V. I. Il'ichev
V. F. Kalinin
P. L. Kirillov
Yu. I. Koryakin
E. V. Kulov
B. N. Laskorin
V. V. Matveev
I. D. Morokhov
A. A. Naumov
A. S. Nikiforov
A. S. Shtan'
B. A. Sidorenko
M. F. Troyanov
E. I. Vorob'ev

Copyright © 1983, Plenum Publishing Corporation. *Soviet Atomic Energy* participates in the program of Copyright Clearance Center, Inc. The appearance of a code line at the bottom of the first page of an article in this journal indicates the copyright owner's consent that copies of the article may be made for personal or internal use. However, this consent is given on the condition that the copier pay the stated per-copy fee through the Copyright Clearance Center, Inc. for all copying not explicitly permitted by Sections 107 or 108 of the U.S. Copyright Law. It does not extend to other kinds of copying, such as copying for general distribution, for advertising or promotional purposes, for creating new collective works, or for resale, nor to the reprinting of figures, tables, and text excerpts.

Consultants Bureau journals appear about six months after the publication of the original Russian issue. For bibliographic accuracy, the English issue published by Consultants Bureau carries the same number and date as the original Russian from which it was translated. For example, a Russian issue published in December will appear in a Consultants Bureau English translation about the following June, but the translation issue will carry the December date. When ordering any volume or particular issue of a Consultants Bureau journal, please specify the date and, where applicable, the volume and issue numbers of the original Russian. The material you will receive will be a translation of that Russian volume or issue.

Subscription (2 volumes per year)
Vols. 52 & 53: $440 (domestic); $489 (foreign)
Vols. 54 & 55: $500 (domestic); $555 (foreign)

Single Issue: $100
Single Article: $7.50

CONSULTANTS BUREAU, NEW YORK AND LONDON

233 Spring Street
New York, New York 10013

Published monthly. Second-class postage paid at Jamaica, New York 11431.

Declassified and Approved For Release 2013/03/04 : CIA-RDP10-02196R000300010004-7

Declassified and Approved For Release 2013/03/04 : CIA-RDP10-02196R000300010004-7

SOVIET ATOMIC ENERGY

A translation of *Atomnaya Énergiya*

April, 1983

Volume 53, Number 4 October, 1982

CONTENTS

		Engl./Russ.
ARTICLES		
Some Results of the Parametric Analysis of the Technicoeconomic Indices of a Power Plant with the Trol Hybrid Ambipolar Reactor — N. N. Vasil'ev, I. N. Golovin, and M. G. Kuznetsov	655	211
Analysis of the Routes to an Economically Advantageous Reorganization of the VVÉR-440 Fuel Cycle — V. D. Simonov, V. I. Pavlov, and S. F. Popilyuk	659	213
Use of Nuclear Fuel to Cover the Seasonal Maximum Electric Load — V. M. Boldyrev, M. V. Sigal, and S. A. Skvortsov	664	218
Measurement of Fuel Burnup in VVÉR-365 and VVÉR-440 Fuel-Element Assemblies by Gamma Spectroscopy — B. A. Bibichev, V. P. Kruglov, V. P. Maiorov, Yu. M. Protasenko, M. A. Sunchugashev, P. I. Fedotov, and A. F. Shvoev	669	222
Tritium Content in Water Systems of a Reactor of the Fifth Unit of the Novovoronezh Nuclear Power Plant — V. P. Kruglov, V. M. Ilyasov, I. G. Golubchikova, B. N. Mekhedov, L. N. Sukhotin, S. V. Popov, V. M. Arkhipkin, and A. G. Babenko	673	225
Problem of Predicting the Radiation Conditions in an Atomic Power Station A. M. Luzhnov, V. P. Romanov, R. F. Tagi-Zade, and S. G. Tsypin	677	227
Small Steam Leaks into Sodium in a Reverse Steam Generator—F. A. Kozlov, G. P. Sergeev, L. G. Volchkov, A. R. Sednev, V. M. Makarov, and B. I. Tonov	682	231
Effect of Gas Dissolved in Water on the Heat-Exchange Crisis — V. V. Lozhkin, Yu. A. Smirnov, Yu. Yu. Shtein, and R. V. Shumskii	687	234
Influence of Both Reactor Irradiation and Helium Isotopes upon the Mechanical Properties of Titanium and α-Titanium Alloys — V. N. Tebus, É. F. Alekseev, Yu. V. Bobkov, F. P. Butra, A. M. Glazyrin, I. V. Golikov, B. V. Grigorovich, A. M. Kaptel'tsev, Yu. N. Sokurskii, and V. I. Chuev	690	237
Effects of Heat Treatment and Alloying on the Radiation Erosion of Austenitic Stainless Steels and Alloys — E. E. Goncharov, M. I. Guseva, B. A. Kalin, O. A. Kozhevnikov, A. N. Lapin, A. N. Mansurova, A. M. Parshin, D. M. Skorov, I. N. Chernov, G. N. Shishkin, and V. D. Yaroshevich	697	243
Results with Pilot Bitumening Plants — I. A. Sobolev, L. M. Khomchik, V. V. Kulichenko, N. A. Rakhov, S. A. Dmitriev, and V. M. Chebyshev	707	250
Prospects for the Development of Neutron-Activation Analytical Facilities Based on Powerful Antimony—Beryllium Sources — G. N. Flerov, Yu. N. Burmistenko, Yu. V. Dyadin, Yu. S. Zamyatnin, A. A. Medvedev, A. A. Sal'nikov, and Yu. G. Teterev	714	255

Declassified and Approved For Release 2013/03/04 : CIA-RDP10-02196R000300010004-7

Declassified and Approved For Release 2013/03/04 : CIA-RDP10-02196R000300010004-7

CONTENTS

(continued)

Engl./Russ.

LETTERS TO THE EDITOR

Stability of a Nuclear Reactor with Natural Circulation of a Liquid Fuel — V. A. Blinkin and E. I. Emel'yanov 720 261

Indicator of the Energy Distribution in the RBMK-1000 Field — G. N. Aleksakov, S. A. Gavrilyuk, A. V. Kudryavtsev, and G. P. Terekhov 724 263

Diffusion of ^{131}I and ^{103}Ru in Single-Crystal Tungsten — E. S. Bekmukhambetov, D. K. Daukeev, Zh. R. Zhotabaev, and R. T. Musurmankulov. 727 265

Characteristics of Reflected γ Rays with a Short Distance between the Detector and the Scattering Surface — V. I. Kulikov, K. K. Popkov, and V. I. Titov. 729 266

Creep in a Carbon–Carbon Material — Yu. A. Kalinkin, Yu. N. Podladchikov, O. P. Popov, V. N. Stetsyuk, and A. R. Khenven 732 268

Formation of Bubbles of Radiolytic Gas in Polyethylene — N. N. Alekseenko, P. V. Volobuev, and S. B. Trubin 734 269

Effect of the Geometry of Measurement on the Attenuation of β Particles — K. M. Erokhin, V. A. Mashinin, and E. V. Skachkov. 736 270

Mechanism of Formation of Deposits on Heating Surfaces Cooled by Organic Coolants — A. I. Gavrilin, N. G. Gataullin, B. A. Mikhailov, V. E. Fedoseev, and Yu. V. Chechetkin. 738 271

Temperature Fields of Electricity Generating Thermal Emission Elements in Changes of the Width of the Gap between the Electrodes — A. G. Tsitsin. 741 273

Calculations of the Irradiation Characteristics in Reactor Tests — E. S. Glushkov, N. N. Ponomarev-Stepnoi, and I. G. Timofeev. 743 274

The Russian press date (podpisano k pechati) of this issue was 9/28/1982. Publication therefore did not occur prior to this date, but must be assumed to have taken place reasonably soon thereafter.

Declassified and Approved For Release 2013/03/04 : CIA-RDP10-02196R000300010004-7

Declassified and Approved For Release 2013/03/04 : CIA-RDP10-02196R000300010004-7

SOME RESULTS OF THE PARAMETRIC ANALYSIS OF THE TECHNICOECONOMIC INDICES OF A POWER PLANT WITH THE TROL HYBRID AMBIPOLAR REACTOR

N. N. Vasil'ev, I. N. Golovin, and M. G. Kuznetsov

UDC 621.039.624

In recent years, in investigations of engineers on the problem of controlled thermonuclear fusion, great attention has been paid to the study of the "reactor prospects" of ambipolar open traps. For this purpose, several conceptual projects of "pure" [1, 2] and hybrid reactors with both a thorium (TMHR project [3]) and a uranium blanket (TROL project [4]) have been developed.

In the TMHR project, a detailed parametric analysis was carried out of the principal design solutions achieved by taking account of the nuclear fuel balance in the power generating system. This analysis allowed the optimal ratios of the physics and design parameters of this power plant to be established, and the factors most strongly affecting its technico-economic indices to be developed. In the TROL project, a reactor was considered with a uranium blanket, in which plutonium is produced. Because of the significantly higher value of the multiplication factor of the energy in the uranium blanket by comparison with the thorium blanket, and also as a result of the use of more conservative concepts of plasma containment, the parameters of the TROL design were found to be markedly different from the parameters of the TMHR design. The power generation parameters of these reactors are given below:

	TROL	TMHR
Thermal power, MW	6500	4000
Electrical power, kW		
gross	2400	1440
net	1550	890
Thermonuclear power, MW	780	915
Neutron loading on first wall of central trap, MW/m²	1.0	1.5
Power enhancement factor	2.25	2.0
Magnetic field, T:		
in central trap	1.1	1.7
in "plugs"	14	12
Injection energy, keV:		
into central trap	20	20
into barrier traps	1400	400
Injection current into central trap, A	400	350
Injection power into barrier traps, MW	400	670
Uhf-heating power, MW	0	470
Average power, released in the nuclear zone of the blanket per 1 thermonuclear neutron, MeV	120	72
Nuclear fuel made per 1 thermonuclear neutron	1.5	0.8
Tritium breeding factor	1.05	1.0
Nuclear zone coolant	Boiling water and superheated steam	Helium

Translated from Atomnaya Énergiya, Vol. 53, No. 4, pp. 211-213, October, 1982. Original article submitted May 4, 1982.

0038-531X/82/5304-0655$07.50 © 1983 Plenum Publishing Corporation

Declassified and Approved For Release 2013/03/04 : CIA-RDP10-02196R000300010004-7

Declassified and Approved For Release 2013/03/04 : CIA-RDP10-02196R000300010004-7

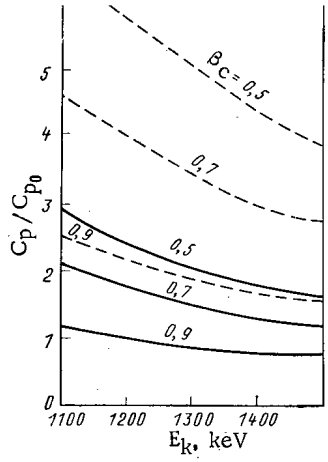

Fig. 1. Dependence of the purposeful function on the injection energy into the barrier traps, for different values of β_c and $\gamma_k = 1$ (——) and $\gamma_k = 0.5$ (– – –).

Nuclear zone fuel	Metallic uranium	Metallic thorium
Power conversion system	Steam-turbine	

In the present paper, we discuss the results of an analysis of the effect on technico-economic indices of deviations of the parameters of the power plant with the TROL reactor from their design values.

Choice of Specific Functions for Parametric Analysis. The efficiency of one concept or another, set as the basis of the power plant, is determined by its technicoeconomical index. For conventional power stations, this index is the specific calculated cost of the production of 1 kWh of electric power, taking into account the once-only capital costs and the annual operating costs. For a hybrid facility, producing power and plutonium, it is difficult to use this criterion. The most objective estimate of the efficiency of a hybrid power plant can be obtained by considering the nuclear power generation from hybrid reactors as a whole. However, at this level of knowledge, in view of the considerable indeterminacy of the physical and technical solutions and the cost indices of the basic plant, this approach is unjustifiably complex. In the present paper, therefore, for the parameter characterizing the relative efficiency of the different design solutions, the magnitude of the costs per 1 g plutonium produced was chosen, after taking account of the cost of the electric power generated by the reactor, C_p. The "pure" costs of the production of plutonium, obtained in this way, should not give an absolute value, and it is meaningful to consider them only as a certain factor which will allow different alternatives to be compared, which should not differ too severely from the "basic" version. In the contrary case, the extrapolation functions used for the physical and engineering parameters and the limitations imposed on these parameters may prove to be incorrect.

Plasmaphysical Model of the Reactor. At the basis of the model lies the procedure described in [5], but taking account of the spatial nonuniformity of the plasma density in the barrier traps.

Cost Indices. The use in the analysis of the economic efficiency criteria of the power plant bears an additional indeterminacy (in addition to the indeterminacy related with the inadequate knowledge of the reactor physics), due to the fact that very many capital systems of the reactor do not have industrial similarities. In order that a unified system of cost indices should be used, the indices given in [3] were assumed in the present paper. In this case, the principal factors most severely affecting the final result are the specific costs of the blanket (per unit length), the superconducting magnet system (per kAm), and the injection systems (per unit intensity of the bunch for different current values). Certain articles of the costs are almost constant with variation of the parameters (the costs of buildings and plant, energy conversion system, etc.).

Declassified and Approved For Release 2013/03/04 : CIA-RDP10-02196R000300010004-7

Declassified and Approved For Release 2013/03/04 : CIA-RDP10-02196R000300010004-7

Limitations on the Physical and Structural Parameters of the Reactor. The power generation regime of an ambipolar reactor is determined by more than two dozen parameters. Since many of them cannot be chosen arbitrarily, limitations are imposed on them, related either to the plasma containment physics or to the technical feasibilities of creating some other systems. The optimum values of the injection energy into the barrier traps E_k, the thermonuclear plasma density in the central trap n_c, the average particle density in the barrier traps $< n_k >$, and the neutron flux at the first wall S_n do not coincide with the maximum permissible values. They were computed in the calculations being described.

In addition, in the calculations, we considered the effect of the indeterminacy associated with the possible anomalous reduction of the plasma containment time in the barrier traps, which is described by the coefficient $\gamma_k = \tau_k/\tau_k^{cl}$ (τ_k^{cl} is the classical time of containment), and also with the possibility of the onset of MHD-instability, restricting the limiting values of β_c.

Method of Solution. In the present paper, the parametric analysis is formulated as finding the minimum value of the purposeful function C_p with a defined assignment of one of the parameters and with different values of the coefficient of anomalousness γ_k. Finding the optimum value of the function C_p in the presence of limitations is effected by the method of variable directions, in conjunction with the method of penalty functions [8].

Discussion of Results. The results of the calculations are shown in Figs. 1 and 2. Figure 1 shows how the purposeful function depends on the injection energy for different values of β_c and γ_k. Each point corresponds to the minimum value of C_p with respect to the variable of the parameters for a given value of E_k. It was found that the optimum values of the parameters investigated are very stable: In the range represented, $E_k n_c \approx 5 \cdot 10^{13}$ cm^{-3}, $< n_k > = 1.7 \cdot 10^{14}$ cm^{-3} for a coefficient of nonuniformity $n_k^{max}/< n_k > = 2$, and $S_n = 100$ W/cm^2 with a length of the central trap of 43 m and with a fixed radius of 2.25 m. It can be seen that the dependence of C_p on E_k is relatively weak, especially for high values of β_c. This provides the basis for further planning, to consider versions with a lower injection energy by comparison with that stated in [4]. However, C_p increases very rapidly (i.e., the economic efficiency of the power plant decreases rapidly) with reduction of β_c and γ_k. If the curve of the purposeful function C_p versus the power enhancement factors in the plasma Q, calculated for each version (i.e., different values of β_c, γ_k, and E_k) is plotted, then all points lie well on a single curve (see Fig. 2). The values of Q are determined by the necessary injection power and the secondary heating of the electrons in order to obtain the optimum reactor parameter stated above. It can be seen from Fig. 2 that with increase of Q the purposeful function falls sharply at first, and then after $Q \approx 2$ the dependence becomes relatively weak. This implies that within the limits of the considered concept of containment, any measures contributing to an increase of Q do not give an appreciable economic effect.

When determining the total costs of individual elements of the power plant, it was established that the most expensive systems are the magnetic system and the blanket. Thus, the capital costs of the blanket with the magnetic system of the central trap (using the cost indices of [3]) amount to 30% of the costs of the entire power plant. Of the other systems, the injection and secondary heating systems make an appreciable contribution to the capital costs.

In the design of a power plant with the TROL reactor, optimistic assumptions were accepted in relation to the plasma containment in the reactor traps ($\beta_c = 0.9$; $\gamma_k = 1$). At the present time, there are theoretical considerations about the fact that "balloon" instability in the central trap can limit β_c to the level of ~ 0.3. At the same time, as experiments on the TMX (USA) show, the plasma remains stable even at a pressure appreciably exceeding the "balloon" limit [7], so that it is difficult to assign an exact value of the maximum permissible value of β_c at the present time. Therefore, β_c is considered as a free parameter in the calculations.

When analyzing the experiments on plasma containment in open traps, it was found [7] that the containment time of particles is a factor of 2 to 3 less than the classical time, and therefore in the present paper a version with $\gamma_k = 0.5$ is considered. Estimates of the absolute values of the capital costs for the TROL facility indicate that even with $\beta_c = 0.9$ and $\gamma_k = 1$, the use of this reactor may prove to be economically inefficient. With a reduction of β_c and γ_k by at least two times, the capital costs increase by a factor of 5-6, which makes the reactor absolutely unprofitable.

Declassified and Approved For Release 2013/03/04 : CIA-RDP10-02196R000300010004-7

Declassified and Approved For Release 2013/03/04 : CIA-RDP10-02196R000300010004-7

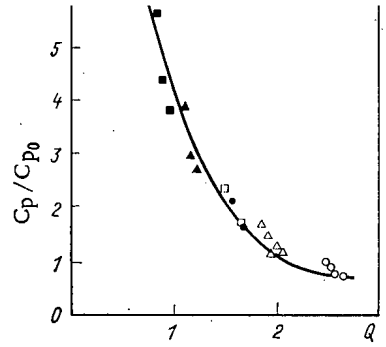

Fig. 2. Dependence of the purposeful function on the power-enhancement coefficient Q for different values of β_c, γ_k, and E_k: ○, △, □) β_c, = 0.9, 0.7, and 0.5, respectively, for γ_k = 1 and E_k = 1200-1500; ●, ▲, ■) same values of β_c for γ_k = 0.5 and E_k = 1200-1500.

The urgent necessity of finding solutions significantly improving plasma containment in the reactor, by comparison with the classical ambipolar trap, is obvious. The use of "thermal barriers" [8] may be shown by some of these solutions. In this case, as calculations show, it is possible to obtain $Q \approx 10$-20 [2, 3] with relatively high parameters of the magnetic system and of the injection system, which would allow an economically attractive reactor even with small values of β_c and γ_k. It is proposed to verify this idea in 1982-1983 on the specially constructed facilities TMX-Upgracle and TARA (USA), and GAMMA-10 (Japan), and somewhat later on the MFTF-B facility (USA), with the plasma parameters similar to the reactor parameters.

LITERATURE CITED

1. R. Moir et al., Preliminary Design Study of the Tandem Mirror (TMR), LLL, UCRL-53302 (1977).
2. B. Balger et al., Witamir-1A University of Wisconsin, Tandem Mirror Design, Madison, Wisconsin, UWFDM-400 (1980).
3. R. Moir et al., Tandem Mirror Hybrid Reactor Design Study Report, TMHR, LLL, UCID-18808 (1980).
4. N. N. Vasil'ev et al., At. Energ., 52, No. 2, 113 (1982).
5. Yu. V. Gribov and V. A. Chuyanov, Hybrid Thermonuclear Reactor Based on a Trap with Double Plugs [in Russian], Proceedings of the Second Soviet—American Seminar on "Fusion—Fission," Moscow (1977).
6. V. É. Lukash et al., Determination of the Optimum Parameters of a Thermonuclear Power Plant with a Tokamak and an MHD generator [in Russian], Proceedings of the First All-Union Conference on the Engineering Problems of Thermonuclear Fusion, Leningrad (1977).
7. T. Simonen, Nucl. Fusion, 21(12), 1667 (1981).
8. D. Baldwin and B. Logan, Phys. Rev. Lett., 43, No. 18 (1979).

Declassified and Approved For Release 2013/03/04 : CIA-RDP10-02196R000300010004-7

Declassified and Approved For Release 2013/03/04 : CIA-RDP10-02196R000300010004-7

ANALYSIS OF THE ROUTES TO AN ECONOMICALLY ADVANTAGEOUS REORGANIZATION OF THE VVÉR-440 FUEL CYCLE

V. D. Simonov, V. I. Pavlov, and S. F. Popilyuk

UDC 621.039.003:621.039.516

Makeup with fresh fuel is stipulated for the VVÉR-440 once per year. The residence time of the fuel-element assemblies in the reactor is limited to three runs. Therefore, approximately one-third of the 349 fuel-element assemblies forming the core is replaced with each recharging. The running time between rechargings usually is calculated on 7000 effective hours, so that with an average reactor power during the operating period of 85-90% of nominal, and with a recharging duration of 30 days, the annual utilization factor of the installed capacity of the power unit amounted to 0.8.

Taking account of what has been said, the fuel cycle (FC) typical for the VVÉR-440 is described in [1]. In it, the average duration of the reactor operating period (700 eff. h) in shut-down conditions of recharging is ensured with fuel of two enrichments. In the composition of the makeup fuel there are 84 fuel-element assemblies with an enrichment of 3.6% and 36 or 31 fuel-element assemblies (after odd and even operating periods, respectively) with an enrichment of 2.4%. Thus, the average enrichment of the makeup fuel is 3.24-3.28%. The fuel elements with 3.6% enrichment operate for three runs, which on conversion to the duration of operation of the reactor at nominal power, amounts to 940 eff. days for the assemblies of the first charge and 875 eff. days in steady-state conditions. At the instant of discharging, the average buildup of slags in them amounts to 31.6-29.1 kg/ton U, and in the most spent fuel-element assemblies it is 34.3-32.9 kg/ton U. The nonuniformity of the fuel burnup (the ratio of the accumulated slags in the maximum and minimum burned-up fuel elements) amounts to 1.15-1.20. The greater part of the fuel with an enrichment of 2.4% also operates for three runs, and in this case up to 27.7 kg/ton U is burned up on average. However, as 17% of the fuel-element assemblies are withdrawn from the cycle after two runs, the average burnup over the operating period of the reactor of this fuel is 25.4 kg/ton U, and the nonuniformity of burnup is 1.6.*

In addition to the large nonuniformity of fuel burnup of the fuel-element assemblies with an enrichment of 2.4% in this fuel cycle (we shall call it the reference fuel cycle — RFC), it is noteworthy that after three runs the energy potential of the 3.6% enriched fuel is not completely exhausted: Of every additional (with respect to the 2.4% enriched fuel) 12 kg of ^{235}U contained in each ton, only approximately one-quarter is burned. The reasons for this are in some way related to the limitations imposed on the recharging periodicity of the reactor, the fuel burnup, and, consequently, the operating period of the fuel-element assemblies, and are also related to the choice of fuel enrichment.

It is logical to suppose that the fuel cycle indices of the VVÉR-440 can be improved if a more complete utilization of the energy potential of the fuel can be achieved, primarily of a fuel of higher enrichment.

Two methods for achieving this reserve, which are not connected with structural changes or the improvement of the physical characteristics of the reactor, seem to be the most possible. In using the first method, it is proposed to change the fuel enrichment while maintaining all the other RFC limitations. It will not cause any serious technical problems. The

*Without taking account of the central fuel-element assembly, which has a special recharging cycle and is changed after even runs with a burnup of ∿ 16 kg/ton U and six fuel-element assemblies discharged after the first run with an average burnup of 11.2 kg/ton U.

Translated from Atomnaya Énergiya, Vol. 53, No. 4, pp. 213-218, October, 1982. Original article submitted January 11, 1982.

0038-531X/82/5304-0659$07.50 © 1983 Plenum Publishing Corporation

Declassified and Approved For Release 2013/03/04 : CIA-RDP10-02196R000300010004-7

Declassified and Approved For Release 2013/03/04 : CIA-RDP10-02196R000300010004-7
second method is associated with definite technical complications, as it stipulates a departure from certain customary limitations, which are not always essential to the operating conditions. First and foremost, this concerns the periodicity of the reactor recharging and the depth of burnup of the fuel. The fuel enrichment can remain unchanged.* The technical difficulties can be prevented by reorganizing the fuel cycle on the basis of the second method. At the same time, its consideration will be advantageous, as it will allow the effect of certain limitations of the fuel cycle to be assessed and, in the final count, the advantages of the removal of each limitation to be compared with the costs of solving the corresponding technical problems.

Before discussing the results of the investigations into reorganizing the fuel cycle by the first method, we note that the makeup fuel enrichment, necessary for a specified reactor run, can be provided by fuel-element assemblies of one or a different enrichment. However, if it is oriented on the enrichment specification accepted for the VVER reactors and it does not take account of the use of any other fuel then, obviously, a greater flexibility of control in the composition of the makeup fuel is provided by fuel-element assemblies of a different composition. Moreover, it will be useful to pay attention to the data on the burnup of fuel-element assemblies with 3.6% enrichment in the reference fuel cycle. For operating periods equal to 7000 eff. h, with a limitation on the duration of operation of the fuel-element assemblies to three such runs, the maximum fuel enrichment is chosen much too high.

Taking account of these considerations and also of the undesirability of using a large diversity of fuel enrichment, fuel cycles were calculated which satisfy all the RFC limitations, but which are more economical. It was found that such a fuel cycle is one with fuel-element assemblies with an enrichment of 2.4 and 3.3%, when the composition of the makeup is varied from run to run with a periodicity dependent upon a three-year period of operation of the fuel and with the geometrical special features of the core; in this case, combinations of these fuel-element assemblies are always maintained: 12, 13 and 102, 108; the average enrichment of the makeup fuel is 3.20-3.21%.

In this region of makeup, fuel with 2.4% enrichment was found only in the brackets of the control and safety rod cassettes. Recorder charts of the fuel charges were formed by the method in [2], but in this case a further condition of observance of a uniform scheme of periodic reorganization of the fuel-element assemblies was introduced.

The principal characteristics of this fuel cycle, calculated by the BIPR-5 program [3], on the assumption that the absorbers of a working group of control and safety rod cassettes are inserted into the core to 75 cm and are withdrawn from it only after the final withdrawal of boron from the coolant,† are shown in Table 1. It follows from Table 1 that the buildup of slags in the most spent fuel-element assemblies does not exceed 33.1 kg/ton U, and the average buildup of slags for the fuel-element assemblies with 2.4 and 3.3% enrichment is established at the level of 26.8-27.1 and 30.2-30.4 kg/ton U, respectively. This is a marked improvement of the similar indices for the RFC. The fuel cycle being considered is not inferior even according to the value of the coefficients characterizing the nonuniformity of the power distribution of the reactor.

As transition to this fuel cycle does not increase the constant component of the specific normalized costs of the production of electric power, in order to show its economic advantages, it is sufficient to estimate the change of the fuel component. This can be done most clearly if we assume equality of the relative changes of the fuel component and the specific consumption of natural uranium.‡ By comparing the data about the consumption of natural uranium, we see that the fuel component for the cycle with fuel of 3.3% enrichment is less by 3.6% than for the RFC. This is an appreciable effect, even taking into account that the fraction of the fuel component in the normalized costs on actual units with VVER according to the data of [4], is estaimated at 0.25-0.35.

*Obviously, combinations of these methods are also possible. In this case, the technical complexity of the practical embodiment is a classification criterion.

†The other results given here are also obtained on this same procedural basis and with the same assumptions.

‡The assumption is valid with the accuracy applicable for a comparative estimate, as the fuel cycle being considered differs only a little in enrichment. It leads to an understated estimate.

Declassified and Approved For Release 2013/03/04 : CIA-RDP10-02196R000300010004-7

Declassified and Approved For Release 2013/03/04 : CIA-RDP10-02196R000300010004-7

TABLE 1. Fuel Cycle with a 3.3% Fuel Enrichment

Characteristics	Reactor charge								
	2	3	4	5	6	7	8	9	10
Operating period, eff. days	274	306	289	289	303	291	290	302	291
No. of makeup fuel-element assemblies with 3.3 and 2.4% enrichment	102 / 12	108 / 12	102 / 13	102 / 12	108 / 12	102 / 13	102 / 12	108 / 12	102 / 13
Coefficient of nonuniformity at start of run:									
by power of fuel-element assemblies	1,32	1,28	1,26	1,26	1,27	1,25	1,26	1,27	1,27
volume	1,77	1,78	1,71	1,74	1,69	1,72	1,73	1,69	1,72
Average buildup of slags in discharged fuel, kg/ton U	21,9	29,8	30,0	29,9	30,0	30,1	29,9	30,0	30,1
including in fuel with 3.3 and 2.4% enrichment	— / 21,9	30,4 / 25,0	30,4 / 26,9	30,2 / 27,0	30,4 / 26,8	30,4 / 27,1	30,2 / 27,0	30,4 / 26,8	30,4 / 27,1
Average buildup of slags in fuel-element assemblies with greatest burnup, with 3.3 and 2.4% enrichment, kg/ton U	— / 22,8	33,1 / 28,1	32,5 / 29,4	32,5 / 29,7	32,2 / 30,0	32,5 / 29,8	32,3 / 29,7	32,2 / 29,8	32,5 / 29,8
Nonuniformity of fuel burnup with 3.3 and 2.4% enrichment	— / 1,12	1,19 / 1,27	1,16 / 1,21	1,18 / 1,22	1,13 / 1,29	1,09 / 1,23	1,17 / 1,22	1,13 / 1,28	1,09 / 1,23
Specific consumption of natural uranium (eff. days)$^{-1}$	0,911 (0,932)	0,860 (0,870)	0,869 (0,904)	0,863 (0,889)	0,868 (0,901)	0,863 (0,895)	0,860	0,871	0,863

Note. In the first charge, in addition to the 133 and 102 fuel-element assemblies with 2.4 and 3.3% enrichment, there are 114 fuel-element assemblies with 1.6% enrichment, which are discharged after the first run.

Here and in Table 2, the consumption of natural uranium is estimated on the assumption that the enrichment of the tailings amounts to 0.25%; values are given in brackets for the fuel cycle of [1].

The results obtained confirm the prospects for the considered method of reorganization of the VVÉR fuel cycle which, as calculations show, can be achieved without difficulties, starting from any run of the RFC. It should be added that the reorganization does not impose additional limitations on the solution of the current operating problems. The possibility is established in the fuel cycle, in the case of necessity, of both shortening individual runs by increasing the fraction of fuel-element assemblies with 2.4% enrichment in the fresh fuel, as well as lengthening the run by the introducing fuel with 3.3% enrichment into the brackets of the control and safety rod cassettes.

We shall now evaluate the advantages of the second route for reorganization, if fuel with 2.4 and 3.6% enrichment is used. It seems most reasonable to conduct this analysis by successively removing the limitations on the burnup and the fuel recharging periodicity. First of all, let us return to the results of [5], where the fuel cycle of the VVÉR-440 with a fuel enrichment of 2.4 and 3.6% is optimized with respect to the economic criterion and more than a four-year operation of the fuel-element assemblies is allowed. It follows that part of the reserve of the energy potential of the fuel with 3.6% enrichment, which is not used in the RFC, can be used successfully with an annual recharging periodicity and a constant duration of the operating run (7000 eff. h), if the least spent fuel-element assemblies of this enrichment remain in the fourth year of operation. Transition to a four-year run of 36 of these fuel-element assemblies with the simultaneous reduction of the number of makeup fuel-element assemblies to 108-109 and an increase of the fraction of the fuel-element assemblies with 3.6% enrichment among them to 83% is equivalent to a reduction of the number of recharging of this fuel after the run to 3.4 and is accompanied by an increase of the average time of operation to 900 eff. days. This is expressed beneficially on the natural cost indices. The average burnup of fuel with 3.6% enrichment increases to 33.8-33.9 kg/ton U, and the specific consumption of natural uranium is reduced by 3.5% in comparison with the RFC. The gain in the fuel component of the normalized costs also will be almost the same, since the constant component, just as in the previous case, is unchanged. Thus, this fuel cycle promises approximately the same economic advantages as the fuel cycle with 3.3% enrichment.*

*This procedure of delaying a part of the fuel-element assemblies to a fourth year of operation, determined by a duration of the run of 7000 eff. h, does not give an appreciable effect in the fuel cycle with 3.3% enrichment.

Declassified and Approved For Release 2013/03/04 : CIA-RDP10-02196R000300010004-7

Declassified and Approved For Release 2013/03/04 : CIA-RDP10-02196R000300010004-7
An additional effect can be obtained by the direct utilization of the fuel-element assemblies withdrawn earlier from the RFC.

In analyzing this fuel cycle, it is impossible not to touch upon the technical difficulties which may be caused by the transfer of the fuel-element assemblies to a four-year operating cycle.* The most problematic are questions of the durability of the fuel elements and also transportation into the cooling pond and storage of the spent fuel.

The existing experience in the bulk operation of the fuel-element assemblies of the VVÉR inspires some optimism with respect to the maintenance of the efficiency of the fuel elements during four runs, when the average buildup of slags in them is greater than in the RFC by 7-11% and by a maximum of 18-20%. It is true that it concerns only regulation conditions and does not give direct information about the behavior of the fuel in accident situations, which also must be taken into account. This experience indicates that the annually undertaken increase (after exhaustion of the reactivity margin on burnup) of the 10-20% effective duration of the operating time of the reactors in conditions of reduction of power and temperature of the coolant, which is widespread in the practice of operating the units of nuclear power stations, leads to an increase of burnup of almost all fuel-element assemblies by 10-15%. For example, at the Kol'sk nuclear power station, an average burnup in the discharged fuel of $\sim 33 \cdot 10^3$ MW•days/ton ($\sim$34.3 kg/ton) is achieved, with a burnup of up to $37 \cdot 10^3$ MW•days/ton in individual fuel-element assemblies. This has not been accompanied by a loss of pressurization of the fuel elements above the permissible limits. At the present time, these conditions for VVÉR are accepted as ordinary and no counterindications are recorded, either from the point of view of durability of the fuel elements, or from the point of view of operations with spent fuel at nuclear power stations [4, 6-10].

Even on the understanding that these problems will require additional close study and that the discussions presented cannot serve as the technical basis for the safe operation of the fuel-element assemblies above the design period, it can be asserted that such a fuel cycle is not without promise. There are specific realistic prerequisites to be considered for the feasibility of its achievement without significant additional costs.

Finally, let us remove at once both limitations involved in the RFC, by simultaneously postulating that the fuel-element assemblies can function for longer than 940 eff. days with a burnup above average equal to 31.6 kg/ton U, and that the effective duration of the run of the reactor between rechargings can amount to less than 7000 eff. h. An analysis of the reorganization of the fuel cycle on the shortened operating period is not deprived of practical meaning since quite often, according to the conditions in the power system or some other reasons, the power plants of nuclear power stations are operated with a utilization factor of the installed capacity (UFIC) of less than 0.8. For example, the average value over many years of this factor for the Novovoronezh nuclear power station amounted to 0.7 [11], and for the Kol'sk nuclear power station it was 0.65 [10]. There are similar data also for PWR reactors: The average UFIC over the whole time of operation cited in [12] is less than 0.73. For almost one-half of the reactors of this type, it does not exceed 0.7. In these case, when maintaining an annual periodicity of recharging, it should be directed to an operating period of less duration. Not taking this into account will lead to an unjustified increase of cost of electric power, in the avoidance of which the enrichment of the makeup fuel can be reduced by increasing in it the fraction of fuel-element assemblies with 2.4% enrichment.

But a fuel cycle is found to be more economical in which the fuel with 2.4% enrichment operates for three runs and the fuel with 3.6% enrichment operates for four runs, and during recharging about one-quarter of the core is replaced. It is not complicated to convert to this regime after any normal run of the RFC, e.g., after the first — to a fuel cycle for which the characteristics are given in Table 2. In this case, the reactor emerges into the steady-state recharging cycle with a constant interchange scheme of the fuel-element assemblies and with an operating period of about 6200 eff. h. As the number of rechargings of the fuel-element assemblies with 3.6% enrichment during the run (1030 eff. days) is increased up to four, their average and maximum burnup increases by 13-15% in comparison with the RFC. The coefficients of nonuniformity of power distribution and the spread of the average burnup of the fuel-element assemblies are found to be small. The specific natural uranium consumption is less by 7.8% than in the RFC.

*The discussion here will not fall beyond the bounds of the technical aspects. It is inappropriate to touch upon the specific questions concerning bilateral commitments of the suppliers and customers of fuel or the guarantees of the IAEA.

Declassified and Approved For Release 2013/03/04 : CIA-RDP10-02196R000300010004-7

Declassified and Approved For Release 2013/03/04 : CIA-RDP10-02196R000300010004-7

Table 2. Fuel Cycle with Shortened Operating Period and Quadruple Recharging of the Fuel-Element Assemblies with 3.6% Enrichment

Characteristics	Reactor charge								
	2	3	4	5	6	7	8	9	10
Operating period, eff. days	274	244	253	261	256	259	256	256	259
No. of makeup fuel-element assemblies with 3.6 and 2.4% enrichment	78 / 36	78 / 12	78 / 13	78 / 12	78 / 12	78 / 13	78 / 12	78 / 12	78 / 13
Coefficient of nonuniformity at start of run:									
by power of fuel-element assemblies	1,26	1,28	1,28	1,24	1,25	1,27	1,26	1,27	1,27
volume	1,69	1,68	1,75	1,69	1,65	2,00	1,66	1,66	2,00
Average buildup of slags in discharged fuel, kg/ton U	22,4 (22,2)	27,6 (30,7)	33,2 (29,4)	33,6 (29,3)	33,6 (29,3)	33,8 (28,3)	33,8	33,6	33,7
including in fuel with 3.6 and 2.4%	— / 22,4	31,7 / 24,9	35,8 / 26,3	34,9 / 24,6	35,1 / 24,2	35,2 / 24,7	35,2 / 24,6	35,1 / 24,5	35,1 / 24,7
Average buildup of slags in fuel-element assemblies with greatest burnup, with 3.6 and 2.4% enrichment, kg/ton U	— / 23,3	32,0 / 28,3	38,7 / 25,4	37,1 / 25,1	37,4 / 25,3	37,5 / 25,5	37,6 / 25,3	37,4 / 25,3	37,5 / 25,4
Nonuniformity of fuel burnup with 3.6 and 2.4% enrichment	— / 1,06	1,05 / 1,10	1,15 / 1,05	1,10 / 1,06	1,12 / 1,09	1,12 / 1,06	1,12 / 1,06	1,11 / 1,10	1,10 / 1,06
Specific consumption of natural uranium, (eff. days)$^{-1}$	0,935	0,891	0,865	0,833	0,849	0,845	0,849	0,849	0,845

As a result of this reorganization of the fuel cycle, a significant part (about 30%) of the loss in the normalized costs can be compensated due to the lower UFIC (because of the specific operating conditions).

A reduction of the fuel component can also overlap the increase of the constant component. A loss of 1.5-2% in the normalized costs is revealed in the case when the considered and reference fuel cycles are compared for identical average charges (80-90% of nominal) during a run and with an identical time of standstill of the unit for each recharging (25-30 days [4]).* Undoubtedly, more frequent shutdowns can create definite drawbacks for the power distribution systems, into which the nuclear power station is connected, and this must take into account the specific situation. From the point of view of costs of the production of electric power, this fuel cycle is interesting. The technical difficulties because of the deeper fuel burnup in it are not worsened by comparison with the difficulties of the preceeding fuel cycle.

When operating a power plant with an even lower UFIC (0.5-0.6), a fuel cycle may be advantageous where all the fuel-element assemblies with 2.4 and 3.6% enrichment operate for four and five runs, respectively. It allows 15-20% of the unavoidable increase of the normalized costs to be compensated in this case. If, however, this fuel cycle is used for a reactor with a high (∿0.8) UFIC, more frequently carrying out makeup, then the loss in the specific normalized costs will be even less (∿1%) than that expected in the similar situation with the previous fuel cycle.

The analysis of different alternatives for the reorganization of the VVÉR fuel cycle shows that there are realistic prerequisites for reducing the normalized costs of the production of electric power by a nuclear power station with reactors of this type by 2.5%, The effect can be obtained both as a result of conversion to the use of fuel with 3.3% enrichment and also by increasing the number of rechargings of fuel of the enrichment used at the present time. In the latter case, it will be necessary technically to justify the feasibility of the safe operation of the fuel-element assemblies with a burnup 10-20% higher than that accepted as permissible.

Since these reorganizations do not require a structural change of the reactor or of the fuel-element assemblies and do not worsen the physical characteristics of the reactor, they

*Despite the more frequent shutdowns with the shortened operating period, the reduction of the UFIC in comparison with that in the RFC in this case amounts to about 1%.

Declassified and Approved For Release 2013/03/04 : CIA-RDP10-02196R000300010004-7

Declassified and Approved For Release 2013/03/04 : CIA-RDP10-02196R000300010004-7
can be achieved at any stage of its planning and operation. This possibility of a smooth adaptation of the VVÉR-440 fuel cycle to different situations, affecting the economics of electric power generation at nuclear power stations, is exceptionally advantageous.

The authors are deeply greatful to V. A. Sidorenko for interest in the work and for valuable comments, and also to A. N. Noviko for useful discussions of the problems touched upon here.

LITERATURE CITED

1. L. V. Kokhanovskaya, Kernenergie, 20, No. 10, 307 (1977).
2. V. V. Pobedin and V. D. Simonov, At. Energ., 46, No. 5, 357 (1979).
3. D. M. Petrunin, E. D. Belyaeva, and I. A. Kireeva, Preprint IAÉ-2518, Moscow, 29 (1975).
4. F. Ya. Ovchinnikov et al., Operating Regimes of Water-Cooled/Water-Moderated Nuclear Reactors [in Russian], Atomizdat, Moscow (1977).
5. V. I. Pavlov et al., At. Energ., 51, No. 3, 161 (1981).
6. F. Ya. Ovchinnikov et al., in: Affective Experience in the Operation of the Novovoronezh Nuclear Power Station [in Russian], Novovoronezh (1974), p. 51.
7. L. I. Golubev, V. D. Dobrynin, and V. M. Tsybenko, ibid., p. 68.
8. V. P. Kruglov and A. F. Shvoev, ibid., p. 85.
9. F. Ya. Ovchinnikov, V. K. Sedov, and V. B. Netesin, in: Nuclear Power Stations [in Russian], No. 1, Énergiya, Moscow (1977), p. 82.
10. A. A. Mateev et al., At. Energ., 51, No. 2, 87 (1981).
11. V. A. Sidorenko, At. Energ., 43, No. 5, 325 (1977).
12. Yu. V. Smirnov et al., Nuclear Industry of Foreign Countries [in Russian], Atomizdat, Moscow (1980).

USE OF NUCLEAR FUEL TO COVER THE SEASONAL MAXIMUM ELECTRIC LOAD

V. M. Boldyrev, M. V. Sigal, and S. A. Skvortsov

UDC 621.31:621.311.2:621.039

The operation and structure of the generating capacities of united electrical power systems (UEPS) in the USSR are related to the seasonal nonuniformity of electricity consumption. The fluctuations in electricity consumption are usually very significant. Thus, in some UEPS the summer minimum in the electrical load curve reaches 30% of the winter maximum. A forecast of electrical power indicates that the spread in the seasonal load curve will increase.

At the present stage of development of nuclear power, nuclear power plants (NPP) operate only on the base part of the electrical load curve. The seasonal maximum is covered by thermoelectrical power plants using fossil fuels. At the same time, the increasing total power of nuclear power plants on line raises the possibility of using nuclear fuel together with fossil fuel at the time of the seasonal load maximum.

The operation of a nuclear reactor with seasonal variation of its thermal power does not give rise to any special technical problems and is more a problem of economics, since the use of nuclear power plants for 4000-5000 h/yr with steam turbines will for a long time be less useful than fossil-fuel-fired stations (even including the increase in the price of fossil fuel). It may be economically expedient to use nuclear fuel as well in nuclear thermoelectric central system (NTES) for seasonal regulation. This proposition is based on similarities of the configurations of seasonal electricity and heat consumption curves. In this connection, it is interesting to create NTES with special turbines with back pressure, generating electrical power only for heating. Such NTES, as will be described in what follows, likewise have definite ecological advantages over the first generation NTES, currently being planned, with TK-type turbines with fixed steam capacity ($NTES_{TK}$).

Translated from Atomnaya Énergiya, Vol. 53, No. 4, pp. 218-222, October, 1982. Original article submitted December 3, 1981.

 0038-531X/82/5304-0664$07.50 © 1983 Plenum Publishing Corporation

Declassified and Approved For Release 2013/03/04 : CIA-RDP10-02196R000300010004-7

Declassified and Approved For Release 2013/03/04 : CIA-RDP10-02196R000300010004-7

The main purpose of the program for constructing NYES and nuclear thermal power stations (NTP), which has already begun, is to replace in the heating-electrical power sector very scarce (especially in the European part of the USSR) fossil fuel [1], consumed in large quantities for producing heat for public and industrial consumers. At the same time, due to the type of turbine with fixed steam capacity for NTES that are planned and currently being constructed and the possibility of operating such stations all year at a constant steam flow rate in the head part of the turbine [2], these NTES help solve other problems as well, namely, problems of increasing the nuclear base electrical generating power and the problem of summer maintenance reserve.

Usually, in power systems, power stoppages for planned maintenance are timed to the seasonal minimum. At the same time, according to the power balance, it ofter occurs that in addition to the blocks being serviced, it is also necessary to stop operating blocks, which are thus forced to participate in the regulation of the electrical load schedule. In many cases thermoelectric power plants (TEP) with K-200-130 and K-300-240 turbines contribute to such seasonal regulation.

As new nuclear power stations are brought on line, primarily in UEPS in the northwest and central parts of the country, a situation will occur in the future in which the summer load decrease will also affect the nuclear power plants. In this situation it will not be advisable to increase power generation at NTES during a period of no heating (stations with TK turbines). This will justify the use of TR-type central heating turbines with back pressure in NTES and electrical power generation in such stations ($NTES_{TR}$) exclusively for heating in order to cover the fall—winter load maximum.

Thus, a situation in which it will be necessary to choose one of the following combinations of power sources in order to supply the fixed electricity and heat requirements of a region is realistic: I) $NTES_{TR}$ + PB + NPP; II) TEP + $NTES_{TK}$ + PB; III) TEP + NTP + PB + NPP (PB is the peak reserve fossil-fuel-fired boiler source).

In the first variant, nuclear fuel is used both for producing heat and generating electricity for heating for seasonal regulation of its output.

In the alternative second and third variants, fossil-fuel-fired steam thermal power stations are used for seasonal regulation of power generation, while NTES with TK-450/500-60 turbines and NTP are used for generating heat.

The PB sources are included in the combinations listed above due to the necessity for their operation in combination with heat sources in order to optimize the heat supply system. The combinations of power sources are supplemented by nuclear steam electrical power plants due to the necessity of meeting the total fixed power demand, as shown in Fig. 1.

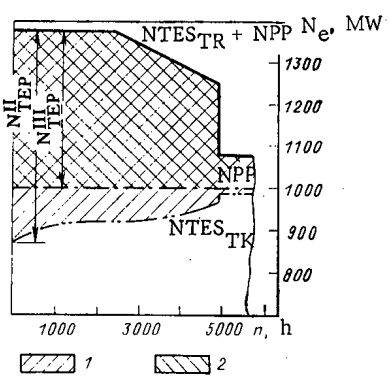

Fig. 1. Graph of annual electrical power generation in the electrical supply systems analyzed: 1, 2) electrical power generation by thermoelectric stations in variants TEP + $NTES_{TK}$ and TEP + NTP + NPP, respectively.

Declassified and Approved For Release 2013/03/04 : CIA-RDP10-02196R000300010004-7

Declassified and Approved For Release 2013/03/04 : CIA-RDP10-02196R000300010004-7

It is useful to consider in greater detail the specific characteristics of $NTES_{TR}$ entering into the first combination of power sources.

First, we note that the absence of TR turbines in the scheme of the low-potential part [low-pressure cylinders (LPC), condensers] decreases the capital investment required in constructing the station both due to the decreased cost of equipment and the decrease in the amount of construction and assembly work: The layout of the engine room is simplified, it is not necessary to construct cooling towers which are expensive and require special equipment, etc. The system for supplying water to the station itself may also decrease the required capital investment. For the conditions under which saturated steam turbines are used in nuclear power plants and NTES, much larger amounts of steam are used than in modern fossil fuel fired thermoelectric power plants with the same rated capaicity. This in its turn requires much larger amounts of water in the turbine condensors than in large state regional electic power stations and complicates the problem of supplying water for cooling and industrial use due to the uneven distribution of water resources in various territories of the USSR. Taking into account the fact that NTES by their nature are attracted more to regions where heat is consumed than to water sources, the decrease in the assured steam capacity of NTES increases the freedom of choice (quite limited for nuclear power supplies) of area for constructing the plant. This greatly decreases the economic losses related to dispossessing land, as well as losses in transporting heat. The maximum effect could be obtained by completely eliminating condensers, i.e., by installing TR-type turbines in the NTES.

In making a decision to construct $NTES_{TR}$ the characteristics of reverse pressure turbines should not be forgotten, namely, the close match of electrical power generation to the thermal loads and thus to climatic factors as well. At the same time, the problems related to the decreased maneuverability of $NTES_{TR}$ compared to fossil-fuel-fired thermoelectric power plants, are technically completely solvable. In particular, when the electrical power generation at the NTES deviates from the planned level, a corresponding redistribution in the heat output between PB_{TR} and $NTES_{TR}$ or $NTES_{TK}$ operating in the same power system can be effectuated. It may also be useful to connect for a short time water—water heat exchangers with circulating water as the cooling agent into the makeup supply line [3] and to introduce other measures as well.

A characteristic of $NTES_{TR}$ in contrast to $NTES_{TK}$ is the necessity of switching it into preheated water boilers (later transferrable into the peak load regime).

While $NTES_{TR}$ are less universal than $NTES_{TK}$, they undoubtedly are preferable ecologically. Located near large cities, $NTES_{TK}$ must have a cooling system with cooling towers, which are a source of concentrated thermal and steam emissions into the atmosphere. These emissions, as studies have shown [4], are much greater than for any natural process occurring in the atmosphere and can generate considerable atmospheric effects (cloud formation, increased precipitation, formation of fogs, etc.). $NTES_{TR}$ do not have such negative side effects on the environment, which is especially valuable in connection with the perspective application of technical solutions that permit placing NTES near the region where heat is consumed (as done, e.g., in developing NTES based on the VK-500 reactor).

TR-type turbines having the same initial steam parameters as TK turbines can handle a much higher user heat load. In this connection, $NTES_{TR}$ based on the VK-500 reactor being developed or some other promising reactors with the same unit capacity could be more widely used than similar power plants based on a more powerful reactor of the VVÉR-1000 type. At the same time, because of the tendency for planners to create large territorial formations including a group of cities and population centers with total heat load of the order of 10,000 Gcal/h and higher $NTES_{TR}$ with VVÉR-1000 reactors will also find application. It may also be useful to create mixed central steam thermal power plants, where turbines of type K and type TR could also be used in the block, e.g., with a VVÉR-1000 reactor. Determining the expedience of using $NTES_{TR}$ is a regional problem. In each case, it must be examined taking into account the specific conditions under which the power system operates and the structure of its power-generating capacities.

The conditions for variants I-III being analyzed to be competitive are determined using the technique of technicoeconomic calculations in energetics by comparing the total computed reduced expenditures when supplying the same power in all variants. The criterion for economic efficiency in this case is minimum expenditures.

Declassified and Approved For Release 2013/03/04 : CIA-RDP10-02196R000300010004-7

Declassified and Approved For Release 2013/03/04 : CIA-RDP10-02196R000300010004-7

Evidently, the competitiveness of $NTES_{TR}$ can be ensured if the following conditions are satisfied:

$$Z_{TR} + Z_{PB_I} + Z_{C_I} + Z_{NPP} \leqslant Z_{TEP_{II}} + Z_{TK} + Z_{PB_{II}} + Z_{C_{II}} \quad (1)$$

and

$$Z_{TR} + Z_{PB_I} + Z_{C_I} + Z_{NPP} \leqslant Z_{TEP_{III}} + Z_{NTP} + Z_{PB_{III}} + Z_{C_{III}} + Z_{NPP} \quad (2)$$

Here Z_{NPP}, Z_{TK}, Z_{TR}, Z_{NTP}, Z_{TEP}, and Z_{PB} are the computed reduced expenditures on power generation by the power sources being analyzed (NPP, $NTES_{TK}$, $NTES_{TR}$, NTP, TEP, and PB, rubles/yr); Z_C are the computed reduced expenditures on transporting fuel, rubles/yr. The numerical indices indicate the power source combination.

Depending on the problem formulated, expressions (1) and (2) can be transformed accordingly. In particular, in the present work, where $NTES_{TR}$ are being examined from the point of view of the usefulness of including them in seasonal regulation of the electrical load curve as alternatives to fossil fuel fired sources, it is more convenient to write conditions (1) and (2) in the form

$$Z_{TEP} \geqslant \frac{Z_{NPP}Z_E + Z_{TR} - Z_{TK} + Z_{C_I} + Z_{PB_I} - Z_{C_{II}} - Z_{PB_{II}}}{Z_{NPP} + Z_{TR} - Z_{TK}} \quad (1a)$$

and

$$Z_{TEP} \geqslant \frac{Z_{TR} - Z_{NTP} + Z_{C_I} + Z_{PB_I} - Z_{C_{III}} - Z_{PB_{III}}}{Z_{TR} + Z_{NTP}^{CN}} . \quad (2a)$$

Here Z_{TEP} are the proportionate reduced expenditures on the power generated by the fossil-fuel-fired thermoelectric power plant, operating in the seasonal regulation mode, rubles/(MW·h); Z_E, proportionate computed expenditures on the electrical power supplied by a nuclear power plant operating in the base regime, rubles/(MW·h); Z_{NPP}, Z_{TR}, and Z_{TK}, electrical power supplied per year by the nuclear power plant being analyzed, NPP, $NTES_{TR}$, and $NTES_{TK}$, MW·h; Z_{NTP}^{CN} electrical power consumed over the same time period by the NTP for its own needs, MW·h.

The right-hand sides of expressions (1a) and (2a) determine the limiting values of the proportionate computed expenditures on electrical power supplied by maneuverable thermoelectric power plants, above which these plants become economically less efficient than the $NTES_{TR}$ being analyzed.

The initial stage in the program for assimilating nuclear heat supply sources (NTES and NTP) do not yet permit determining uniquely and with sufficient reliability the capital investment required for constructing them. There is also some uncertainty in estimates of the reserve expenditures on electrical power. Under these conditions, it is interesting to determine the competitiveness of $NTES_{TR}$ relative to alternative power sources by varying over a wide range such indicators as the proportionate capital investment in constructing nuclear heat supply sources and the proportionate computed expenditures on electrical power supplied by the NPP and by substituting maneuverable TEP.

In the calculations, the results of which are discussed in the present paper, we examine a variant for supplying power to a region whose rated heat load Q = 1500 Gcal/h, which permits performing a technicoeconomic analysis using both NTES and NTP. The base part of the heat load is supplied by nuclear sources, while the peak part is supplied by gas- and oil-fired-boiler sources with KVGM-100 boilers. The base heat sources are either $NTES_{TR}$ or NTES with TK-450/500-60 UTMZ turbines or NTP with AST-500 reactor installations. We also analyzed the use of TR turbines, consisting of high- and medium-pressure cylinders combined with TK-450/500-60.* The calculations show that such a turbine provides maximum electrical power of 380 MW while supplying 950 Gcal/h. Thus, the computed fraction of the thermal load supplied by nuclear power sources to the overall thermal load of the region in variants I-III constitutes: $\alpha_{TR} = 0.63$, $\alpha_{TK} = 0.60$, and $\alpha_{NTP} = 0.57$.

*The structure and the useful unit capacity of turbines for $NTES_{TR}$ should be analyzed separately.

Declassified and Approved For Release 2013/03/04 : CIA-RDP10-02196R000300010004-7

Declassified and Approved For Release 2013/03/04 : CIA-RDP10-02196R000300010004-7

The electrical load of the adjoining region in all variants was assumed to be identical. Its variation over the course of a year and the fractional participation of power sources entering into combinations I-III in covering the load correspond to the data presented in Fig. 1. The utilization factor of the rated capacity of the nuclear reactor for nuclear power plants and $NTES_{TK}$ is $\varphi = 0.8$, which corresponds to the technically and economically well-founded regime of its operation [5].

The calculations were performed for the climatic conditions of the central region of the European part of the USSR. The fraction of the load used for hot-water supply in the total thermal load of the region was taken as 0.2 $NTES_{TR}$ and $NTES_{TK}$ based on VVÉR-1000 and VK-500 reactors were examined. In doing so, we took into account the difference in the distances between the nuclear power source and the region where the heat is consumed determined by radiation safety. The specific capital expenditures were varied in the range 300-500 rubles/kW* for $NTES_{TK}$ and 120-140 thousand rubles/(Gcal/h) for NTP. The total capital investment in $NTES_{TR}$ with the same thermal reactor power as for $NTES_{TK}$ was reduced, according to estimates, by 14.2 million rubles per turbine unit. This sum included only the minimum expected difference in capital investment, related to the absence of low-pressure cylinders, condensers, and cooling towers. In this case, the savings owing to the lower cost of the first fuel loading, lower construction costs due to the smaller size of the engine room, as well as more favorable than in variants with $NTES_{TK}$, possibilities for choice of location, were not included (resulting in a definite disadvantage for variants including $NTES_{TR}$). The technicoeconomic operational indicators of nuclear sources, which together with the capital investments determine the computed reduced expenditures on power generation entering into (1) and (2), were determined from completed projects.

The results of calculations determining the competitiveness of variants incorporating the use of nuclear and fossil fuel, respectively, for covering the fall—winter maximum electrical load are presented in Fig. 2 for the case of heat supplied by NTES. The conditions for equal economic efficiency correspond to equality of the left and right sides of expression (1). Economically preferable combination of power sources, including $NTES_{TK}$, for which fossil fuel is used to cover the seasonal maximum in the consumption of electricity, is situated below the straight lines, while the region of economically preferable combination of power sources including $NTES_{TR}$, for which the seasonal maximum is covered with the help of nuclear fuel, is shown above the straight lines.

As follows from the dependences shown in Fig. 2, even for the specific computed expenditures already attained at the present time for nuclear power plants Z_E = 14.5 rubles/MW·h, the use of $NTES_{TR}$ is economically justified beginning with Z_{TEP} = 19 rubles/MW·h). In the future, when nuclear power plants with high unit power (e.g., 1500 MW and then 2400 MW) are assimilated, as well as with the introduction of multiblock plants, Z_E will decrease. The limiting value Z_{TEP} determined by expression (1a), will decrease correspondingly.

The data in Fig. 2 concern the variant of $NTES_{TR}$ based on the VK-500 reactor. For the VVÉR-1000 reactor, the nature of the dependences will be analogous to that shown but in the range of variation of C_{sp} and Z_E examined, the limiting values of Z_{TEP} will be lower (due to the difference in the technicoeconomic indicators for operation of the reactors). For example, for C_{sp} = 300 rubles/kW and Z_E = 14.4 rubles/(MW·h), the limiting value of Z_{TEP} is of the order of 17.5 rubles/(MW·h).

It is easier to see the economic efficiency of $NTES_{TR}$ if as an alternative we examine a combination in which heat is supplied by NTP. Multivariant calculations using (2a) showed that even with the least favorable, for $NTES_{TR}$, combination of parameters being varied, its use is economically justified already for Z_{TEP} of the order of 8 rubles/(MW·h) and higher.

In evaluating the results obtained, it should be kept in mind that for coal-fired thermoelectrical power plants with K-200-130 and K-300-240 turbines and the K-500-130 turbine being developed, for a fuel cost expected in the near future not lower than 34-36 rubles/ton per turbine unit, the specific computed expenditures on the electrical energy supplied when these power plants operate in the seasonal regulation mode is of the order of 19.5 rubles/(MW·h) and higher.

Thus, based on what has been said above, we can conclude that the creation of NTES with turbines with back pressure is promising and economically efficient.

*Referred to maximum electrical power in the heat-supply operational regime.

Declassified and Approved For Release 2013/03/04 : CIA-RDP10-02196R000300010004-7

Declassified and Approved For Release 2013/03/04 : CIA-RDP10-02196R000300010004-7

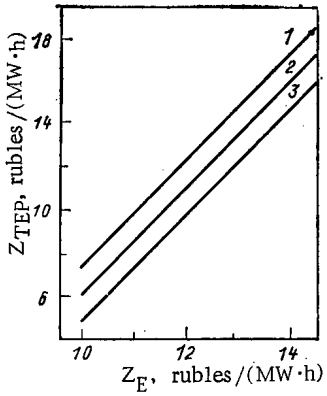

Fig. 2. Conditions for equal economic efficiency in utilizing nuclear and fossil fuel for covering the seasonal peak electrical load as a function of the specific computed expenditures on supplying electrical power by nuclear power plants (Z_E) and maneuverable fossil-fuel-fired thermoelectric power plants TEP (Z_{TEP}) for the following specific capital investments (C_{sp}) in $NTES_{TK}$, rubles/kW: 1) 300; 2) 325; 3) 350.

It is also very important that $NTES_{TR}$ with the same power output as alternative variants will permit replacing an additional amount of fossil fuel (up to 610-690 thousand tons per turbine unit) and, in addition, from that part of the fuel-power balance where nuclear fuel is not presently being used. Thus, one of the most important problems of power engineering, namely, replacing fossil fuel by nuclear fuel in the fuel-energy balance of this country, can be largely solved.

LITERATURE CITED

1. L. A. Melent'ev, Teploenergetika, No. 11, 4 (1976).
2. V. M. Boldyrev et al., Teploenergetika, No. 4, 32 (1978).
3. G. Stempen', Byulleten' Postoyannoi komissii SEV po élektroénergii (Bulletin of the Permanent Commission of the Council of Mutual Economic Assistance of Electrical Power), No. 2, 82 (1972).
4. M. Chaudrakaut, Bhumralkar in: Proc. IIASA Workshop on Climate and Solar Energy Conversion, December 8-10, 1976.
5. B. B. Baturov et al., At. Energ., 43, No. 6, 438 (1977).

MEASUREMENT OF FUEL BURNUP IN VVÉR-365 AND VVÉR-440 FUEL-ELEMENT ASSEMBLIES BY GAMMA SPECTROSCOPY

B. A. Bibichev, V. P. Kruglov,
V. P. Maiorov, Yu. M. Protasenko,
M. A. Sunchugashev, P. I. Fedotov,
and A. F. Shvoev

UDC 621.039.524.4

The improvement of programs for calculating fuel burnup in a VVÉR core requires experimental data on the distribution of fuel burnup and fission products over the height and cross section of fuel-element assemblies (FEA). Such experimental data for VVÉR-70 and VVÉR-210 FEA obtained by gamma spectroscopy are presented in [1-3]. Calculated values of the average fuel burnup in VVÉR-440 FEA are compared in [4] with experimental data obtained by monitoring the coolant temperature in the assemblies. In the present article we present experimental and calculated distributions of fuel burnup over the height of several VVÉR-365 and VVÉR-440 FEA.

Four VVÉR-365 and three VVÉR-440 FEA from the Novovoronezh nuclear power plant (NVNPP) with various fuel enrichments and various irradiation histories were examined (Table 1). In none of the runs were assemblies DR-3 No. 80, RP-3 No. 223, RI-2,4 No. 03, and RI-3,3 No.

Translated from Atomnaya Énergiya, Vol. 53, No. 4, pp. 222-224, October, 1982. Original article submitted November 18, 1980; revision submitted January 28, 1982.

0038-531X/82/5304-0669$07.50 © 1983 Plenum Publishing Corporation

Declassified and Approved For Release 2013/03/04 : CIA-RDP10-02196R000300010004-7

Declassified and Approved For Release 2013/03/04 : CIA-RDP10-02196R000300010004-7

TABLE 1. Principal Operating Data of FEA Examined

Number of FEA	Initial enrichment in ^{235}U, %	Type of reactor	Number of runs	Total length of irradiation, eff. days
DR-3 № 80	3	VVER-365, II unit	1	311
RP-3 № 223	3	" "	4	819
OI-3M-5 № 12	3	" "	3	929
RI-2,4 № 03	2,4	" "	4	1239
RP-3,3 № 71A	3,3	VVER-440, III unit	1	320
R-3,6 № 213	3,6	VVER-440. IV unit	3	1032
R-3,6 № 216	3,6	" "	3	1032

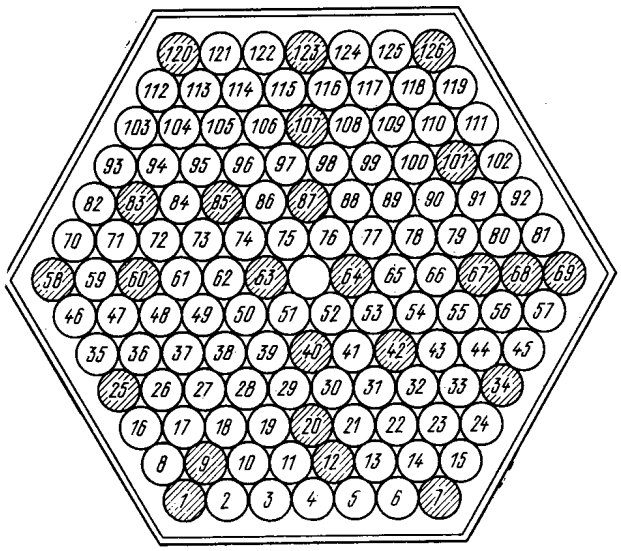

Fig. 1. Chart of positions of fuel elements examined (shaded) in FEA R-3,6 No. 216.

71A located at the core edge (outside row) or adjacent to a reactor power control FEA. In the first run FEA R-3,6 No. 213 and R-3,6 No. 216 were located at the core edge, and during all three runs OI-3M-5 No. 12 was located adjacent to a reactor power control FEA. The FEA were cooled for 1-2 years before measurements were begun.

The measurements were performed in a protection cell at the NVNPP. To eliminate self-absorption of gamma radiation the FEA were separated into individual fuel elements before measurements were begun. Only 26 of the 126 fuel elements in each FEA were examined. Several fuel elements of each row were selected for measurement (Fig. 1). Gamma spectra of fission fragment nuclides were measured every 25 cm along the height of these fuel elements, starting at 12.5 cm from the lower end of the fuel element (bottom of the core).

The measuring equipment (Fig. 2) consisted of a three-section slit collimator, a Ge(Li) detector, and spectrometric apparatus. The first section of the collimator was located inside the protection cell on the FEA dismantling table, whose height is continuously adjustable. The collimator slits of the first and third sections were 2 mm high, and the second slit was 6 mm high. The collimator was aligned optically by using a cathetometer.

The efficiency of the measuring equipment was determined by using one of the fuel elements of each FEA under study as a standard source. At the end of the measurements a sample was cut from the standard fuel element at one of the positions of measurement in the middle of the fuel element. The sample was dissolved, and the concentrations of U, Pu, Am, Cm and ^{137}Cs were measured. The ^{137}Cs concentration at the n-th point along the height of the fuel element being measured was calculated from the relation

Declassified and Approved For Release 2013/03/04 : CIA-RDP10-02196R000300010004-7

Declassified and Approved For Release 2013/03/04 : CIA-RDP10-02196R000300010004-7

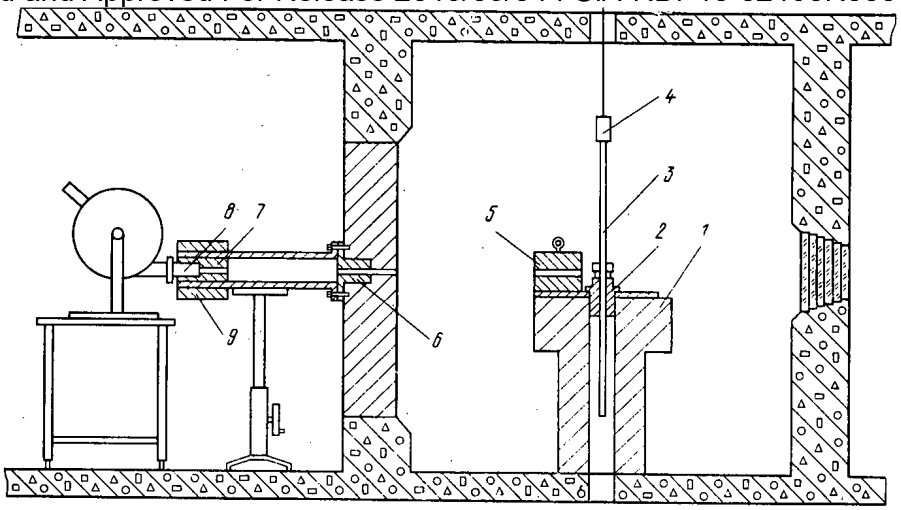

Fig. 2. Schematic diagram of measuring equipment: 1) table for dismantling FEA; 2) centering bushing; 3) fuel element; 4) fuel element holder; 5-7) sections of collimator 8) Ge(Li) detector; 9) detector shield.

$$C_{137}^{n} = \frac{S_{137}^{n} F_{137}}{S_0} C_0, \tag{1}$$

where S_{137} and S_0 are the areas of the ^{137}Cs photopeaks in the spectrum of the fuel element being measured and in that of the standard fuel element; F_{137} is a factor taking account of the decrease of ^{137}Cs during irradiation and cooling of the fuel element being measured; C_0 is the ^{137}Cs concentration in the standard fuel element, atoms/g of initial uranium. The values of S_{137} and S_0 were calculated with the program described in [5]. The fuel burnup was determined from the following relation [6]:

$$W^{n} = \frac{\overline{M}^{n} C_{137}^{n}}{N_A \overline{Y}_{137}^{n}} 10^3, \tag{2}$$

where W^n is the fuel burnup in kg/ton of U; $\overline{M}^n$ is the average molar mass of the fissioned nuclei; $\overline{Y}^n$ is the effective yield of ^{137}Cs for the mixture of fissioned nuclei; N_A is Avogadro's number.

W^n was calculated by assuming that the values of $\overline{Y}_{137}^n$ in the fuel element being measured (at all points along its height) and at the middle of the standard fuel element are identical. Since the cumulative yields of ^{137}Cs from the fission of ^{235}U, ^{239}Pu, and ^{241}Pu by thermal neutrons, and ^{238}U by fast neutrons, differ by only 7% [7], the contribution of each fissionable isotope to $\overline{Y}_{137}^n$ can be taken into account only approximately. $\overline{Y}_{137}^n$ for the standard fuel element was determined from the concentration of the isotopes of U, Pu, and the transplutonium elements [6]. The error resulting from the approximate calculation of $\overline{Y}_{137}^n$ was less than 1.5% for all FEA examined. The total error in the determination of W^n was 3.5-6% for fuel elements from various FEA. The largest contribution to this value was introduced by the reproducibility of the measurements of the standard fuel elements (1.5-2.0%) and the reproducibility of the measurements of the fuel elements being examined (1.5-5.0%). The poor reproducibility of the measurements of the fuel elements for FEA was due mainly to the partial disintegration of the pellets in these fuel elements. In calculating the total error the technological spread of the density of the pellets in unirradiated fuel was also taken into account. The contribution of this effect to the total error was 1.2%.

The measured values of W^n in 26 fuel elements of one FEA were used later to calculate $\overline{W}^n$, the average value of the burnup at a given point along the height of the assembly. In

Declassified and Approved For Release 2013/03/04 : CIA-RDP10-02196R000300010004-7

Declassified and Approved For Release 2013/03/04 : CIA-RDP10-02196R000300010004-7

TABLE 2. Calculated and Experimental Values of the Average Fuel Burnup

Number of FEA	Burnup, kg/ton of U		Deviation of calculated from measured burnup, %
	calculated	measured	
DR -3 № 80	12,7	11,9±0,5	+2
RP -3 № 223	30,2	26,7±1,0	+12
OI -3M-5 № 12	34,1	33,1±1,3	+2
RI -2,4 № 03	41,6	36,1±1,4	+15
RP -3,3 № 71A	14,3	16,0±0,6	−11
R-3,6 № 213	32,7	31,1±1,0	+5
R-3,6 № 216	34,3	32,9±1,1	+4

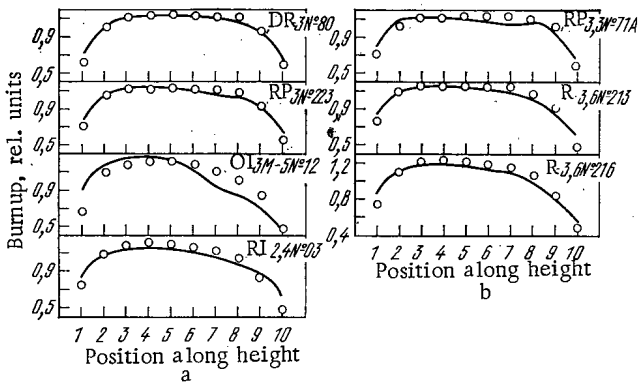

Fig. 3. Calculated (——) and measured (O) distributions of fuel burnup as functions of height along an FEA of a) VVÉR-365; b) VVÉR-440 reactor.

calculating $\overline{W}^n$ it was assumed that it varied only radially with the distance between the axis of the FEA and the axis of the fuel element; the azimuthal dependence was neglected [2]. The error in determining $\overline{W}^n$ was 3-4% for the various FEA.

Figure 3 shows the experimental and calculated distributions of the relative values of the fuel burnup along the height of the FEA examined. The values of the burnup were calculated by using the BIPR-4 and ROR-2 programs [8] at the NVNPP. The relative values of the burnup were obtained by normalizing the calculated and experimental values of the fuel burnup at a given point along the height of the FEA to the calculated or experimental average value of the fuel burnup in the given assembly. Figure 3 shows that for all FEA except OI-3M-5 No. 12 the calculated and experimental values of the burnup agree at all heights except near the ends. At the ends of FEA the difference between the calculated and experimental relative values of the burnup reaches 30% (RI-2,4 No. 3, OI-3-M-5 No. 12, and R-3,6 No. 213) and the calculation systematically overestimates the burnup. The average difference between the calculated and experimental relative values of the burnup at the first and tenth points along the height was 15% for all FEA examined. The difference between the calculated and measured values of the burnup at the ends of FEA is possibly related to the error in calculating the logarithmic derivatives of the slowing-down neutron flux at the fuel-reflector boundary and the deviation of the neutron spectrum from the asymptotic form.

For element OI-3M-5 No. 12 the calculations overestimate the values in the lower part of the FEA, and underestimate them in the upper part. This can be accounted for by the fact that in all three runs the assembly was located adjacent to a reactor power control FEA. In the calculational model it is assumed that the neutron flux in the transition region between the absorber of an assembly of control and safety rods (CSR) and the fueled portion is small in comparison with the neutron flux in the fueled part, and that the 12th group of assemblies of CSR is always at a height of 150 cm during reactor operation at power. Actually the neutron flux in the transition region between the absorber and the fueled part of a CSR assembly is not negligibly small, and in addition the assemblies of the 12-th group of CSR

Declassified and Approved For Release 2013/03/04 : CIA-RDP10-02196R000300010004-7

Declassified and Approved For Release 2013/03/04 : CIA-RDP10-02196R000300010004-7

are gradually withdrawn from the core toward the end of each run. These approximations of the computational model can explain why the calculations underestimate the fuel burnup in the upper part of element OI-3M-5 No. 12 at the seventh, eighth, and ninth points along the height.

Table 2 shows that the deviation of the calculated from the experimental values of the burnup in the FEA examined varies from 2.0 to 13%, and the average difference for the seven FEA is 8%. It should also be noted that for FEA which have been irradiated in three runs (OI-3M-5 No. 12, R-3,6 No. 231, and R-3,6 No. 216) this deviation is appreciable smaller.

Thus, a comparison of the calculated and experimental distributions of fuel burnup in VVÉR-365 and VVÉR-440 FEA showed that at the end portions systematic deviations of the calculated from the measured values reach 30%. In addition, for individual FEA the deviations of the calculated from the experimental values of the average fuel burnup exceed the experimental errors. Therefore, further accumulation of experimental data on the distribution of fission products and fuel burnup over the height and cross section of FEA is necessary for a more detailed check and correction of the programs for calculating fuel burnup.

LITERATURE CITED

1. H. Graber, G. Hofmann, and S. Nagel, Kernenergie, 17, No. 3, 73 (1974).
2. H. Mehner, H. Graber, and G. Hofmann, Kernenergie, 20, No. 8, 242 (1977).
3. L. I. Golubev et al., At. Energ., 40, No. 3, 207 (1976).
4. L. Golubev and V. Subenko, Kernenergie, 20, No. 7, 206 (1977).
5. V. P. Maiorov, M. A. Razuvaeva, and B. A. Bibichev, Preprint Rad. Inst. RI-61, Leningrad (1977).
6. V. Ya. Gabeskiriya et al., At. Energ., 43, No. 4, 278 (1977).
7. M. Meek and B. Rider, Compilation of Fission Product Yields, NEDO-12154-1 (1974).
8. E. D. Belyaeva and D. M. Petrunin, Preprint IAÉ-2093, Moscow (1971).

TRITIUM CONTENT IN WATER SYSTEMS OF A REACTOR OF THE FIFTH UNIT OF THE NOVOVORONEZH NUCLEAR POWER PLANT

V. P. Kruglov, V. M. Ilyasov,
I. G. Golubchikova, B. N. Mekhedov,
L. N. Sukhotin, S. V. Popov,
V. M. Arkhipkin, and A. G. Babenko

UDC 621.039.524.44

The sources of tritium in the VVÉR-1000 reactor are reactions of the ternary fission of fuel, reactions with fission products and with ^{10}B flowing into the coolant and control devices, and reactions with deuterium and the lithium contaminant entering the coolant with the chemical reagents KOH and H_3BO_3 [1, 2].

Table 1 lists the amounts of tritium formed, calculated by using known parameters of the VVÉR-1000 reactor [3] and data on the yields of tritium, ^3He, ^6He, and ^6Li per uranium fission [4]. The rate of formation of tritium was calculated by using the values of the thermal neutron flux $\overline{\varphi}_T$ and the fast flux $\int_0^\infty \varphi(E)\,dE$ averaged over the volume of the reactor. The fact that the fast neutron spectrum in the VVÉR core is close to the ^{235}U fission spectrum [5] was taken into account. In this case the neutron fluxes can be found from the following relations:

$$N_5^5 \sigma_f \overline{\varphi}_T = W n_5; \tag{1}$$

Translated from Atomnaya Énergiya, Vol. 53, No. 4, pp. 225-227, October, 1982. Original article submitted January 11, 1982.

 © 1983 Plenum Publishing Corporation

Declassified and Approved For Release 2013/03/04 : CIA-RDP10-02196R000300010004-7

Declassified and Approved For Release 2013/03/04 : CIA-RDP10-02196R000300010004-7

TABLE 1. Formation of Tritium in the VVÉR-1000 Reactor During a 300-Day Run

Source of tritium formation	Nuclear reaction	Amt. of tritium	
		Bq	%
Nuclear fuel	Ternary fission of ^{235}U	$3{,}56 \cdot 10^{14}$	75,7
	Ternary fission of ^{238}U	$3{,}59 \cdot 10^{13}$	7,6
	$^{3}He\,(n,\ p)\,^{3}H$	$3{,}33 \cdot 10^{11}$	0,06
	^{6}He, ^{6}Li	$1{,}81 \cdot 10^{13}$	3,9
	$(^{6}He \xrightarrow[0{,}797\,s]{\beta^-} {}^{6}Li)$		
Chemical reagents in coolant	$^{10}B\,(n,\ 2\alpha)\,^{3}H$	$1{,}89 \cdot 10^{13}$	4,0
	$^{7}Li\,(n,\ \alpha n)\,^{3}H$	$3{,}7 \cdot 10^{10}$ *	0,01
	$^{6}Li\,(n,\ \alpha)\,^{3}H$	$4{,}07 \cdot 10^{13}$ *	8,7
Natural deuterium in coolant	$^{2}H\,(n,\ \gamma)\,^{3}H$	$1{,}48 \cdot 10^{11}$	0,03

*The experimental value of 0.2 mg/liter for the concentration of lithium in the primary loop was used in the calculation.

$$N_8^8\bar{\sigma}_f \int_0^\infty \varphi(E)\,dE = Wn_8, \tag{2}$$

where N_5 and N_8 are, respectively, the numbers of ^{235}U and ^{238}U isotopes in the reactor; $^{5}\sigma_f$ is the ^{235}U thermal neutron fission cross section; $^{8}\bar{\sigma}_f$, the ^{238}U fission cross section averaged over the ^{235}U fission spectrum; W, the thermal power of the reactor; n_5 and n_8, the numbers of ^{235}U and ^{238}U fissions necessary to obtain a unit of energy; n_5 and n_8, were calculated from the equations

$$\varepsilon = \frac{n_8}{n_5}\frac{1}{\nu_5}(\nu_8 - 1 - \alpha) + 1; \tag{3}$$

$$1 = n_5E_5 + n_8E_8. \tag{4}$$

Equation (3) is taken from [6]. The numerical value of the fast fission factor ε was found by the method of [7]; ν_5 and ν_8 are the average numbers of neutrons per fission of ^{235}U and ^{238}U, respectively; α is the ratio of the effective radiative capture cross section to the ^{238}U fission cross section; E_5 and E_8 are the energies liberated per fission of ^{235}U and ^{238}U. The formation of tritium in the reactions $^{10}B(n,\ 2\alpha)^{3}H$ and $^{2}H(n,\ \gamma)^{3}H$ was calculated by the method of [1], using 5.5×10^{-2} day^{-1} for the decontamination factor of the coolant from deuterium as a result of leakage, which corresponds to a coolant leakage rate of 20 m^3/day. The amount of tritium formed in reactions with lithium was found for lithium of natural isotopic composition with an average concentration of 0.2 mg/liter in the coolant of the primary loop.

This permits an upper estimate of the tritium yield from ^{6}Li, since the relative content of ^{6}Li is decreased during reactor operation as a result of the formation of ^{7}Li in the reaction $^{10}B(n,\ \alpha)^{7}Li$ and the burnup of ^{6}Li [8].

Table 1 shows that 87.3% of the total amount of tritium formed in the VVÉR-1000 reactor comes from the fuel elements, and the remainder mainly from boric acid (4%) and the lithium contaminant (8.7%). A study of the dynamics of the tritium content in the water system of the first unit of the Novovoronezh nuclear power plant (NVNPP) in which there is only rod control of power i.e., no formation of ^{3}H from B and Li, permitted an estimate of the tritium escape from fuel elements into the coolant; 0.12% of the tritium formed in the ternary fission of uranium, which amounts to $\sim 4.8 \times 10^{11}$ Bq per 300 days for the fifth unit. A comparison of

Declassified and Approved For Release 2013/03/04 : CIA-RDP10-02196R000300010004-7

Declassified and Approved For Release 2013/03/04 : CIA-RDP10-02196R000300010004-7

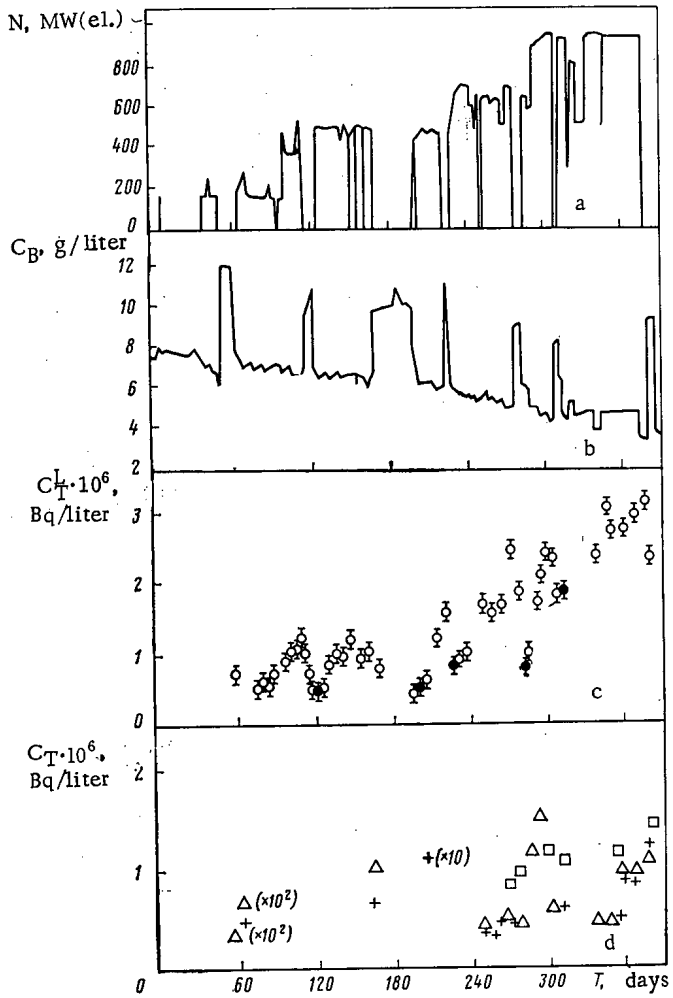

Fig. 1. Time dependence of a) reactor power; b) H_3BO_3 concentration; c) tritium concentration in primary loop [● calculated with Eq. (5)]; d) tritium concentration in water exchange system tanks: +, Δ, □, tritium concentration in tanks B9 and B10 of pure condensate, and in tanks of H_3BO_3 solution averaged over tanks B 8/1, B 8/2, and B 8/3.

this value with the amount of tritium formed from boron and lithium in the coolant (Table 1) shows that boric acid and the lithium contaminant make the main contribution to the tritium in the water systems of the reactor.

From the moment of startup of the fifth unit of the NVNPP with VVÉR-1000 reactors the concentration of tritium in the coolant of the primary loop and in the tanks of the water supply system was measured systematically by a liquid scintillation method, using an SBS-2 set-up. Figure 1 shows data on the power of the fifth unit, the H_3BO_3 concentration, the tritium concentration in the primary loop and in the tanks of the water supply system during the period from May 1980 to May 1981. The frequent unloading of the unit was necessitated by dynamical tests and equipment repair.

Figure 1 shows that during reactor operation at nominal power the tritium content in the primary loop increased to 4.1×10^6 Bq, and varied considerably with time. This variation correlated positively with the power level and negatively with the boric acid concentration during normal reactor shutdowns. This can be explained by the fact that during shutdown part of the coolant is replaced from tanks of fresh boric acid solution, while during power production water lost from the primary loop is replaced from tanks of the makeup system. This process can be described by a system of first degree differential equations for the tritium concentration in the primary loop, the tanks of boric acid solution, and the pure condensate tanks [1]. The solution of this system of equations can be written in the form

$$C_T(\tau') = \left\{[C_T(0) - C_T^b]\frac{C_b^b - C_b^L(\tau)}{C_b^b - C_b^L(0)} + C_T^b - C_T^M\right\}\frac{C_b^L(\tau')}{C_b^L(\tau)} + C_T^M, \quad (5)$$

where $C_T^L(0)$ and $C_B^L(0)$ are the tritium and H_3BO_3 concentrations in the coolant of the primary loop at the instant of reactor shutdown, C_T^B and C_B^B are the tritium and H_3BO_3 concentrations

Declassified and Approved For Release 2013/03/04 : CIA-RDP10-02196R000300010004-7

Declassified and Approved For Release 2013/03/04 : CIA-RDP10-02196R000300010004-7

in the boric acid solution tank, $C_B^L(\tau)$ is the maximum concentration of H_3BO_3 in the primary loop during shutdown; $C_B^L(\tau')$ is the H_3BO_3 concentration in the primary loop at the instant the reactor starts producing power, and C_T^M is the tritium concentration in the makeup water.

The rate of water exchange during reactor shutdown was calculated from the change in the boric acid concentration in the primary loop. The results of the calculations of the tritium concentration during water exchange are in good agreement with experimental data (Fig. 1c). This procedure permits a prediction of the change in tritium concentration in the coolant during normal reactor shutdowns.

Measurements of the tritium concentration in the water supply system show high values in the pure condensate tanks $(0.37-1.5) \times 10^6$ Bq/liter, in the boric acid solution tanks $(0.74-1.5) \times 10^6$ Bq/liter, in the control tanks 7.4×10^5 Bq/liter, and in the liquid wastes settling tanks $(3.7-7.4) \times 10^5$ Bq/liter (Fig. 1d). Thus, after a year of operation of the VVER-1000 reactor at power, the tritium concentration in the coolant reached a level of 4.1×10^6 Bq/liter. The appreciable time variations of the tritium concentration can be accounted for by the exchange of water between the primary loop, the boric acid solution tanks, and the pure condensate tanks. The rapid water exchange while the reactor is developing power, and the resulting rapid spread of tritium through the water supply system, shows the necessity of developing measures to localize the tritium in order to improve the radiation environment and to solve ecological problems.

LITERATURE CITED

1. L. I. Golubev, At. Energ., 46, No. 2, 79 (1979).
2. K. Langeker and H. Graupe, Kernenergie, 15, No. 5, 165 (1972).
3. F. Ya. Ovchinnikov et al., Operating Conditions of Water-Moderated/Water-Cooled Power Reactors [in Russian], Atomizdat, Moscow (1979).
4. V. M. Gorbachev et al., in: Interaction of Radiation with Heavy Nuclei and Nuclear Fission [in Russian], Atomizdat, Moscow (1976), p. 353.
5. L. I. Golubev and S. S. Lomakin, Teploenergetika, No. 10, 57 (1971).
6. Yu. B. Novikov et al., At. Energ., 43, No. 4, 240 (1977).
7. G. Ya. Rumyantsev, Calculation of a Thermal Reactor [in Russian], Atomizdat, Moscow (1967).
8. L. I. Golubev et al., At. Energ., 45, No. 5, 362 (1978).

Declassified and Approved For Release 2013/03/04 : CIA-RDP10-02196R000300010004-7

Declassified and Approved For Release 2013/03/04 : CIA-RDP10-02196R000300010004-7

PROBLEM OF PREDICTING THE RADIATION CONDITIONS IN AN ATOMIC POWER STATION

A. M. Luzhnov, V. P. Romanov,
R. F. Tagi-Zade, and S. G. Tsypin

UDC 621.039-78

The authors of [1-3] have described a method of calculating the dose rate of the γ-radiation from heterogeneous cylindrical and spherical sources. The reliability of the results obtained was assessed in comparisons with calculations made with the Monte Carlo method. In predicting the radiation conditions in an atomic power station with the aid of the LUCh-1 and LUCh-2 programs using the above technique, a computational model must be designed, i.e., the radioactive components of the equipment must be represented by a set of cylindrical and spherical sources. The extent to which a well-designed model reflects reality can be assessed by comparing the calculations with experimental results.

The present article reports on examples of using the method in problems of practical importance. Computational models are described. The results of the calculations are compared with experimental results.

Predicting the Radiation Conditions in the Instrument Section of the Atomic Power Station Block of the VVÉR-1000 Reactor. During the start-up of the energy generation of the fifth block of the AVAÉS power station (atomic power station block with the VVÉR-1000 reactor), the distribution of the γ-radiation exposure dose rate in the steam generator and the tube duct corridor was obtained. The measurements were made with a DRGZ-03 dosimeter.

The main radiation of the coolant stems from the radioactive ^{16}N nuclide whose concentration in the coolant is directly proportional to the thermal power of the reactor. When the reactor is operated at low power (the measurements were made with about 1% of the power), power fluctuations can occur and the fluctuations imply that changes in the distribution of the specific activity of the coolant in the circuit occur in the course of time. The specific activity of the coolant is one of the basic initial data for the calculations. A comparison with calculations is possible only when the experimental data correspond to a known activity distribution of the coolant in the circuit.

The change in the specific activity of the coolant within the second main circulation loop (ML-2), in which all the measurements were made, was checked with the aid of a loop monitor [4]. The loop monitor continually determined changes in the specific activity of the coolant. This information then made it possible to analyze the experimental data.

All experimental points were divided into groups each of which is characterized by a certain direction l_n in space (n = 1-4; see Figs. 1 and 2). Some of the experimental dependencies obtained at various heights h reckoned from the 23.10 mark correspond to each direction l_1, l_2, and l_3.

Several series of measurements were made for specific l_n and h values. The time required for making one series of measurements did not exceed 1-2 min. By using the monitor, the measurements were started at the moment in which the specific activity of the coolant in ML-2 had become stable. Furthermore, before and after each measurement series the exposure dose rate at the reference point P_0 was checked with the DRGZ-03 dosimeter. The reference point P_0 was situated on the surface of the thermal insulation of the Du-850 tube duct (see Fig. 1).

When the results of the measurements were evaluated, series for which the initial and final dose rate values at the point P_0 differed by more than 10% were rejected. In this fashion each series of measurements was set in corespondence to a certain value of the dose rate at the point P_0. When the initial and final values differed by less than 10%, the average value was employed. It was therefore possible to normalized all the series to a single dose rate of $2.2 \cdot 10^{-2}$ μA/kg at the point P_0 (this value will be denoted by $\dot{X}_e$). This is

Translated from Atomnaya Énergiya, Vol. 53, No. 4, pp. 227-230, October, 1982. Original article submitted January 29, 1982; revision submitted April 6, 1982.

0038-531X/82/5304-0677$07.50 © 1983 Plenum Publishing Corporation

Declassified and Approved For Release 2013/03/04 : CIA-RDP10-02196R000300010004-7

Declassified and Approved For Release 2013/03/04 : CIA-RDP10-02196R000300010004-7

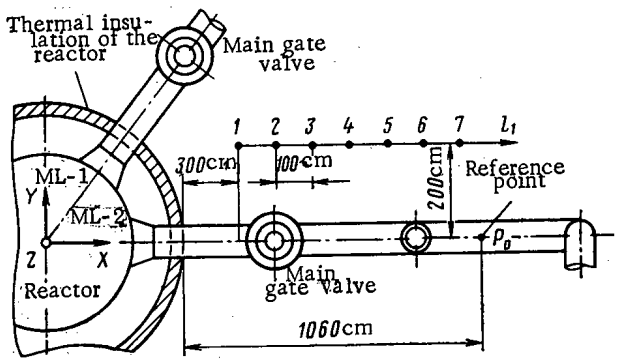

Fig. 1

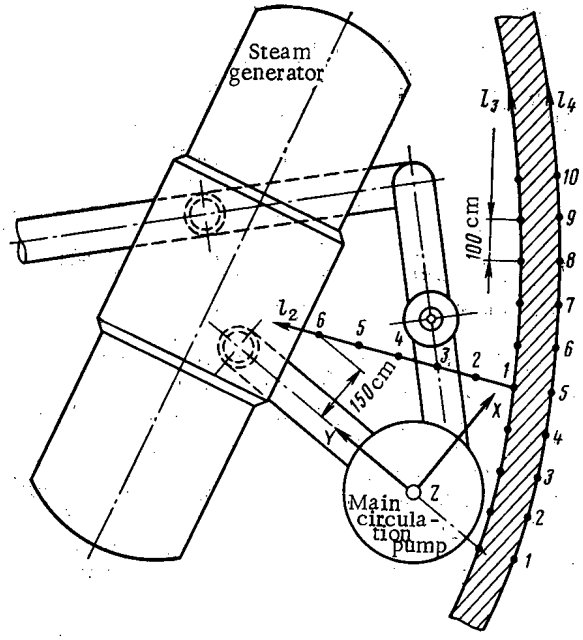

Fig. 2

Fig. 1. Scheme of the measurements in the region of the reactor.

Fig. 2. Scheme of the measurements in the main circulation pump.

equivalent to reducing all experimental data to a single distribution of the specific activity in the ML-2. After normalization and after averaging over the results of the measurements at identical points and calculating the statistical error, final distributions are shown in Figs. 3 and 4 were obtained.

The specific-activity distribution in ML-2, which corresponds to the experimental data shown in Figs. 3 and 4 was determined with $\dot{X}_e$, i.e., the dose rate value at the reference point. The position of this point makes it possible to confirm that the dose rate at the point is produced entirely by the neighboring section of the Du-850 tube duct. The other points are either far away or their radiation is shielded by some construction elements. It was therefore possible to use the PEGAS-4 program [5], which executes the Monte Carlo technique in cylindrical geometry, to calculate $\dot{X}_e$, i.e., the dose rate value at the point P_0 for the case in which the specific activity of the coolant (Q_p) in the adjacent section of the tube duct is 1 Bq/cm³. Thereafter the formula

$$Q_0 = Q_p \dot{X}_e / \dot{X}_p$$

was used to determine the specific-activity value of the coolant in the Du-850 tube duct section adjacent to the point P_0. This specific-activity value corresponds to the dose rate $\dot{X}_e$ at this point:

$$Q_0 = (3.5 \pm 0.5) \cdot 10^4 \text{ Bq/cm}^3.$$

With this Q_0 value, with the known coolant flow of 5.28 m³/sec, and with the known coolant dwell time of 2.36 sec in the steam generator, the specific activity of coolant in any section of ML-2 can be assessed.

In order to calculate the exposure dose rate distribution in the directions l_1 (reactor region) and l_2, l_3, and l_4 (main circulation pump region), various models consisting of ten and nine cylindrical sources, respectively, were devised. The equipment not only of the main circulating loop ML-2 but also of the circulating loop ML-1 was modeled for the calculations pertaining to the reactor region. The specific activity of the sources modeling the ML-1 section was assumed equal to the activity of the sources modeling the corresponding ML-2

Declassified and Approved For Release 2013/03/04 : CIA-RDP10-02196R000300010004-7

Declassified and Approved For Release 2013/03/04 : CIA-RDP10-02196R000300010004-7

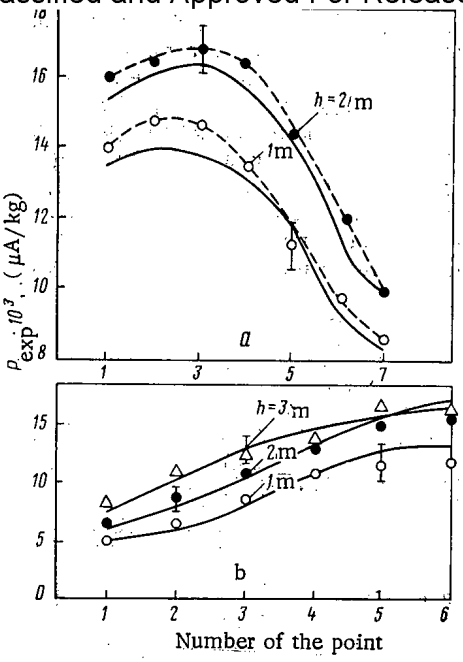

Fig. 3

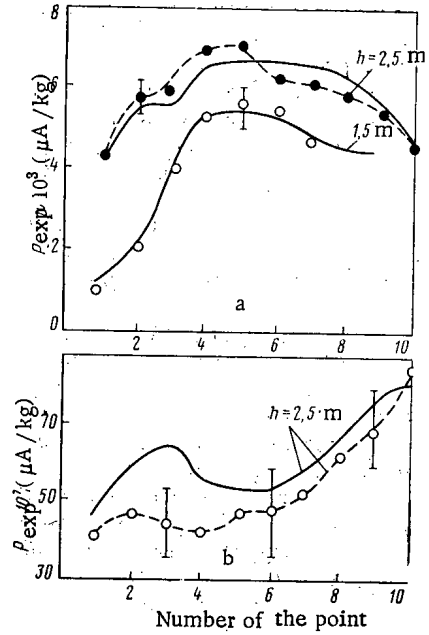

Fig. 4

Fig. 3. Distribution of the exposure dose rate in (a) l_1 direction and (b) l_2 direction: △, ○, and ● refer to the experiment; —— refers to the calculations.

Fig. 4. Distribution of the exposure dose rate in (a) l_3 direction and (b) l_4 direction: ○ and ● refer to the experiment; —— refers to the calculations.

TABLE 1. Activity of the Deposits on Steam Generator Collectors before Deactivation

Nuclide	Average energy (MeV) of the γ radiation	Specific activity Q_5 (10^{-7} Ci*/cm^2)	Nuclide	Average energy (MeV) of the γ radiation	Specific activity Q_5 (10^{-7} Ci*/cm^2)
^{60}Co	1,25	1,0	^{110m}Ag	0,86	0,22
^{140}La	1,1	0,58	^{65}Zn	0,7	0,35
^{54}Mn	0,842	1,5	^{99}Mo	0,21	1,7
^{58}Co	0,5	3,1	^{103}Ru	0,46	0,83
^{95}Zr	0,73	1,5	^{51}Cr	0,125	1,5
^{59}Fe	1,2	0,36			

*1 Ci = $3.700 \cdot 10^{10}$ Bq.

sections. All geometrical parameters of the models were determined from the assembly drawings.

Having gathered all the initial data, the LUCh-2 program was used to calculate the exposure dose rate distribution in all directions under consideration from points which coincided with the experimental points. Figures 3 and 4 show the results of calculations. Obviously, for all directions before the shield (l_1, l_2, l_3) and also for the direction behind the shield (l_4) the calculated curves repeat in their form the experimental curves and the exposure dose rate values coincide at almost all points with the experimental data within the error limits.

Predicting the Radiation Conditions in Inspection and Maintenance Work on Steam Generators of Atomic Power Stations with the VVÉR Reactors. The steam generators are one of the main sources of external γ radiation for atomic power station personnel performing inspection and maintenance work [6]. In Russian steam generators used in the atomic power stations with serial VVÉR-440 reactors, the major portion of the work is made from the side of the second circuit in the region of the collectors (inside the steam generator). The authors of [7]

Declassified and Approved For Release 2013/03/04 : CIA-RDP10-02196R000300010004-7

Declassified and Approved For Release 2013/03/04 : CIA-RDP10-02196R000300010004-7

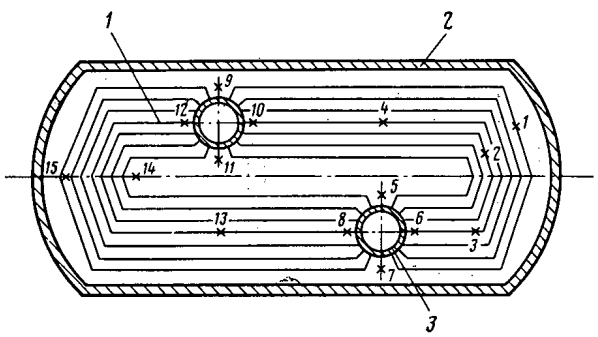

Fig. 5

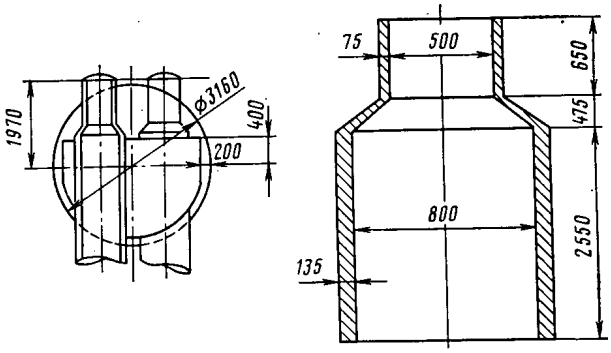

Fig. 6

Fig. 5. Schematic cut along the horizontal axis of the steam generator: 1) tube system; 2) housing; 3) collector (the asterisks denote the experimental points).

Fig. 6. Geometrical dimensions of the steam generator.

have attempted to predict the dose rate in inspection and maintenance work on the steam generator in the third block of the NVAÉS atomic power station: The experimental dose rate values near the outer surface of the steam generator housing and at inspection points of the inner surface were stated; a comparison was made with calculations performed with the ray-analysis technique. But the authors could make the calculations only for the simplest geometrical configurations, namely for points located in the collectors near the upper part of the steam generator housing. No calculations were made for points inside the steam generator on the side of the second circuit, i.e., where most of the inspection and maintenance work is done.

The authors of the present work had to consider the following problems:

1. Based on the experimental data, show the possible use of the ray-analysis technique for predicting the radiation conditions ruling during inspection and maintenance work on the steam generator.

2. Assess the importance of various sources for the development of the γ-radiation field inside the steam generator.

3. Assess the efficiency of various measures taken to improve the irradiation conditions.

All experimental data on the positions and dose rate values were obtained on one of the steam generators of the first block of the Kola Atomic Power Station while the block was shut down.

Figure 5 depicts schematically the steam generator used in the atomic power station with the VVÉR-440 reactor. The figure also shows the main points at which people are during maintenance work. The dose rate values at point 1-15 are 50, 200, 300, 150, 150, 100, 150, 100, 200, 350, 200, 150, 150, 200, and 150 μR/sec, respectively ($1\ R = 2.58 \cdot 10^{-4}$ C/kg). The points are situated 10 cm above the level of the tube system. Two collectors in the tube system are the γ-radiation sources. During operation radioactive deposits accumulate on the inner surfaces of those elements. Data on the nuclide composition of the radioactive deposits are listed in Table 1.

The real geometry of the steam generator is shown in Fig. 6. Additional data for the calculation: volume fraction of the steel in the space occupied by the tube system — 0.07; area of the inner surface of the tubes — $2.17 \cdot 10^7$ cm^2; and total volume occupied by the tube system — $4.66 \cdot 10^7$ cm^3. The collectors and the tube system of the steam generator are surface sources. Only volume sources can be introduced in the LUCh-2 program which we employed. Therefore, the surface sources were modeled by volume sources with the same total activity. The conversion of the specific activity was made with the formula $Q_V = (S/V)Q_S$. The Q_S values are listed in Table 1 (these values were experimentally obtained for the collectors; the same values were assumed in the tube system).

All active components of the steam generator are represented by five cylindrical sources. Each collector is represented by two sources as indicated in Fig. 7. The outer cylinder is introduced to account for the shielding of the lower collector portion by the tube system. The mutual positions of the sources are indicated in Fig. 8.

Declassified and Approved For Release 2013/03/04 : CIA-RDP10-02196R000300010004-7

Declassified and Approved For Release 2013/03/04 : CIA-RDP10-02196R000300010004-7

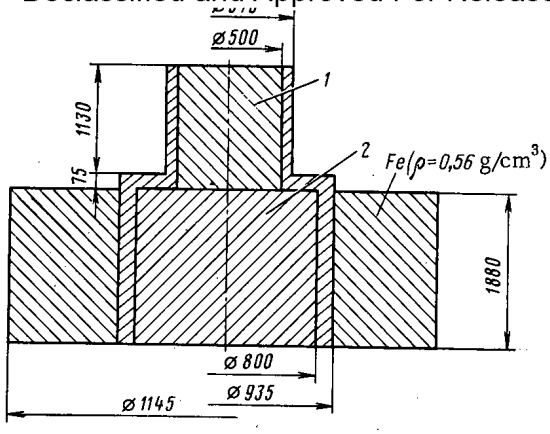

Fig. 7

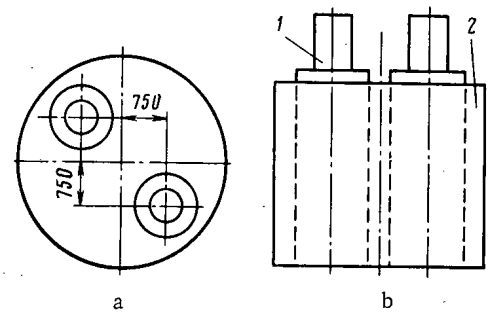

Fig. 8

Fig. 7. Geometry of the sources used to model the collector of the steam generator.

Fig. 8. Mutual positions of the sources in the calculations: a) top view; b) side view (the cylinders modeling the screening of the collectors (1) by the tube system (2) are not shown in the drawing).

The results of the calculation coincide with the experimental data within the error limits (30-40%). It can be concluded from the comparison that the proposed calculation model of the steam generator is fully adequate for predicting the radiation conditions. An analysis of the computational data shows that the total contribution of the two collectors to the dose rate does not exceed 0.1%. This implies that in all subsequent calculations only the tube system should be considered. This makes it possible to obtain correct results on the basis of a very simple model of the steam generator.

From the viewpoint of practical application it is clear that an improvement in the radiation conditions can be reached by attenuating the radiation from the tube system. Calculations have shown that in a steam generator filled with water to the level of the tube system the dose rate is reduced by a factor of 2.6. When, in addition, a 0.5-cm-thick lead shield is put onto the tube system, the initial dose rate is reduced by a factor of 5.4; when the sheet thickness is 1 cm, the reduction is by a factor of 8.7. Quantitative estimates of the influence which various factors have upon the radiation conditions are a very valuable result because the resulting data are not related to the absolute value of the specific activity of the deposits.

LITERATURE CITED

1. A. M. Luzhnov and S. G. Tsypin, in: Trans. of the All-Union Inst. of Heat Engineering [in Russian], No. 26 (1979), p. 50.
2. A. M. Luzhnov, R. F. Tagi-Zade, and S. G. Tsypin, in: Trans. of the All-Union Inst. of Heat Engineering [in Russian], No. 26 (1979), p. 57.
3. A. M. Luzhnov, R. F. Tagi-Zade, and S. G. Tsypin, in: Trans. of the All-Union Inst. of Heat Engineering [in Russian], No. 26 (1979), p. 110.
4. A. A. Alekseev et al., in: Abstracts of the Reports of the 3rd All-Union Conf. on Shielding from Ionizing Radiations [in Russian], Tbilisi State Univ. (1981), p. 115.
5. É. B. Brodkin, A. N. Kozhevnikov, and A. V. Khrustalev, in: Trans. of the All-Union Inst. of Heat Engineering [in Russian], No. 26 (1979), p. 30.
6. V. N. Sedov, M. A. Baranov, and V. N. Vlasenko, in: Reports on the Joint Anglo-Russian Symposium "Exploitation of Atomic Power Stations," [in Russian], Izd. Vsesoyuz. Teplotekh. Inst., Moscow (1977), p. 27.
7. M. A. Baranov et al., in: Radiation Safety and Shielding of Atomic Power Stations [in Russian], No. 2, Atomizdat, Moscow (1976), p. 5.

Declassified and Approved For Release 2013/03/04 : CIA-RDP10-02196R000300010004-7

Declassified and Approved For Release 2013/03/04 : CIA-RDP10-02196R000300010004-7

SMALL STEAM LEAKS INTO SODIUM IN A REVERSE STEAM GENERATOR

F. A. Kozlov, G. P. Sergeev,
L. G. Volchkov, A. R. Sednev,
V. M. Makarov, and B. I. Tonov

UDC 621.039.526

The processes accompanying small leaks of water into sodium for a reverse steam generator,* as shown in [1], can greatly differ from similar phenomena for a forward steam generator. In particular, due to the characteristics of the hydrodynamic state arising in a defective tube in a reverse steam generator, when a water leak appears into the sodium the rate of damage to the structural materials of the tube both in the immediate vicinity of the defect and in the zone opposite to the location of the leak can decrease. However, the influence of such factors as the location of the leak, type of structural material, and the diameter of the steam generator tubes on corrosive effects were not investigated in [1]. We conducted experiments to study these problems and the results are reported in this paper.

A model of a reverse steam generator is shown in Fig. 1. The working tubes with dimensions 15 × 2, 32 × 3.5, and 48 × 4 mm (the first number indicates the diameter and the second indicates the thickness of the wall) had protective casings. The ring-shaped gaps between the tubes and casings were under an argon pressure of 5.0 MPa during the experiments. In the initial variant, the entire model was made out of 12Kh18N10T steel. After the model was tested for the second stage of the experiments, the stainless steel tubes with diameters of 15 and 32 mm were replaced by tubes made of 10Kh2M steel with dimensions 16 × 2.5 and 33 × 3 mm. Magnetic flow meters were located at the bottom of the working tubes. We monitored the

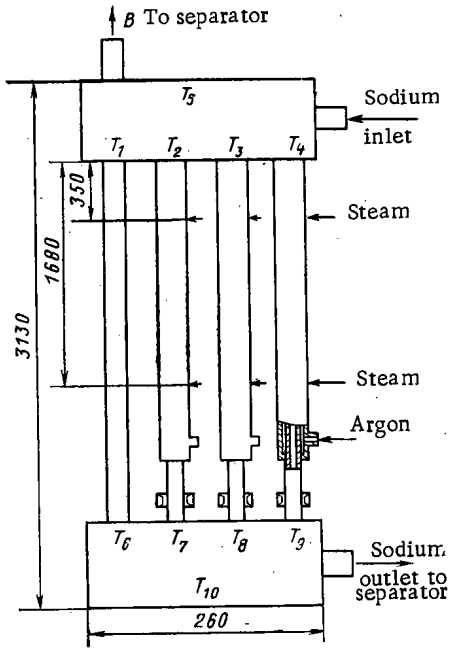

Fig. 1. Experimental section: model of a reverse steam generator.

*In a reverse steam generator, sodium flows along the tubes and water flows in the space between the tubes.

Translated from Atomnaya Énergiya, Vol. 53, No. 4, pp. 231-234, October, 1982. Original article submitted December 30, 1981.

 0038-531X/82/5304-0682$07.50 © 1983 Plenum Publishing Corporation

Declassified and Approved For Release 2013/03/04 : CIA-RDP10-02196R000300010004-7

Declassified and Approved For Release 2013/03/04 : CIA-RDP10-02196R000300010004-7

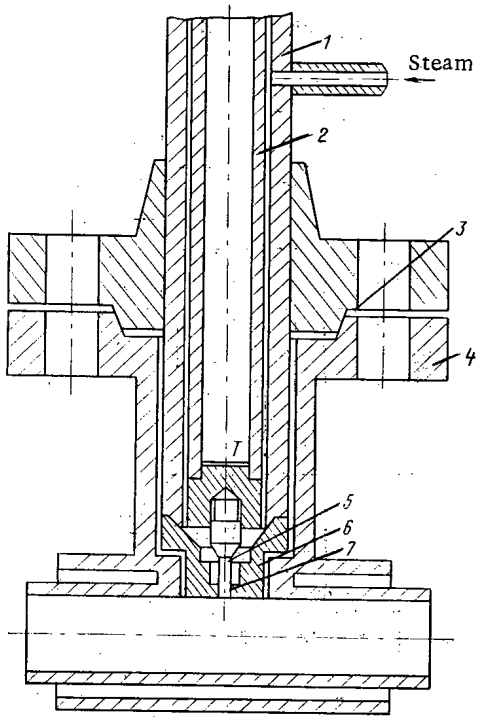

Fig. 2. Steam injection unit: 1) housing; 2) steam; 3) seal; 4) pipe flange; 5) valve; 6) seat; 7) valve sealing flange.

sodium temperature with thermocouples at the inlet and outlet of each tube and at the centers of the upper and lower collectors of the section. Leak simulators could be placed on the working pipes at a distance of 350 and 1680 mm from the upper collector. The construction of the lead simulator is shown in Fig. 2. Its replaceable parts (seat and valve) were made of the same material as the working tube on which the leak simulator was located. The thickness of the seat of the simulator equals the thickness of the wall of this working tube. A longitudinal groove, whose cross section had the shape of an equilateral triangle, was cut on the pivot of the valve. This artificial defect served to create the initial steam leak into the sodium, the spontaneous development of which we investigated during the experiment.

During the experiments, we continuously recorded: the temperature in the upper and lower collector of the model; the temperature at the inlet and outlet of the working tube into which steam was injected; the sodium flow rate through the model and the working tube with the leak simulator; the steam temperature in the leak simulator; the amount of steam introduced into the model and its flow rate. We usually terminated an experiment as soon as the steam leak into the working tube of the model increased spontaneously (>1 g/sec). In several cases, in order to obtain data on the further evolution of the lead after this stage and its action on the opppsite wall of the tube, we continued the experiment for some time under conditions such that the leak exceeded 1 g/sec. The conditions and the results of the experiments on the model of the reverse steam generator are presented in Table 1 and in Figs. 3-5. It should be noted that the experiments were performed in the absence of heat extraction from the working tubes of the models.

In the model used in the experiments, when the leak through the upper simulator accompanied the formation of a steam-hydrogen bubble in the working tube and cessation of the sodium flow in it, the lead was located under the sodium level and not in the gas bubble. In the experiments, the minimum size of the steam leak leading to cessation of sodium flow in the 16 × 2.5-mm working pipe constituted $\sim 2.10^{-2}$ g/sec.

In all the experiments, with the exception of experiment 10, we observed spontaneous development of the steam leak independent of the initial leak, its location, and the diameter of the working tube. During the spontaneous process, two stages can be distinguished. At the first stage, the changes in the size of the leak compared to the initial value were not

Declassified and Approved For Release 2013/03/04 : CIA-RDP10-02196R000300010004-7

Declassified and Approved For Release 2013/03/04 : CIA-RDP10-02196R000300010004-7

TABLE 1. Conditions and Results of Experiments (in all experiments the sodium and steam temperature was 450°C; the pressure of the injected steam was 5.0 MPa)

Parameters	Number of experiments									
	1	2	3	4	5	6	7	8	9	10
	12Kh18N10T					10Kh2M				
Steam flow, g/sec initial	0,002	0,006	0,006	0,023	0,009	0,008	0,32	0,002	0,008	0,9
maximum	0,22	1,1	2,95	0,37	0,32	1,64	3,9	6,61	11,5	0,9
First stage of expt.:										
duration, sec	1300	1356	3240	1805	1825	217	53	3090	828	—
amount of water injected, g	8,2	28	31	52	43	14	17	23	12	—
average size of leak, g/sec	0,006	0,0206	0,0097	0,029	0,023	0,064	0,32	0,0075	0,015	—
Total duration of exp., sec	9480	2220	3960	2040	2200	240	148	3240	2520	2370
Amt. of water injected over time of exp., g	1052	1005	920	142	145	49	388	678	2025	758
Sizes of water leaks at end of exp., g/sec	0,2	1,2	0,1	0,4	0,8	1,6	3,9	6,6	11,5	0,1
Wall thickness of leak simulator, mm	3,0	3,0	4,5	3,5	3,5	2,0	2,5	2,5	3,0	2,5
Tube diameter and thickness, mm	15×2,5	32×3,5	32×3,5	48×4	48×4	16×2,5	16×2,5	33×3	33×3	16×2,5
Location of leak	Top	Bottom	Top	Top	Bottom	Bottom	Bottom		Bottom	
Working-tube condition after expt	Tube bottom plugged with oxides	No changes		Upper thermocouple malfunctioned	Bottom thermocouple malfunctioned	No changes	Tube burn-through		Tube at inlet collector crumpled	

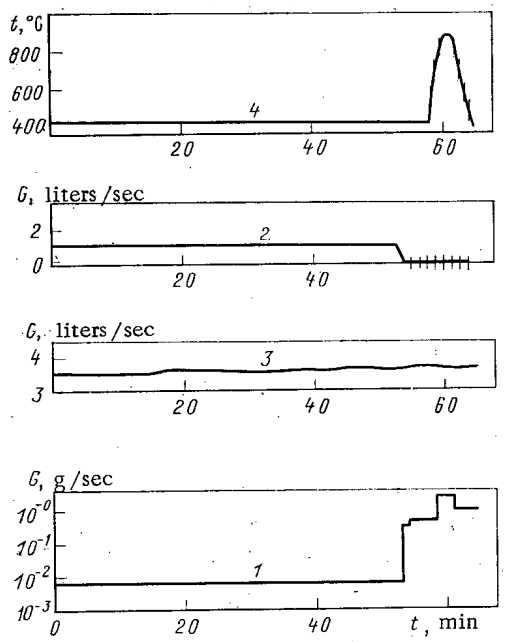

Fig. 3. Parameters of experiment 3: 1) steam flow rate, g/sec; 2, 3) rate of sodium flow through the working tube and through the section, liters/sec; 4) sodium temperature at the inlet to the working tube, °C.

sharp and were small. At the second stage, the leak increased rapidly and exceeded the initial level by more than two orders of magnitude (see Fig. 3). The first stage is characterized by a very limited (⩽50 g) total amount of steam entering the working tube of the experimental model. At the same time, the experiments showed that that total amount of steam at the second stage for leaks near the upper tube plate can exceed 10^3 g without built-up damage to the wall of the working tube, made of 10Kh2M or 12Kh18N10T steel, opposite the location of the leak.

The possibility of relatively rapid burn-through (at the second stage of spontaneous leak development) of the tube opposite the location of the lead was established in experi-

Declassified and Approved For Release 2013/03/04 : CIA-RDP10-02196R000300010004-7

Declassified and Approved For Release 2013/03/04 : CIA-RDP10-02196R000300010004-7

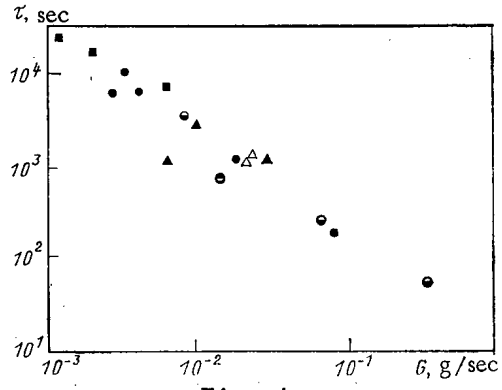

Fig. 4

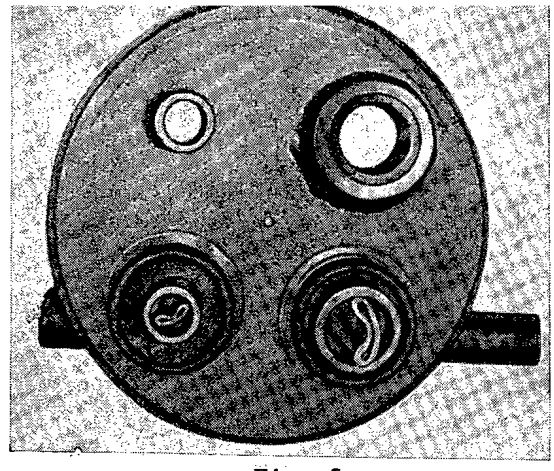

Fig. 5

Fig. 4. Time of spontaneous development of a water (steam) leak in sodium in the forward and reverse steam generator at a sodium temperature of 450°C and tube wall thickness 2.5 mm. For steam leaks according to data in Table 1: ◒, ◓) 10Kh2M, leak at the top and bottom; △, ▲) 12Kh18N10T, leak at the top and bottom, for water leaks in the forward steam generator according to data in [2]: ●) 10Kh2M; ■) 12Kh18N10T.

Fig. 5. View of the tube plate of the upper chamber of the section after the pipes were cut off.

ments 7 and 8 with steam leaks in the lower part of the working tube. In these experiments, the duration of the second stage before the complete damage to the opposite wall constituted 95 and 150 sec, respectively.

During the course of experiment 10, lasting for ∿0.66 h, the leak gradually decreased from the starting level of 0.9 g/sec approximately to 0.12 g/sec. The total amount of steam, introduced through the leak simulator in experiment 10, was ∿760 g, i.e., it was greater than in experiments 7 and 8 up to the time of burn-through of the tube (∿390 and ∿680 g, respectively). The depth of the damage to the wall of the 16 × 2.5-mm 10Kh2M steel working tube in this experiment was 1.25 mm. The wall of the 33 × 3-mm 10Kh2M steel working tube also did not burn through in experiment 9, in which the total amount of steam introduced was maximum: $\sim 2 \cdot 10^3$ g. The depth of the damage to the wall of the tube in this experiment was ∿1.2 mm. During the examination following experiments 9 and 10, it was found that in the upper part, the working tubes are crumpled on sections with length 300 and 150 mm, respectively, immediately adjacent to the upper pipe plate (see Fig. 5). The erosion of material over the thickness of the tube (maximum thinning ∿1.2 mm) is noted in the crumpled part of the 33 × 3-mm tube.

The indications of the magnetic flow meter, placed in the lower part of the working tube and monitoring the flow rate of sodium along it, at the second stage of spontaneous development of a leak were of a different nature depending on the location of the leak (upper or lower leak simulator). Thus for steam leaks in the lower part of the working tube, after the leak as a result of spontaneous development exceeded the critical value determined by the condition of termination of the sodium flow in the working tube [1], sodium motion appeared in this tube in a direction opposite (bottom to top) to the initial direction (see Table 1, experiments 2, 5, and 7).

A characteristic of the hydrodynamic state in the working tube of the section with steam leaks through the upper injection units (experiments 1, 3, 4, 9, and 10) is the almost total absence of average sodium flow rate along the tube when the size of the leak exceeds some critical value. The lower corrosion rate of the wall of the working tube opposite to the location of the leak in this case can be related to a deficiency of sodium in the leak zone as a result of the absence of a sodium flow through the working tube.

The thermocouples recording the temperature in the upper and lower collectors of the experimental model during the experiments (with the exception of experiment 9) did not essen-

Declassified and Approved For Release 2013/03/04 : CIA-RDP10-02196R000300010004-7

Declassified and Approved For Release 2013/03/04 : CIA-RDP10-02196R000300010004-7
tially change their indications. In experiment 9, the temperature at the second stage of spontaneous development of a lead in the upper collector of the model increased up to 650°C.

Large temperature fluctuations were observed in experiments 1, 2, 3, and 6 at the inlet to the working tube. In addition, these fluctuations occurred only at the second stage of the spontaneous development of the leaks, i.e., after termination of the initial sodium flow in the working tube (see Fig. 3). We can conjecture that the increased temperature (the maximum temperature attained 1200°C) at the inlet to the working tube at this stage was related to the fact that the steam entering the tube did not have time to react completely with the sodium as it moved in the tube and partially exited into the upper collector.

In experiments 6 and 7, an increased temperature (up to 500°C) was measured at the second stage of the spontaneous development of the leak also by the thermocouples located in the outlet from the working tube. Evidently, this was a result of the displacement of sodium from its volume in the tube by the steam-hydrogen mixture, which as a result entered into the upper and lower collectors of the model.

Figure 4 shows, based on data in Table 1 for conditions of the reverse steam generator, the duration of the small steam leaks up to the time at which they sharply increased. As follows from Fig. 4, the results of the present experiments and the experiments in [2] agree. After the experiments, the two 32 × 3.5-mm 12Kh18N10T steel working tubes (experiments 2 and 3) and 33 × 3-mm 10Kh2M steel tubes (experiments 8 and 9) were subjected to metallographic analysis, which confirmed the previously obtained data for conditions of the forward steam generator concerning the presence of an intergrain interaction in 12Kh18N10T steel specimens affected by the products of the reaction of water with sodium and concerning the predominantly frontal type of corrosion of 10Kh2M steel specimens.

In the sections of the working tube made of 10Kh2M steel, located above the leak simulators, changes in the microstructure of the steel compared to the starting structure were observed. Thus, in the zone between the flow simulators, the structure of the steel became purely ferritic. Such structural changes can be explained by the prolonged operation of this zone of the experimental model at a temperature of 700-750°C, when the perlite component of the steel decomposes. The structure of the 10Kh2M steel in the zone opposite the upper leak simulator, as well as in the upper part of the working tube, where the tube was crumpled, was a fine grained structure with precipitation of excess phases. These structural changes, evidently, were related to the fact that in the zones indicated, the temperature fluctuated around a level corresponding to the transition of the α phase into the γ phase ($\sim$900–920°C). At this temperature, the strength characteristics of 10Kh2M steel decrease sharply, which most likely was the reason for the loss of stability of the tube and its crumpling.

We thank O. V. Starkov, M. P. Filin, and M. Kh. Kononyuk for performing the metallographic investigations of the specimens of material after the experiments.

LITERATURE CITED

1. V. S. Sroelov, A. A. Saigin, and P. P. Bocharin, Preprint NIIAR P-33(327) Dimitrovgrad (1977).
2. F. A. Kozlov et al., in: Proc. Int. Conf. on Liquid Metal Technology in Energy Production. Seven Springs Mountain Resort, Champion, 3-6 May 1976, p. 202.

Declassified and Approved For Release 2013/03/04 : CIA-RDP10-02196R000300010004-7

Declassified and Approved For Release 2013/03/04 : CIA-RDP10-02196R000300010004-7

EFFECT OF GAS DISSOLVED IN WATER ON THE HEAT-EXCHANGE CRISIS

V. V. Lozhkin, Yu. A. Smirnov,
Yu. Yu. Shtein, and R. V. Shumskii

UDC 536.248.2

Experimental investigations of the heat-exchange crisis in water containing various amounts of dissolved gas performed in [1] have not revealed connections between the critical thermal flux q_{cr} and the gas content of the coolant C. Since then this fact has not been subjected to questions and verifications for a long time. However, data have recently been published [2] from which it has followed that gas dissolved in water affects the heat-exchange crisis. The extent of this effect exceeded the experimental errors. Thus, in tests with a circular tube for boiling with underheating a decrease of q_{cr} by 10% was recorded for the case of a gas content in the water of 1.2×10^3 normal cm^3 N_2/kg H_2O. For volume boiling of water and a gas content of 3.5×10^3 normal cm^3 N_2/kg H_2O the decrease in q_{cr} already reached 30% comparison with q_{cr} for degasified. Such an appreciable dependence of q_{cr} on the gas content has not been explained in [2]. This problem is very urgent from the scientific and practical standpoints in view of the widespread use in nuclear power plants of gas volume compensators — the main source of gas in the circulation loop.

Therefore, the heat-exchange crisis has been investigated experimentally with additional measurements of the gas content of the flow over the cross section of the steam-generating channel, without which it is difficult in our opinion to determine the causes for the discrepancy in the presently existing data on the effect of the gas content on the critical thermal flux.

The tests were performed on a high-pressure test stand, which is a closed circulation loop with forced circulation of the coolant. The gas (nitrogen) is dissolved in water in a saturator specially constructed for these purposes. A vertical continuous tube made out of Kh18N10T steel (12 mm in diameter, wall thickness 1.5 mm, and length 880 mm) heated by a transmitted electric current served as the working section. The time at which the heat-exchange crisis arose was fixed by four Chromel—Copel thermocouples welded on the perimeter of the outer wall of the working section directly beneath the upper current-conducting spine. A movable isokinetic sampler is mounted at the exit from the working section at a distance of 20 mm from the current-conducting spine. Structurally, the probe is made out of two noncorroding capillaries 1.2 mm in diameter with a wall thickness of 0.1 mm. Its radial displacement was accomplished with the help of an electric drive through a sylphon seal; the position of the probe in the channel was specified to an accuracy of 0.01 mm.

The isokinetic sampling procedure is described in detail in [3] and consists of the following with regard to this investigation (Fig. 1). With valves *a* and f closed and valve g open a sample selection rate established through the probe by the valve d, at which the difference between the static pressure in the probe orifice and on the wall of the working section becomes equal to zero (the isokinetic condition) is after complete purging of the pulse lines and the refrigerator valve *a* is opened simultaneously with the closing of valve d so that the isokinetic nature of the sample selection is preserved. Entering the calibration burette, which is filled with carbon tetrachloride, the selected water sample floats in the carbon tetrachloride, expelling the latter into the buffer chamber. Gas liberated from the water is collected in the upper part of the burette above the water level. The gas content of the sample is determined by the ratio of the water and gas volumes. Upon complete purging of the lines into the burette no less than 150 ml of sample was selected. The accuracy class of the apparatus is equal to two.

Translated from Atomnaya Énergiya, Vol. 53, No. 4, pp. 234-237, October, 1982. Original article submitted January 11, 1982.

0038-531X/82/5304-0687$07.50 © 1983 Plenum Publishing Corporation

Declassified and Approved For Release 2013/03/04 : CIA-RDP10-02196R000300010004-7

Declassified and Approved For Release 2013/03/04 : CIA-RDP10-02196R000300010004-7

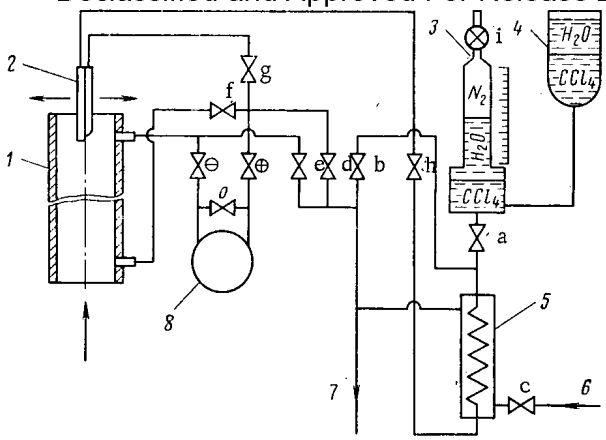

Fig. 1

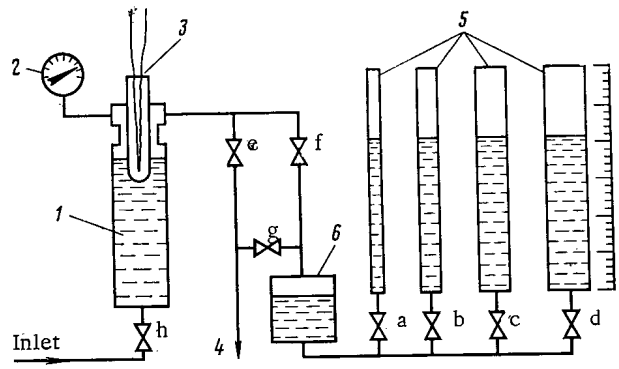

Fig. 2

Fig. 1. Layout of the apparatus for isokinetic selection of samples: 1) working section; 2) isokinetic probe; 3) measuring burette; 4) buffer chamber; 5) refrigerator; 6) cooling water; 7) drain; 8) differential manometer.

Fig. 2. Layout of the detector for determination of the total gas content of the coolant: 1) measuring volume; 2) manometer; 3) thermocouple; 4) drain; 5) measuring burette; 6) buffer chamber.

The total gas content of the coolant was measured by the open method (Fig. 2). To this end a small flow of coolant was effected through a measuring chamber from the loop into the drain line with the goal of heating it up to the coolant temperature at the inlet to the working section. After heating, the chamber with the sample was cut off by valves and cooled to room temperature. With the appropriate valves open the measuring chamber was connected to the atmosphere through the buffer chamber and the burette. The gas liberated in the measuring chamber from the sample expanded to atmospheric pressure, dispelling water from the buffer chamber into the burettes. The volumes of liberated gas and expelled water were assumed to be equal. The detector volume was 875 cm^3. The sample to the detector was removed from the circulation loop directly before the inlet to the working section. The accuracy class was 2.5.

The total gas content was also measured by this method, which one can call the dynamic method [4]. To this end a measurement of the pressure by an electric manometer (accuracy class 1) and the temperature by a Chromel—Copel thermocouple was provided in the measuring chamber. The signals from these detectors were recorded at the rate of one measurement per second on photographic paper by a loop oscillograph. The gas content was calculated from the discontinuity of the curve of the time dependence of the pressure $p(\tau)$ upon cooling of the selected sample, as has been recommended in [4]. Characteristic oscillograms of the dependence $p(\tau)$ under conditions in which the water was and was not subjected to forced saturation with gas are shown in Fig. 3. It is noted that in the second case (curve 1) the form of the dependence $p(\tau)$ differs from that obtained in [4] and better characterizes the process of the transition of the system through a metastable state. The difference between the values of the gas content calculated from the minimum and maximum of the curve $p(\tau)$ reaches 10%.

Prior to the main experiments a calibration series of tests on calibration of the thermocouple, manometers, the measurement unit of the isokinetic probe, the measuring chambers, and so on was run. The efficiency of the isokinetic probe was checked by comparing the velocity profiles in a single-phase flow of water measured by it with a logarithmic one. The maximum discrepancy did not exceed 10% for the center of the flow. The results of simultaneous measurement of C_o, C_d, and C_i turned out to be in satisfactory agreement. In tests without heating of the working section the profiles of the distribution $C_i(r)$ over the cross section of the tube were two-dimensional; therefore the isokinetic probe was located at the center of the flow during the comparative measurements.

The experiments were performed in the following sequence: Specified values of the pressure, mass velocity, and temperature of the water at the inlet to the working section were established. In order to provide an identical gas content through the entire circulation loop, a constant water temperature was maintained. The gas content was measured in three

Declassified and Approved For Release 2013/03/04 : CIA-RDP10-02196R000300010004-7

Declassified and Approved For Release 2013/03/04 : CIA-RDP10-02196R000300010004-7

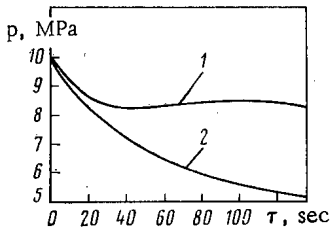

Fig. 3

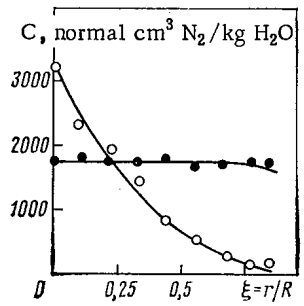

Fig. 4

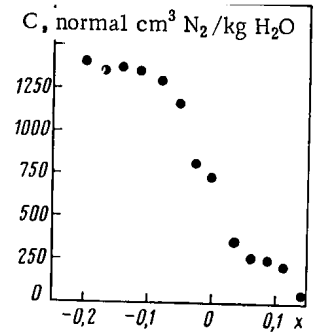

Fig. 5

Fig. 3. Oscillograms of the variation in pressure in connection with the measurement of the gas content by the dynamic method with t_{in} = 260°C: 1) C_o = 53, C_i = 81; 2) $C_o = 1.52 \times 10^3$, $C_i = 1.67 \times 10^3$, $C_d = 1.58 \times 10^3$.

Fig. 4. Distribution of gas over the cross section of the tube measured by the isokinetic method: ○) p = 18 MPa; ρw = 2000 kg/(m²·sec); x_{cr} = −0.19; x_{out} = −0.215; $C_o = 1.45 \times 10^3$ normal cm³ N_2/kg H_2O; ●) p = 10 MPa; ρw = 2000 kg/(m²·sec); x_{cr} = 0.145; x_{out} = 0.113; $C_o = 0.7 \times 10^3$ normal cm³ N_2/kg H_2O.

Fig. 5. Gas content in samples selected from the wall of the working section with ρw = 2000 kg/(m²·sec), $C_o = 1.5 \times 10^3$ normal cm³ N_2/kg H_2O, p = 10 MPa, x_{out} 0.149, and x_{cr} = 0.162.

ways: open C_o, dynamic C_d, and isokinetic C_i. The power liberated in the working section up to the time at which the heat-exchange crisis arises was increased in steps of 1-2 kW. As the thermal flux increases to q_{cr}, the operating parameters were measured at separate power levels by a system of running control and the distribution of gas over the diameter of the working section was measured with the isokinetic probe. The next experimental point was specific to have a different value of the pressure. Then without shutting down the circulation, all the measurements were repeated using water saturated with gas. Experiments were performed in similar fashion for different values of the mass velocity of water. Dissolution of the gas was accomplished in a series of tests at a pressure 2-3 MPa lower than the operating pressure. Then the pressure was increased to the specified level, and the experiments were carried out in the order outlined above.

The basic series of tests was conducted in the following range of variation of the parameters: pressure, 10-18 MPa, mass velocity, 1000-3000 kg/(m²·sec), thermal flux, 0-3.5 MW/m², steam content, 0.2-0.4, and total gas content, 30-1700 normal cm³ N_2/kg H_2O. As a result of the experiments it has been established that for a variation of the gas content from 30 to 1700 normal cm³ N_2/kg H_2O the values of q_{cr} practically coincide, independently of the methods of dissolving the gas in water and the methods for measuring its concentration and the steam content x in the crisis zone. The reliability of the data obtained on q_{cr} has been confirmed by their satisfactory agreement with the tabular data from [5], having a mean-square deviation of 9%. The mean-square deviation of our data from the tabular values is 7.1%.

No accumulation of gas at the heat-exchanging surface of the working section in a single one of the precrisis tests has been detected by local probing of the flow with the isokinetic sampler. Characteristic profiles $C_i(r)$ are shown in Fig. 4. This result has been obtained in experiments on the measurement of the gas content in liquid samples selected at a low rate through holes in the wall of the working section (Fig. 5). In the region of large overheatings ($x < -0.1$) the gas content in the layer near the wall differs hardly at all from the overall gas content in the flow at the inlet to the working section. One can assume that under these conditions no appreciable gas exchange with the central part of the flow occurs due to an insufficient number and intensity of steam generation centers. As the transition to volume boiling occurs, the liberated gas is distributed over the cross section of the flow; the gas content in the layer near the wall is close to zero.

Thus, the measurements of the gas content distribution did not exhibit any kind of peculiarities or tendencies in the gas distribution over the cross section of the steam-generating tube which can produce a dependence of q_{cr} on the concentration of gas dissolved in water up to 2000 normal cm³ N_2/kg H_2O in the investigated range of variation of the coolant parameters.

Declassified and Approved For Release 2013/03/04 : CIA-RDP10-02196R000300010004-7

Declassified and Approved For Release 2013/03/04 : CIA-RDP10-02196R000300010004-7

The results obtained in this paper lead to the following conclusions.

1. With a positive steam content at the exit from the experimental section no decrease of the critical thermal fluxes falling outside the limits of experimental accuracy was exhibited in the 10-18 MPa pressure range, 100-3700 kg/(m^2·sec) mass velocity range, and a gas content up to 4000 normal cm^3 N_2/kg H_2O.

2. A tendency towards a decrease of the critical thermal fluxes is observed in the region of liquid heated to boiling at the exit from the channel in the very same range of variation of the parameters and only for a vapor content higher than 2000 normal cm^3 N_2/kg H_2O. With a gas concentration of 4100 normal cm^3 N_2/kg H_2O this decrease amounted to no more than 20%.

A control experiment was run to determine the critical power for a pressure of 17 MPa, a mass velocity of 2000 kg/(m^2·sec), a water temperature at the inlet to the channel of 200-300°C, and different gas contents. The experimental equipment and procedure for performing the experiments were the same as given in the article. The results of the control experiment have shown that the critical power can decrease by only 3-5% for a coolant with a gas content of 3000 normal cm^3 N_2/kg H_2O. The decrease in the critical thermal fluxes was no greater than 15%.

The authors express their gratitude to P. L. Kirillov for initiative in formulating and conducting this investigation.

LITERATURE CITED

1. V. I. Subbotin et al., in: Investigations of Heat Exchange to Steam and Water Boiling in Tubes at High Pressure [in Russian], Atomizdat, Moscow (1958), p. 83.
2. V. V. Fisenko et al., At. Energ., 48, No. 5, 327 (1980).
3. P. L. Kirillov et al., Preprint FÉI-421, Obninsk (1973).
4. Yu. A. Kalaida et al., At. Energ., 48, No. 2, 91 (1980).
5. "Recommendations on the calculation of the heat exchange crisis upon boiling of water in tubes," Preprint IVTAN SSSR 1-57, Moscow (1980).

INFLUENCE OF BOTH REACTOR IRRADIATION AND HELIUM ISOTOPES UPON THE MECHANICAL PROPERTIES OF TITANIUM AND α-TITANIUM ALLOYS

V. N. Tebus, É. F. Alekseev,
Yu. V. Bobkov, F. P. Butra,
A. M. Glazyrin, I. V. Golikov,
B. V. Grigorovich, A. M. Kaptel'tsev,
Yu. N. Sokurskii, and V. I. Chuev

UDC 620.039.179.15:546.53

Titanium and its alloys recently have been considered promising materials for thermonuclear reactors [1]. The building materials of thermonuclear reactors are subjected not only to mechanical stress and high temperatures but also to neutron irradiation and fluxes of charged particles. Since the papers published relate almost exclusively to the influence of neutron irradiation [2-8], an additional investigation of the influence of other radiation quantities, particularly of helium, upon the mechanical properties of titanium and some of its alloys was made.

Experimental Technique

Materials and Conditions of Irradiation. The mechanical properties of technically pure titanium and three of its α-phase alloys were studied (Table 1). Before the irradiation two lots of samples were annealed at 700°C for 1 h in vacuum. The first lot of samples (titanium and alloy 1) in the form of tubes with a diameter of 12 mm and a wall thickness of 0.5 mm was irradiated in the reactor at the temperature of the cooling water (270°C) with a thermal neu-

Translated from Atomnaya Énergiya, Vol. 53, No. 4, pp. 237-242, October, 1982. Original article submitted August 7, 1981; revision submitted April 15, 1982.

 0038-531X/82/5304-0690$07.50 © 1983 Plenum Publishing Corporation

Declassified and Approved For Release 2013/03/04 : CIA-RDP10-02196R000300010004-7

Declassified and Approved For Release 2013/03/04 : CIA-RDP10-02196R000300010004-7

TABLE 1. Chemical Composition of the Materials

Material	Concentration (mass %)											
	Ti	Al	Mn	Zr	Mo	Nb	C	N	Fe	Si	H	O
Titanium	Base material	0,05	—	—	—	—	0,02	0,01	0,05	0,02	0,003	0,07
Titanium alloy No. 1	Same	5,04	—	—	0,056	0,80	0,04	0,01	0,03	0,01	0,004	0,05
No. 2	» »	2,0	—	2,12	—	—	0,03	0,004	0,08	0,01	0,005	0,06
No. 3	» »	0,73	0,63	—	—	—	0,04	0,01	0,04	0,02	0,005	—

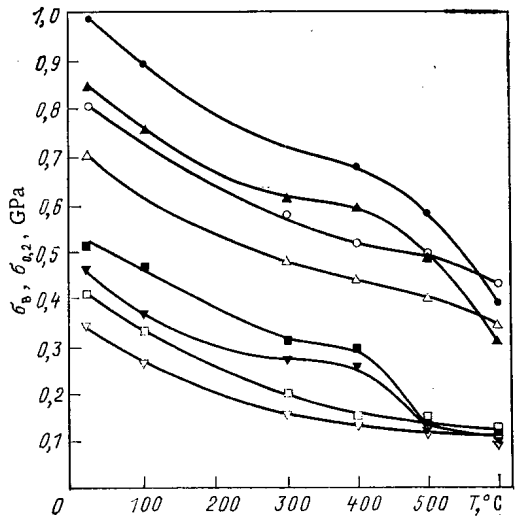

Fig. 1. Influence of irradiation (here and below, □, ▽, ○, and △ refer to the initial samples and ■, ▼, ●, and ▲ refer to the irradiated samples) upon the temperature dependence of the tensile strength and the yield point of titanium (■ and □ refer σ_B; ▼ and ▽ refer to $\sigma_{0.2}$) and of alloy 1 (● and ○ refer to σ_B, ▲ and △ refer to $\sigma_{0.2}$).

tron flux of up to $4 \cdot 10^{20}$ neutrons/cm^2 and a fast (E > 0.1 MeV) neutron flux of $9 \cdot 10^{19}$ neutrons/cm^2. ^{3}He was introduced in the samples by the so-called tritium trick: tritium arrived at the sample in the form of recoil nuclei from the ^{6}Li(n, α)T reaction in lithium contacting the sample [9]; a tritium concentration of $5 \cdot 10^{-3}$ at. %, which according to microautoradiographs was uniform, was created in the sample and after a 2-yr exposure, the tritium decay in the sample left ^{3}He accumulated with a concentration of $5 \cdot 10^{-4}$ at. %.

A second lot of samples (titanium and alloys 2 and 3) was cut from 0.2- and 0.3-mm-thick foil and uniformly saturated with ^{4}He to a concentration of 10^{-2} at. % by bombardment with ^{4}He ions having a maximum energy of 40 MeV; the bombardment took place in a cyclotron [10] at temperatures not exceeding 150°C.

Mechanical tests on annular samples of the first lot were made with the "Instron-1195" machine at a deformation rate of $2.2 \cdot 10^{-3}$ sec^{-1}; the samples of the second lot were tested on a laboratory-type machine for tensile microtesting with automatic recording of the load-elongation curve at a deformation rate of $6.7 \cdot 10^{-4}$ sec^{-1}. The temperature in the tests ranged from 20 to 600°C.

Microhardness and Structure of the Samples Tested. The recovery of the mechanical properties of the irradiated materials was studied by measuring the microhardness on a PMT-3 hardness microtester. The structure of fractures in destroyed samples was studied under an optical MIM-7 microscope and with the scanning electron microscopes "Stereoskan" and "Kvikscan."

Declassified and Approved For Release 2013/03/04 : CIA-RDP10-02196R000300010004-7

Declassified and Approved For Release 2013/03/04 : CIA-RDP10-02196R000300010004-7

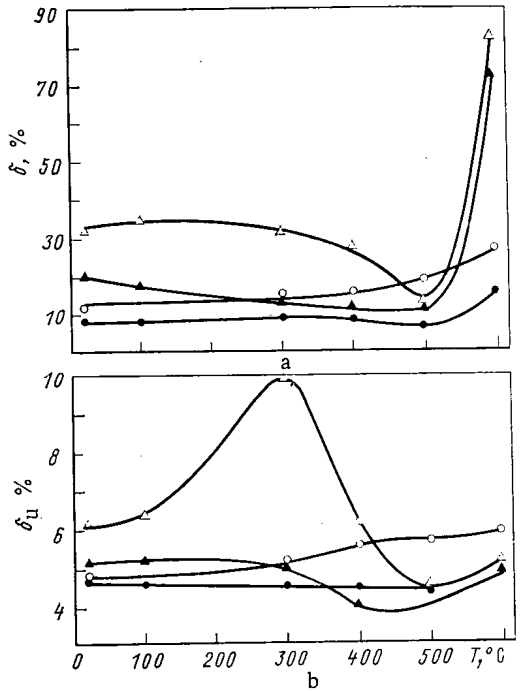

Fig. 2

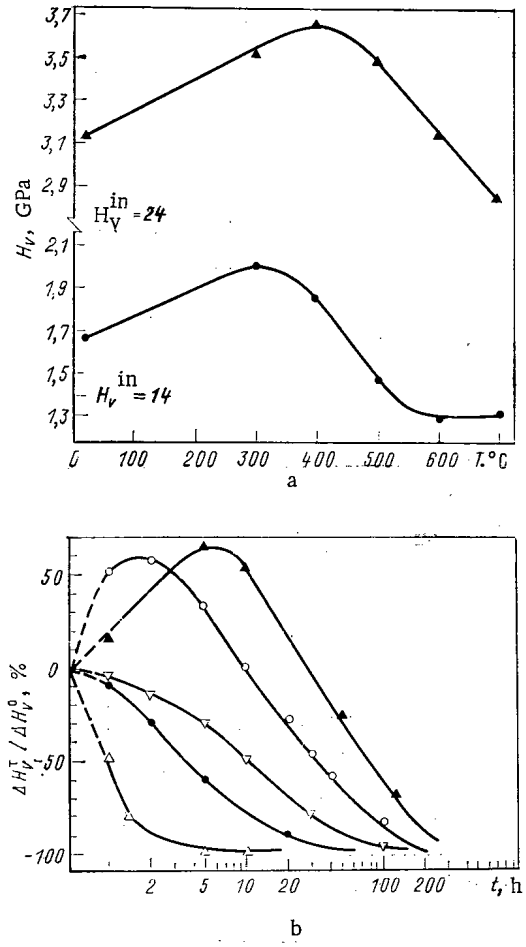

Fig. 3

Fig. 2. Influence of irradiation upon the temperature dependence of the (a) total and (b) uniform elongation of titanium (△ and ▲) and of alloy 1 (○ and ●).

Fig. 3. a) Change of the microhardness H_V of irradiated samples of titanium and alloy 1 subjected for 1 h to isochronous annealing and b) kinetics of microhardness changes (▲ and ● refer to alloy 1 and titanium at T = 600°C; ▽ and △ refer to alloy 1 and titanium at 700°C; ○ refers to titanium at 500°C (ΔH_V^T and ΔH_V^0 denote the temperature-induced and the radiation-induced change in the microhardness, respectively).

Experimental Results

Reactor Irradiation. Figures 1 and 2 depict the results of mechanical tests performed on the initial and irradiated samples of the first lot. The temperature dependencies of the strength properties and of the total elongation of the initial sample are in satisfactory agreement with the published data of [11].

Irradiation increased the strength of the materials examined. The relative increase in strength ($\Delta\sigma_B/\sigma_B$) amounted to 27% and 20% in titanium and in alloy 1 at 20°C, respectively, and to 55% and 24% at 300°C, respectively. The $\sigma_{0.2}$ value changed even more. The influence of irradiation upon the strength hardly manifests itself above 500°C in titanium and above 550°C in alloy 1.

A decrease in the overall elongation (δ) and the uniform elongation (δ_u) is observed in the entire temperature interval of our work though the decrease is substantially smaller at 500-600°C in titanium. The irradiation of the alloy did not change the temperature dependence of the plasticity, whereas the irradiation removed the characteristic increase in plasticity at 90-300°C in the case of titanium.

Figure 3 exhibits the results to isochronous annealing and also the kinetics of recovery. It follows from Fig. 3 that the irradiation increased the microhardness of titanium and alloy

Declassified and Approved For Release 2013/03/04 : CIA-RDP10-02196R000300010004-7

Declassified and Approved For Release 2013/03/04 : CIA-RDP10-02196R000300010004-7

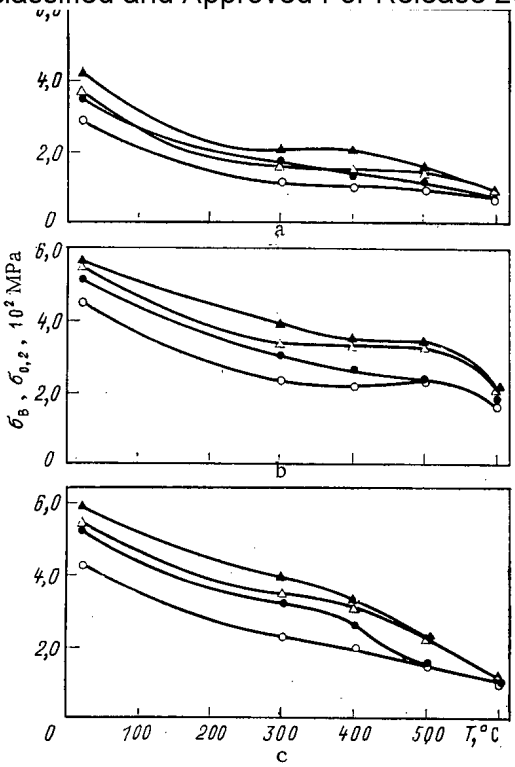

Fig. 4

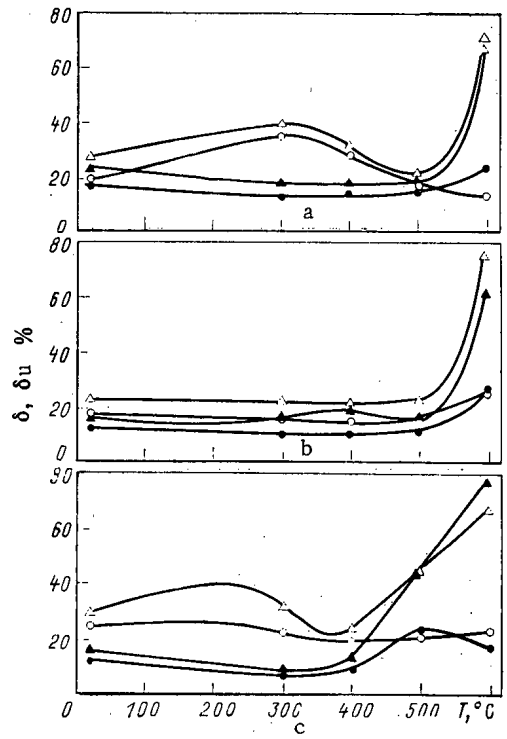

Fig. 5

Fig. 4. Temperature dependence of the tensile strength (△ and ▲) and of the yield point (○ and ●) of a) titanium, b) alloy 2, and c) alloy 3.

Fig. 5. Temperature dependence of the total (△ and ▲) and uniform (○ and ●) elongation of a) titanium, b) alloy 2, and c) alloy 3.

1 by about 30%. The recovery curves of the two materials are smaller. The maximum on the curve pertaining to alloy 1 is shifted toward higher temperatures. Full recovery is observed at 600°C in the case of titanium and at 700°C in the case of alloy 1.

The kinetic curves reveal that the recovery rate increases with increasing temperature and is higher for the titanium samples at a certain fixed temperature (see Fig. 3b). The recovery process is an activation. The activation energy Q is 1.1 eV for titanium and 1.6 eV for alloy 1 (the activation energy for the titanium self-diffusion is 1.27 eV [6]).

Irradiation with ^{4}He Ions. It follows from the temperature dependencies of the mechanical properties of titanium and alloys 2 and 3 that saturation with ^{4}He to a concentration of 10^{-2} at. % causes a noticeable strength increase in the materials at temperatures of 20-400°C but hardly affects the strength of the materials at temperatures in excess of 500°C (Fig. 4). Irradiation did not change the form of the temperature dependence of the strength properties.

Irradiation has a more pronounced influence upon the plasticity of the material. At temperatures of 20-500°C the total elongation and the uniform elongation of irradiated titanium and alloy 3 samples decreased noticeably and depended only slightly upon temperature. In this temperature range the plasticity of irradiated alloy 2 decreased also but the overall form of the change remained preserved. At temperatures of 500-600°C the total elongation of the irradiated samples increased sharply in analogy to the increase observed in the initial samples (Fig. 5).

The recovery of the mechanical properties was investigated by measuring the microhardness of the irradiated samples in 1 h isochronous annealing. Similar microhardness measurements of the same samples irradiated with neutrons at ∿300°C (flux of up to 10^{20} neutrons/cm^2) were made for comparison. Figure 6 shows that, without any dependence on the type of the irradiation, total recovery of the mechanical properties of the materials occurs at 550-600°C.

Structure of the Fractures. It was established in investigations of sample fracture (Figures 7 and 8) that destruction takes place in transcrystalline fashion with a mechanism

Declassified and Approved For Release 2013/03/04 : CIA-RDP10-02196R000300010004-7

Declassified and Approved For Release 2013/03/04 : CIA-RDP10-02196R000300010004-7

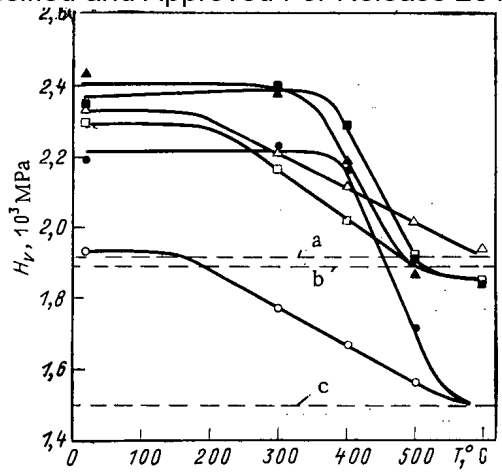

Figure 6. Temperature dependence of the microhardness of irradiated titanium samples (○ and ●), of alloys 2 (△ and ▲), and of alloys 3 (□ and ■) subjected to 1-h isochronous annealing (○, △, and □ refer to samples saturated with ^{4}He; $T_{irr} \leqslant 150°C$; ●, ▲, and ■ refer to samples irradiated with neutrons at $T_{irr} \approx 300°C$; *a*, b, and c indicate H^{in} of alloys 1 and 2 and of titanium respectively).

including nucleation, growth, and merging of microvoids while a cup relief develops on plastic materials. When the temperature is increased above 300°C, the pits on the initial and irradiated samples are enhanced but become slightly smaller on the irradiated samples.

Discussion of Results

It follows from the results described above that both reactor irradiation and irradiation with ^{4}He ions influence in the same fashion the mechanical properties of technically pure titanium and its alloys of the α-phase. At temperatures of 20-400°C the relative change in the strength properties of the materials is in both cases more pronounced at increased temperatures but the form of the temperature dependence is preserved. The total and uniform elongation of irradiated materials depend relatively slightly upon the temperature at 20-400°C though an increase in plasticity at increasing temperatures is observed in the initial samples of titanium and of alloy 3 in this temperature interval and though the form of strain hardening is changed.

At temperatures in excess of 500°C irradiation has reduced influence upon the mechanical properties of the materials: The strength properties of irradiated samples and initial samples are practically identical and the relative reduction of the plasticity is much smaller than at 20-400°C. The curves of the total elongation of the irradiated and initial samples have the same form. It should be noted that the irradiated materials conserve an adequate plasticity reserve ($\delta > 6\%$) at all the temperatures. This is also confirmed by the viscous break-up of the irradiated samples.

These results give reason to assume that the radiation hardening at 20-400°C results from the formation of point defect complexes preventing the movement of dislocations [4] and from the introduction of helium atoms in interstitial points of the lattice. But helium only slightly influences the hardening, as put into evidence by the similar microhardness changes in samples irradiated in the cyclotron and in the reactor. Furthermore, at temperatures in excess of 500°C there is no radiation hardening in both cases. This confirms the results of [8] concerning the irradiation of α-phase titanium alloys in a reactor with a flux of up to $2 \cdot 10^{21}$ neutrons/cm^2 ($E > 0.1$ MeV). This means that the radiation defects are practically fully annealed at this temperature and that the helium present does not enhance the strength of the samples. The plasticity of the materials increases sharply and the influence of irradiation upon the plasticity is substantially reduced; the plasticity of irradiated alloy 3 is even higher than the plasticity of the initial sample. It is a well-known fact that at temperatures in excess of 500°C recrystallization processes, accompanied by a noticeable increase in plasticity [11], are observed in nonirradiated titanium and its α-phase alloys. The presence of helium in the irradiated samples obviously did not have a significant influence upon these processes. This means that the helium atoms incorporated in titanium and in austenitic stainless steels behave in different ways: Helium atoms in austenitic stainless steels significantly slow down recrystallization and polygonization processes and cause high-temperature radiation-induced (helium) embrittlement [10, 12, 13]. We list below the relative values of a parameter expressing the sensitivity to high-temperature radiation-induced embrittlement. The parameter values were calculated with the formula

Declassified and Approved For Release 2013/03/04 : CIA-RDP10-02196R000300010004-7

Declassified and Approved For Release 2013/03/04 : CIA-RDP10-02196R000300010004-7

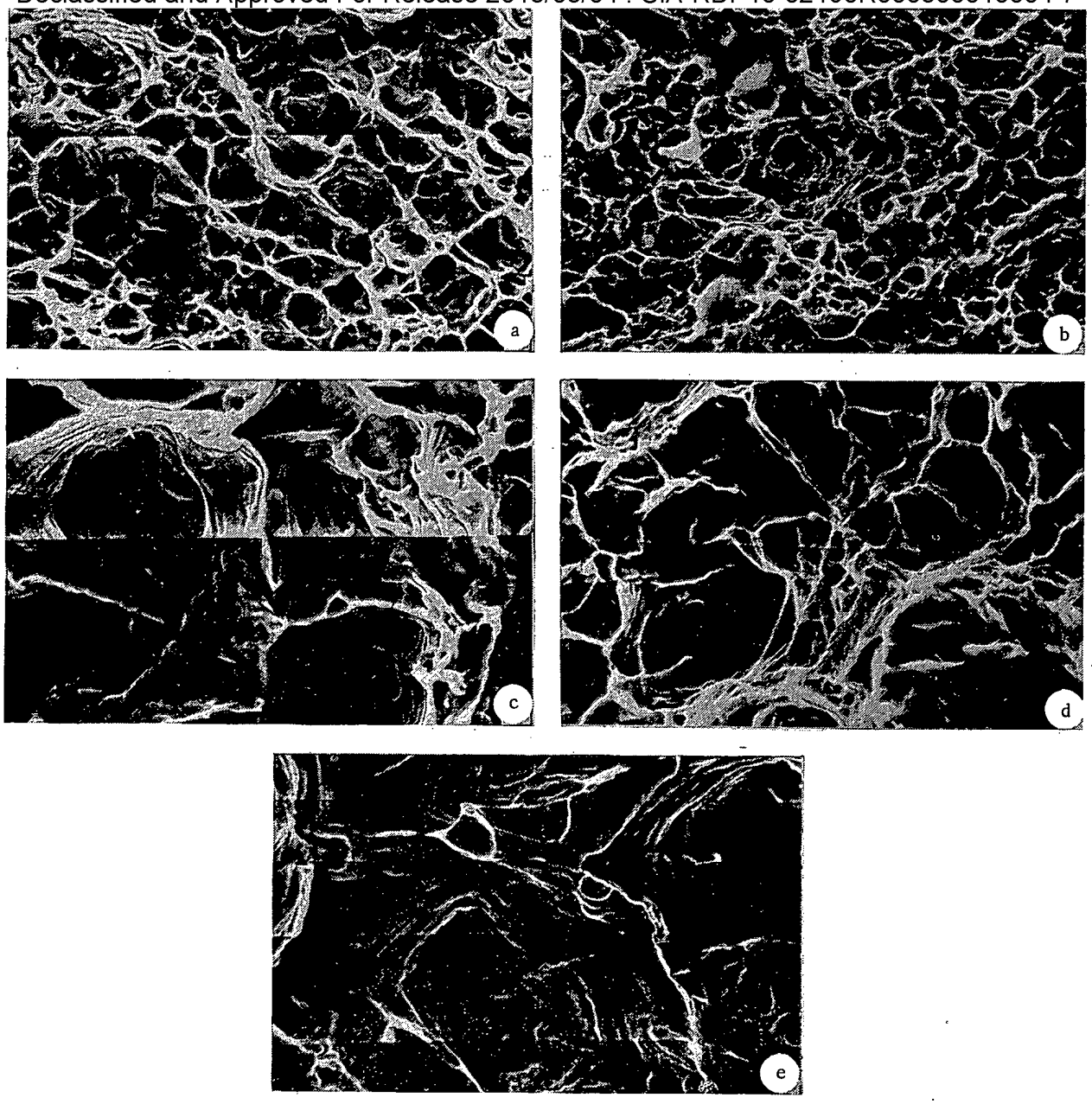

Fig. 7. Titanium microstructure at the fracture point at T = 20°C in (a) initial and (b) irradiated samples; at T = 300°C in (c) initial and (d) irradiated samples; and at T = 500°C in (e) an irradiated sample (× 500).

$$S = (\delta_{in} - \delta_{irr})/(\delta_{in} C_{He}),$$

where δ_{in} and δ_{irr} denote the total elongation of the initial and irradiated samples, respectively; and C_{He} denotes the helium concentration.

Titanium	6.7	316 Steel [9]	300
Alloy 2	18.8	Ti-70A [9]	11.3
Alloy 3	0	Ti-6Al-4V [9]	23.0
OKh16N15MZB Steel [10]	438		

The sensitivity parameter of austenitic stainless steels is much higher than that of titanium and its alloys. This is also confirmed by the data obtained after introducing ^{3}He with the "tritium trick" into titanium alloys [9].

Declassified and Approved For Release 2013/03/04 : CIA-RDP10-02196R000300010004-7

Declassified and Approved For Release 2013/03/04 : CIA-RDP10-02196R000300010004-7

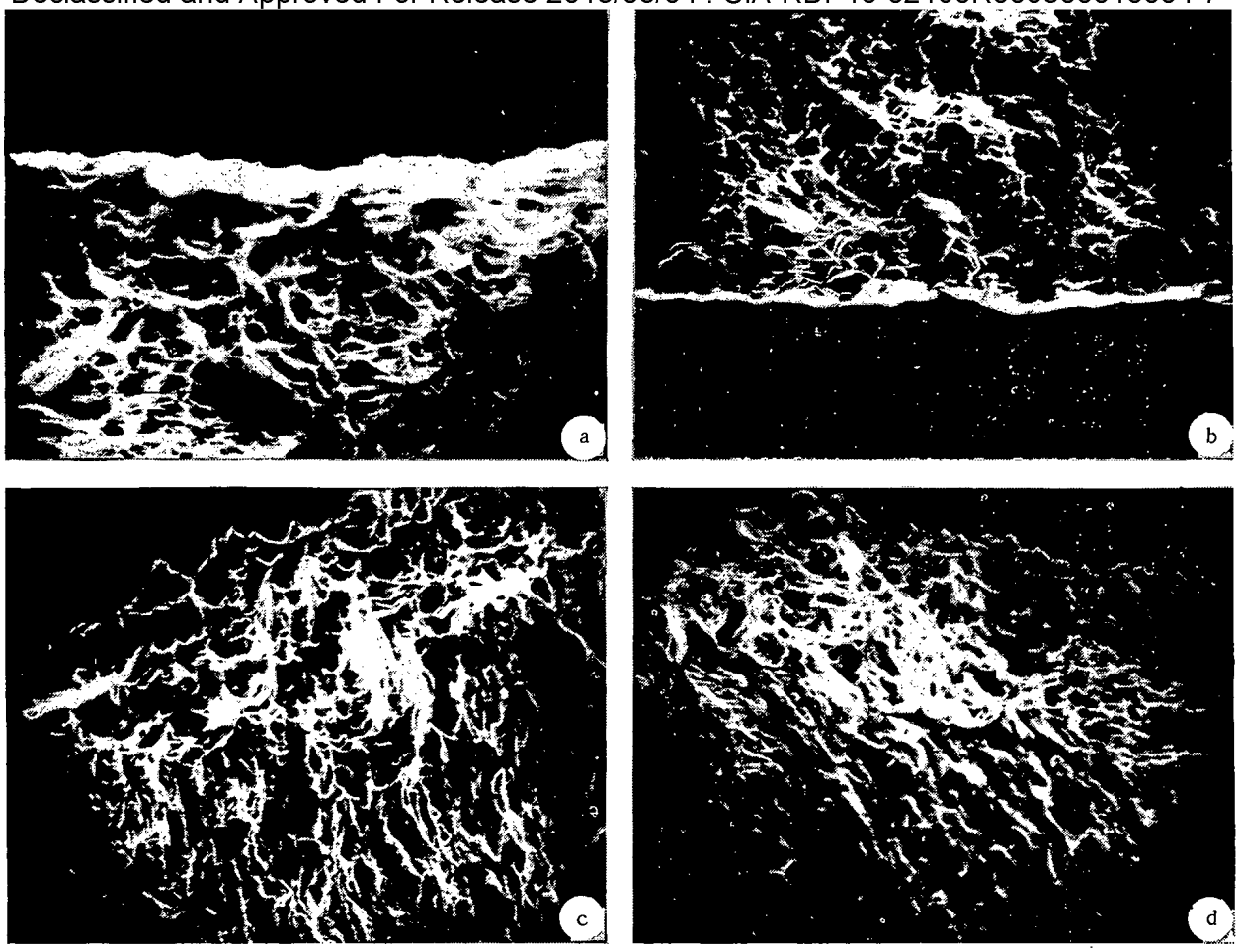

Fig. 8. Relief of (a, b) the rupture surfaces and (c, d) the adjacent side surfaces of samples of alloy 3 tested at T = 300°C: a, c) initial sample; b, d) irradiated sample (× 600).

CONCLUSIONS

Reactor irradiation of titanium and its α-phase alloys containing ^{3}He and irradiation with ^{4}He ions leads to increased strength and reduced plasticity in the temperature range 20-400°C. The influence of the two types of irradiation upon these materials is similar. At 20-600°C the irradiated materials conserve an adequate plasticity reserve ($\delta > 6\%$). Viscous destruction of the initial and irradiated samples of the materials examined takes place in mechanical testing. At the temperature (500-600°C) at which recrystallization of nonirradiated materials begins, total recovery of the strength properties and noticeable recovery of the plasticity are observed in the irradiated samples. Titanium alloys are inclined to high-temperature radiation-induced embrittlement to a lesser degree than austenitic stainless steels.

LITERATURE CITED

1. I. V. Gorynin et al., in: Reports of the All-Union Conf. on Engineering Problems of Thermonuclear Reactors [in Russian], Izd. NIIÉFA, Leningrad, 3, 187 (1977).
2. M. Makin and F. Minter, J. Inst. Met., 85, 397 (1956).
3. Y. Higashiguchi and H. Kayano, J. Nucl. Sci. Technol., 12(5), 320 (1975).
4. I. A. Gindin et al., Probl. Prochn., No. 8, 49 (1973).
5. I. A. Gindin et al., Probl. Prochn., No. 8, 118 (1972).
6. Y. Higashiguchi, H. Kayano, and S. Yayma, J. Nucl. Sci. Technol., 13, 454 (1976).
7. R. Blake, A. Jostons, and P. Kelli, in: Proc. 8th Int. Cong. on Electron Microscopy, Canberra, 1, 610 (1974).
8. I. V. Gorynin et al., in: Radiation Defects in Metallic Crystals [in Russian], Nauka, Alma-Ata (1978), p. 123.
9. R. Jones and L. Charlot, J. Nucl. Mater., 85, 877 (1979).

Declassified and Approved For Release 2013/03/04 : CIA-RDP10-02196R000300010004-7

Declassified and Approved For Release 2013/03/04 : CIA-RDP10-02196R000300010004-7

10. V. D. Onufriev, Yu. N. Sokurskii, and V. I. Chuev, Preprint IAE-3070, Moscow (1978).
11. B. A. Kolachev, V. A. Livanov, and A. A. Bukhanova, in: Mechanical Properties of Titanium and Its Alloys [in Russian], Metallurgiya, Moscow (1974), p. 25.
12. V. F. Zelenskii et al., in: Reactor Materials Science [in Russian], TsNIIatominform, 2, Moscow (1978), p. 192.
13. N. P. Agapove et al., in: Reactor Materials Science [in Russian], TsNIIatominform, 2, Moscow (1978), p. 214.

EFFECTS OF HEAT TREATMENT AND ALLOYING ON THE RADIATION EROSION OF AUSTENITIC STAINLESS STEELS AND ALLOYS

E. E. Goncharov, M. I. Guseva,
B. A. Kalin, O. A. Kozhevnikov,
A. N. Lapin, A. N. Mansurova,
A. M. Parshin, D. M. Skorov,
I. N. Chernov, G. N. Shishkin,
and V. D. Yaroshevich

UDC 621.039.531

Stainless steels and nickel alloys of the austenite class are considered as promising materials for the first wall in a fusion reactor [1-4]. Studies on the damage to such materials by ion bombardment have indicated the effects of the irradiation conditions, the mechanical stresses, preliminary ion implantation, and the surface state. However, not much is known about the dependence of the damage on the amount and form of the alloy elements or on the treatment, nor is much known about the behavior of nickel-rich alloys and nickel-free steels on irradiation by light ions under the conditions of a fusion reactor [5-7].

We have examined the effects of alloying elements and previous treatment on the radiation damage to various steels and alloys of the austenite class on ion bombardment. Table 1 gives the compositions and treatments, while Table 2 gives the irradiation conditions. The surfaces were mechanically and electrolytically polished before ion bombardment. The specimens were annealed in an atmosphere of pure argon. Bombardment with He^+ ions of energy 20 keV was performed in a mass monochromator with double focusing by a method previously described in [8]; the irradiation conditions for ions of energies 40 and 80 keV have been given in [9].

The surface topography was examined with a Stereoscan S4-10 scanning electron microscope. The structure were examined with an ÉVM-100L transmission electron microscope, where the dislocation density was determined by the method described in [10]. The distributions of the alloying elements were examined with a Cameca SMI-300 microanalyzer and also by Auger spectroscopy. The distribution profiles for carbon and boron were examined by successively removing surface layers by sputtering with a rate of 150-200 Å/min (1 Å = 10^{10} m) by bombardment with Ar^+ ions of energy 10 keV. The boron distribution near the surface was also examined by track autoradiography, which has high sensitivity ($\sim 10^{-5}$ mass % B) and provides a localization of $\sim$2 μm in depth and 1 μm over the surface [11]. The blister-formation parameters and the erosion coefficients were determined in a standard way [12]. Figure 1 shows typical photomicrographs. Figures 2-4 and Table 3 gives the results.

These indicate the dependence of the erosion on the austenitization conditions, mode of cold deformation CD, nickel content, and amounts of other alloying elements.

Effects of Cold Deformation. Electron micrographs of steels irradiated in the cold-deformed state show clearly that the blisters are much smaller than those found with annealed

Translated from Atomnaya Énergiya, Vol. 53, No. 4, pp. 243-250, October, 1982. Original article submitted November 23, 1981.

0038-531X/82/5304-0697$07.50 © 1983 Plenum Publishing Corporation

Declassified and Approved For Release 2013/03/04 : CIA-RDP10-02196R000300010004-7

Declassified and Approved For Release 2013/03/04 : CIA-RDP10-02196R000300010004-7

TABLE 1. Chemical Compositions of Materials and Treatment

Specimen No.	Material	Treatment No.	Type of treatment	Chemical composition, mass %													
				C	Mn	Si	P	S	Fe	Cr	Ni	Mo	Nb	Ti	Al	B	Others
1	17Cr-15Mn	0	Austenitization + rolling														
2	18-10	1 2	Annealing at 1170°K, 1 h + Cd 20%, 1170°K, 1 h	⩽0,12	1,02	0,71	0,03	0,010	Remainder	17,9	9,17	—	—	0,5	—	—	—
3	16-15	0 1 2 3 4 5	1320°K, 0.5 h + rolling 1170°K, 1 h + Cd 20% 1170°K, 1 h (1170°K, 15 min) 1320°K, 0,5 h 1390°K, 0,5 h Austenitization and aging at 1070°K, 40 h;	0,07	0,53	0,22	0,018	0,007	Same	16,16	14,75	2,88	0,56	—	—	$<10^{-4}$	0,028 N
4	16-15	4	1390°K, 0,5 h	0,02	0,70	0,30	0,011	0,008	» »	16,35	15,30	2,67	0,38	—	—	—	—
5	16-15	0	1320°K, 0,5 h + rolling	0,07	0,44	0,18	0,009	0,008	» »	15,75	14,80	2,73	0,78	—	—	0,002	0,033 N
6		2	1170°K, 15 min	0,07	0,34	0,12	0,008	0,007	» »	15,78	14,80	2,63	0,79	—	—	0,005	0,030 N
7		3	1320°K, 0,5 h	0,08	0,51	0,27	0,012	0,009	» »	15,80	14,95	2,83	0,78	—	—	0,008	0,040 N
8	20-40	1 2	1170°K, 1 h + CD 20 % 1170°K, 1 h	0,01	0,31	0,17	0,009	0,007	» »	19,95	40,2	—	—	—	—	—	—
9	20-45	2 3 6	1170°K, 15 min 1320°K, 1 h 1470°K, 5 h	0,016	0,55	0,22	0,007	0,005	» »	19,64	45,45	4,00	0,84	0,08	0,10	—	0,07 Cu 0,05 Y
10	20-45	2 3 6	1170°K, 15 min 1320°K, 1 h 1470°K, 5 h	0,022	0,53	0,24	0,009	0,004	» »	19,35	44,9	3,55	0,89	0,02	0,16	0,005	0,04 Cu 0,008 N 0,035 Zr
11	20-80	2	1170°K, 1 h	0,08	0,33	0,60	0,005	0,007	0,53	20,25	Remainder	—	—	0,25	0,03	—	—
12	20-75	2	1170°K, 1 h	0,01	0,03	0,13	0,009	0,008	0,14	20,55	Same	2,23	—	0,58	0,62	—	0,01 Cu 0,01 Ce

Declassified and Approved For Release 2013/03/04 : CIA-RDP10-02196R000300010004-7

Declassified and Approved For Release 2013/03/04 : CIA-RDP10-02196R000300010004-7

TABLE 2. Irradiation Conditions

Specimen No.	j, A/m^2	E, keV	T_{irr}, °K	D, ion/m^2
92, 93, 96; 102, 103, 106	0,5	20	< 370	$5 \cdot 10^{21}$
30, 32, 33; 50, 52, 53; 60, 62, 63; 70, 72, 73	0,5	20	< 370	$7 \cdot 10^{21}$
10; 92, 93, 96; 102, 103, 106	0,3	40	< 420	$1 \cdot 10^{22}$
21, 22; 30, 31, 32, 34, 35; 44; 70; 81, 82; 112; 122	0,3	40	< 420	$2 \cdot 10^{22}$
92, 93, 96; 102, 103, 106	0,3	80	< 420	$2 \cdot 10^{22}$

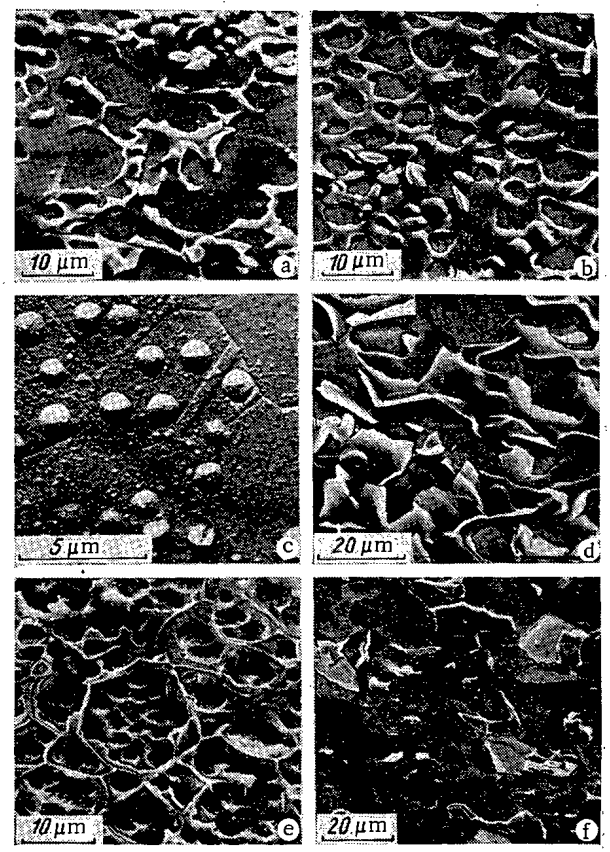

Fig. 1. Radiation erosion in materials irradiated by helium ions: a and b) steels 0Kh16N15M3B and 00Kh16N15M3B (annealed at 1390°K for 0.5 h), He^+ with E = 40 keV, D = 2 × 10^{22} ion/m^2, T_{irr} < 370°K; c) alloy 03Kh20N45M4BCh (annealing at 1170°K for 15 min), He^+ with E = 20 keV, D = 5 × 10^{21} ion/m^2 T_{irr} < 370°K; d, e, and f) alloy 03Kh20N45M4RBTs (annealing at 1170°K for 15 min, 1320°K for 1 h, and 1470°K for 5 h), He^+ with E = 80 keV, D = 2 × 10^{22} ion/m^2, T_{irr} < 420°K.

specimens. An example is provided by steels 12Kh18N10T, 0Kh16N15M3B, and Kh20N40 (specimens 22* and 21, 32 and 31, and 82 and 81 in Fig. 2 correspondingly).

*The first figure of the first two denotes the sequence number of the specimen (Tables 1 and 2), while the latter figure is the treatment number.

Declassified and Approved For Release 2013/03/04 : CIA-RDP10-02196R000300010004-7

Declassified and Approved For Release 2013/03/04 : CIA-RDP10-02196R000300010004-7

TABLE 3. Blister Parameters for 20-45 Nickel Alloys Irradiated with He^+ at E = 20 keV, D = 5 · 10^{21} ion/m^2, T < 370°K

Treatment	$\rho_{irr} \cdot 10^{-11}$, m^{-2}	$(\rho_d < 1\ \mu m)$, $\times 10^{-11}$, m^{-2}	$(\rho_d \geqslant 1\ \mu m)$, $\times 10^{-11}$, m^{-2}	d_{max}, μm	$\bar{d}$, μm
Alloy No. 9					
initial	125,4	124,0	1,4	1,8	0,14
annealing at 1320°K, 1 h	61,0	59,0	2,0	2,0	0,17
the same at 1470°K. 5 h	50,0	48,6	1,4	2,4	0,18
Alloy No. 10					
initial	66,7	65,6	1,1	2,4	0,15
annealing at 1320°K, 1 h	44,4	42,4	2,0	2,6	0,20
the same at 1470°K, 5 h	19,9	17,9	2,0	3,1	0,32

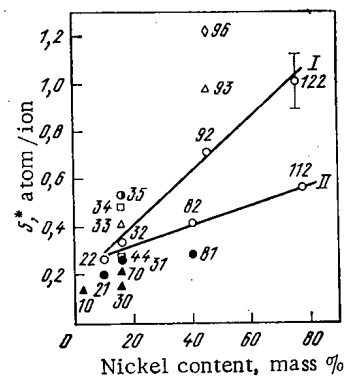

Fig. 2

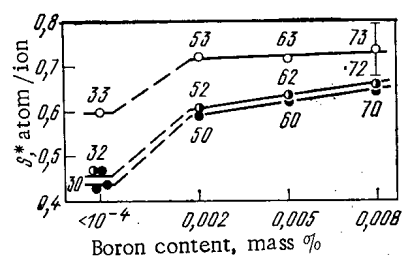

Fig. 3

Fig. 2. Dependence of the erosion coefficient on alloying and form of treatment of irradiation with He^+ with E = 40 keV, D = 2 × 10^{22} ion/m^2, T_{irr} < 370°K (D = 1 × 10^{22} ion/m^2 for alloys 92, 93, and 96): ○) annealing at 1170°K for 1 h (or 15 min); Δ) 1320°K, 1 h (or 0.5 h); □) 1390°K, 0.5 h; ◇) 1470°K, 5 h; ●) 1170°K, 1 h + CD 20%; ▲) 1320°K, 0.5 h + rolling; ◑) 1070°K, 40 h (the numbers in the figures correspond to the materials in Table 1: the number of the first two represents the specimen number, while the last is the treatment number).

Fig. 3. Dependence of the erosion of steel 16-15 on boron alloying on irradiation with He^{3+} with E = 20 keV, D = 7 × 10^{22} ion/m^2, T_{irr} < 370°K: ○) rolling and annealing at 1320°K for 30 min; ◑) rolling and annealing at 1170°K, 15 min; ●) rolling.

Effects of Alloying Elements. We measured the erosion coefficients for the following steels annealed at 1170°K for 1 h: 12Kh18N10T (specimen 22), 0Kh16N15M3B (32), and Kh20N40 (82), along with the alloys 20-45 (92), 20-75 (122), and 20-78 (112), which showed a general tendency for the erosion to increase with the nickel content (Fig. 2). However, the variations in content of Ni, Fe, and Cr in these alloys are accompanied by variations in the minor components (Mo, Nb, Ti, Al, B), which, as shown in Figs. 2 and 3, play an important part in the surface damage on ion bombardment. The results for identically treated materials show that 0.002-0.008 mass % B in steel 16-15 (specimens 3 and 5-7 in Table 1) increases the erosion coefficients considerably, and the same applies to 0.005 mass % B and 0.035 mass % Zr in the high-nickel alloys (specimens 9 and 10), with the same effects for about 4 mass % Mo, ∿1

Declassified and Approved For Release 2013/03/04 : CIA-RDP10-02196R000300010004-7

Declassified and Approved For Release 2013/03/04 : CIA-RDP10-02196R000300010004-7

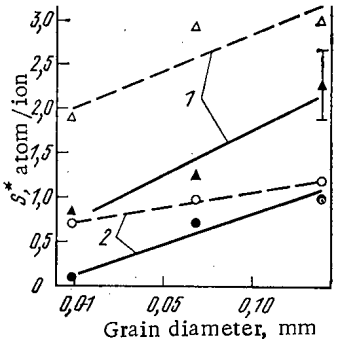

Fig. 4. Dependence of the erosion of alloys No. 10 (1) and No. 9 (2) on grain size (heat treatment) on irradiation with He^+ with E = 40 keV, D = 1 × 10^{22} ion/m^2 (broken line) and with E = 80 keV, D = 2 × 10^{22} ion/m^2 (solid line).

mass % Nb, and Y or B with Zr (specimens 8 and 9, 10), as also for 2.23 mass % Mo and 0.62 mass % Al (specimens 11 and 12), as indicated in Figs. 2-4. The alloying elements also influence the character of the surface damage. In KhN78T (112) there is one-layer exfoliation, whereas in KhN76M2TYu (122) two layers are shed. The highly alloyed materials with intermetalline hardening (line I in Fig. 2) have higher erosion coefficients than do alloys with predominantly carbide hardening (line II in Fig. 2).

Effects of Carbon and Boron. These elements play a considerable part in the irradiation erosion of these materials. For example, double vacuum melting of steel results in purification from carbon and other interstitial impurities, and this reduces the erosion coefficients (Fig. 2, specimens 34 and 44; Fig. 1a and 1b). The blister density on 00Kh16N15M3B steel (44) is lower by about a factor 1.5 than that on steel 0Kh16N15M3B (34), which was given similar treatment. Carbon influence the blistering at the stages of nucleation, growth, and combination of the gas bubbles into blisters, and also at the stage of exfoliation, and its effect is due to changed mechanical properties in the subsurface layer.

These He^+-irradiated surfaces showed that steel containing boron (specimens 5-7 in Table 1) were more liable to erosion (Fig. 3). Also, the increase in the erosion coefficient on alloying with boron for a given density, size, and distribution of the blisters is due to the breakaway of a large number of blister tops. Annealing the material before irradiation alters the erosion coefficients, particularly for steels without boron. Annealing at 1320°K for 30 min greatly alters the boron concentration in the surface layer (thickness <1 μm) for steel 0Kh16N15M3B. In the initial state and after a brief annealing (15 min at 1170°K), the boron content in the surface layer, as determined by track autoradiography, corresponded to the certificate (<10^{-4} mass %), while after high-temperature annealing it rose to 1 × 10^{-3} mass % and the erosion coefficient increased from 0.46 to 0.60 atom/ion (Fig. 3).

There is hardly any effect on the erosion (Fig. 3) from varying the boron content between 0.002 and 0.008 mass % (within the errors of measurement). However, track autoradiography showed that the boron is almost uniformly distributed (Fig. 5a) in hot-rolled steel (specimen 70), whereas in cold-rolled steels (specimens 50 and 60) there was a prominent streaky boron distribution (Fig. 5b), which partially persisted even after annealing for 30 min at 1320°K (Fig. 5c). There was a similar distribution of the carbon along the rolling direction. These nonuniform distributions also influence the surface damage, because the widths of the individual streaky components rich in boron are up to ∿100 μm (Fig. 5b). This is confirmed by the fact that the erosion coefficients for different parts differ only slightly for steel with a uniform boron distribution (specimen 70), whereas in specimens 50 and 60 with prominent streaky boron distributions there is a certain spread in the reduced mean values (Fig. 3).

Declassified and Approved For Release 2013/03/04 : CIA-RDP10-02196R000300010004-7

Declassified and Approved For Release 2013/03/04 : CIA-RDP10-02196R000300010004-7

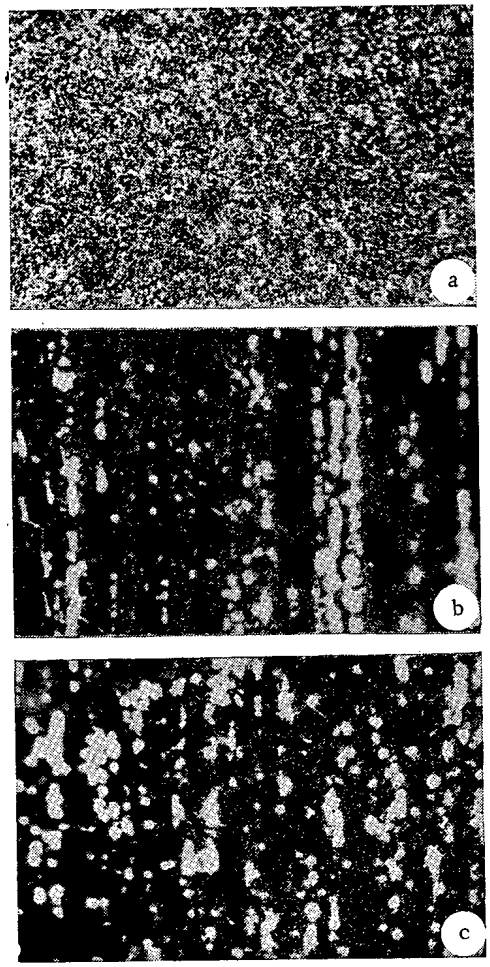

Fig. 5. Autoradiographs of the boron distribution in 0Kh16N15M3BR steel: a) austenitization at 1320°K for 0.5 h + hot rolling; b) austenitization at 1320°K for 0.5 h + cold rolling + annealing at 1170°K for 15 min; c) austenitization at 1320°K for 0.5 h + cold rolling + annealing at 1320°K for 0.5 h; × 130 in all cases.

Nickel alloy 20-45 (No. 10) contains boron and zirconium, and this has a higher erosion coefficient in the analogous alloy (No. 9) alloyed with yttrium (Fig. 4) for all the conditions of irradiation and modes of heat treatment.

Not much is known about the radiation resistance of chromium–manganese alloys, but early results show that the erosion resistance of 06Kh17G15NAB steel corresponds approximately to that of steels 18-10 (Fig. 2, specimen 10).

Dependence of Erosion on Heat-Treatment Conditions. The electron micrographs show that heat treatment has a considerable effect on erosion. The erosion coefficients for 0Kh16N15M3B steel treated under various conditions (specimens 30 and 32-35 in Table 1 and in Fig. 2) indicate that the minimum erosion occurs in steel irradiated in the initial state (30) and in the fine-grained state [32]. The erosion coefficient increases to 0.44 atom/iom (34) after high-temperature annealing. Aging the steel increases the erosion coefficient to 0.56 atom/ion (specimen 35 in Fig. 2).

Figure 1c and Table 3 show that on irradiating alloy 20-45 with He^+ ions of energy 20 keV one gets not only small blisters ($d < 0.4$ μm) of high density ($\sim 10^{12}$–10^{13} m^{-2}) but also large ones ($d > 0.9$ μm) with density $\sim 10^{11}$ m^{-2}; the smallest blisters ($d = 0.14$–0.15 μm) occur in materials irradiated in the initial state. As the temperature and duration of the pre-

Declassified and Approved For Release 2013/03/04 : CIA-RDP10-02196R000300010004-7

Declassified and Approved For Release 2013/03/04 : CIA-RDP10-02196R000300010004-7
liminary annealing are increased, the blisters increase in size but decrease in density, and the certian difference between alloys No. 9 and 10 (Table 3) is ascribed to the effects of the minor alloying elements, particularly boron, on the blister nucleation kinetics.

There are two features of the blistering in complex alloy steels and other alloys. Firstly, helium ions of energy up to 20 keV produce blisters in two groups, of diameter up to 2 μm and < 0.4 μm. There are two maxima on the blister size distribution curve for a material with an fcc lattice, e.g., for the complex nickel alloys types 20-75 and 20-45 (Fig. 1c and Table 3) and also for steel 16-15 annealed at 1023°K for 1 h after irradiation [13]. A similar curve has been recorded for molybdenum [14], i.e., from a metal with a bcc lattice. This indicates that the helium is redistributed during the irradiation. Secondly, helium ions of energy ⩾80 keV produce damage by flaking in a complex alloy, where several layers of material are exfoliated, while in other materials one gets blistering and the breakaway of tops.

The erosion for alloys No. 9 and 10 increases with the energy and dose. The erosion coefficients increase with the temperature and duration of the annealing, i.e., as the grain size increases (Fig. 4). When the energy of the bombarding ions rises to 80 keV, one gets two-layer exfoliation in both alloys (Fig. 1, d-f).

The irradiation resistance of a high-nickel alloy is substantially dependent on the microstructure. Surface swelling and exfoliation of an entire layer (Fig. 1f) are controlled by the grain boundaries, and in some cases damage occurs to the boundary zone only with difficulty (Fig. 1e); various factors may be responsible for this, which act during nucleation of the helium bubbles (a boundary acts as a sink for defects and implanted helium atoms, with the boundary layers free from accumulating helium bubbles) and at the stage where these bubbles link up into cavities and cracks propagate (the boundary layer free from helium bubbles prevents crack propagation).

Discussion and Conclusions. An inhomogeneous tangential-stress distribution arises on ion bombardment of a material having an uneven distribution of the implanted helium, while the surface has a marked effect on the point-defect distribution, and the stresses twice change in direction over a distance equal to the maximum range of the ions in the material. Therefore, there are two zones of zero tangential stress in the implanted layer: near the frontal surface and at the end of the ion range. These zones are the preferential sites of gas-bubble formation, which results in two maxima on the size distribution curve for the blisters. This would explain why the thicknesses of the tops of the main (large) blisters at low ion image always exceed the projected range of the ions, and this explanation does not conflict with the theory of gas cavities and blisters [16].

The release of the implanted helium and the formation of bubbles in the zone with zero tangential stresses must inevitably be dependent on the energy parameters of the point defects and the helium in the lattice. For example, helium in molybdenum behaves differently from that in nickel, which is due to differences in the energies of formation of the point defects and complexes with helium. In molybdenum, inherent interstitial atoms readily displace helium from He—V complexes [17]. This results in redistribution of the implanted helium, part of which is desorbed, while the other atoms are deposited in the surface zone (thickness < 0.01 μm if one judges from the size of the small blisters). A similar displacement may occur in the He_2V and He_3V complexes. Such processes are not favored by energy in a pure fcc metal. In fact, in nickel two interstitial helium atoms displace an atom of the metal. However, various alloying elements (Fe, Cr, Mo, Nb, C, N, B, Zr, etc.) alter the energy for the formation of radiation defects, and as a result helium is displaced from traps and emerges on the surface.

Isothermal annealing of steel at 1023°K for 1 h [13] results in decomposition of the helium-bearing complexes (type $He_n V_m$) and diffusion of the helium to the surface, which also gives two peaks in the helium distribution in depth and therefore two peaks on the blister size distribution.

Therefore, it is difficult to explain the complicated effects of alloying elements and thermal and mechanical treatment on radiation blistering and erosion. These elements and treatments influence the distributions of the minor components and also the microstructure and physicomechanical properties, and they thus influence all stages in the radiation damage to the surface: in the formation of clusters of point defects and complexes, in the formation of helium bubbles, and in the combination of these into cavities (i.e., in blister formation),

Declassified and Approved For Release 2013/03/04 : CIA-RDP10-02196R000300010004-7

Declassified and Approved For Release 2013/03/04 : CIA-RDP10-02196R000300010004-7

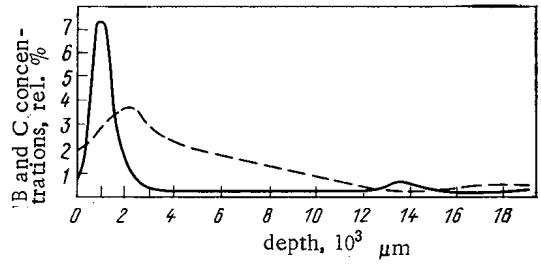

Fig. 6. Distributions of boron (solid line) and carbon (broken line) in OKh16N15M3BR steel on irradiation with He^+ with E = 20 keV, D = 2 × 10^{21} ion/m^2, T_{irr} < 370°K; processing: austenitization + rolling + annealing at 1320°K for 0.5 h.

as well as in disruption of the surface layer. However, during the ion implantation, before the blistering starts one gets very high helium concentrations at a certain depth (up to 1 He atom per Me atom [17]), which should eliminate the differences in the processes preceding the formation of helium bubbles, while also greatly affecting the mechanical properties of the implanted layer and producing microcracks. The course of the subsequent damage recorded from the topography is still dependent on the alloying and heat treatment. Consequently, both of these influence the microdamage. The level of the stresses arising from the helium implantation is important in the production of blisters and erosion (by the detachment of blister tops or flaking), and the same applies as regards the tendency to stress relaxation.

A difference from the vacancy swelling observed on fast-neutron irradiation is that the formation of pores in the material bombarded by helium ions is decisively influenced by the excess number of gas atoms, which at an early stage form complexes of the types He_nV_m, He_KI_l, etc. with vacancies, interstitial atoms, and atoms of alloying components [18-21].

Radiation swelling is particularly reduced by alloying a metal with an element whose atoms are different in size from the solvent [22, 23], and this applies particularly to elements of small atomic radius. For example, alloying nickel with beryllium, carbon, or silicon more greatly suppresses vacancy swelling than does alloying with molybdenum, titanium, aluminum, and so on [23]. It is assumed that the suppression is produced by attachment of point defects to atoms of the alloying elements [24]. However, one gets the contrary effect on implanting helium: Alloying increases the erosion of a chromium–nickel material. The swelling produced by neutrons is similar to that produced by helium only in the early stages of complex formation, i.e., before helium bubbles are formed. By the time blisters appear, one should already speak of embrittlement in the irradiated layer. The alloying elements harden the solid solution and also alter other properties of the matrix [25], which evidently favors damage from ion implantation. In that case, relaxation of the stresses arising on bombardment occurs mainly not by plastic deformation (radiation creep) but by cracking.

Radiation-stimulated impurity diffusion should also play a certain part in the embrittlement and surface damage. For example, we have made secondary-ion emission studies with the SMI-300 Cameca microanalyzer along with Auger measurements, which have shown that helium bombardment produces a prominent maximum in the contents of carbon and boton, and also segregation of chromium in the surface layer (Fig. 6). This indicates that the deterioration in the erosion resistance is due to change in the mechanical properties of a thin surface layer arising from supersaturation with boron, carbon, and other interstitial components, since the depth at which these lie in the irradiated layer corresponds to the thickness of the blister tops (∿0.15 μm for He^+ of energy 20 keV).

Redistribution of the alloying elements is one of the reasons why heat treatment influences the radiation erosion. For example, the austenitization conditions control the distribution of carbon between the solid solution, the carbonitrides Nb(C, N), and the carbides (Fig. 7a). The carbides dissolve, as do the carbonitrides partially, as the austenitization temperature is raised, and the process is more rapid at the grain boundaries (Table 4). After annealing at 1390°K for 30 min (steel 16-15) or at 1470°K for 5 h (alloy 20-45), the austenite is supersaturated with carbon, molybdenum, niobium, chromium, and other elements, which results in many elastically distorted regions in the solid-solution matrix. Although the

Declassified and Approved For Release 2013/03/04 : CIA-RDP10-02196R000300010004-7

Declassified and Approved For Release 2013/03/04 : CIA-RDP10-02196R000300010004-7

TABLE 4. Effects of Heat Treatment on the Parameters of Deposits and the Dislocation Density in 20-45 Nickel Alloys

Heat treatment	Size d of deposits, μm		Deposit density		dislocation density $\rho_d \times 10^{-13}$, m^{-2}
	Along boundaries	in grains	on boundaries, $\rho_b \times 10^{-6}$, m^{-1}	in grain, $\rho_g \times 10^{-12}$ m^{-2}	
1170 °K, 1 h	0,02—0,18	0,03—0,24	15±2	6±1	7±3
1320 °K, 1 h	0,05—0,14	0,04—0,30	7±2	5±1	5±2
1470 °K, 5 h	0,08—0,10	0,05—0,39	3±1	2±1	2±1

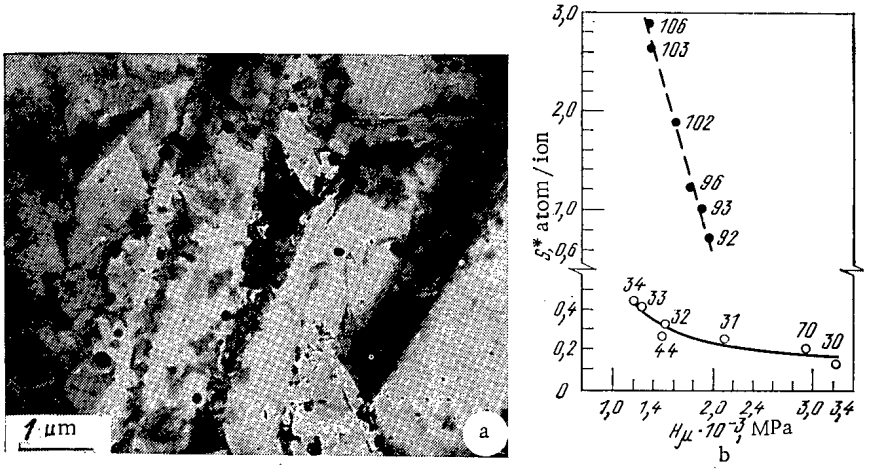

Fig. 7. Microstructure of 03Kh20N45M4BCh alloys annealed at 1320°K for 1 h (a) and correlation between the surface damage (erosion coefficient) and microhardness for steels 16-15 (solid line) and nickel alloys 20-45 (broken line) on irradiation with He^+ with E = 40 keV and D = 1 × 10^{22} ion/m^2 (●) and 2 × 10^{22} ion/m^2 (○): 30, 70) annealing at 1320°K for 5 h + rolling; 31) 1170°K, 1 h + CD 20%; 32) 1170°K 1 h; 92, 102) 1170°K, 15 min; 33) 1320°K, 0.5 h; 93, 103) 1320°K, 1 h; 34, 44) 1390°K, 0.5 h; 96, 106) 1470°K, 5 h.

strength of the matrix on the whole is slightly reduced, as is indicated by the reduction in microhardness after high-temperature annealing (Fig. 7b) and by the fall in dislocation density and the dissolution of dispersed deposits (Table 4), one gets segregation of the interstitial atoms at the surface, e.g., carbon and boron (Fig. 6). This alters the structural state of the surface and produces conditions for large helium bubbles to arise and cracks to originate in response to the gas pressure and the tangential stresses. Subsequent microcrack propagation in the surface layer results in extensive exfoliation, i.e., as occurs in the highly alloyed material 20-45 (106) annealed at 1470°K for 5 h (Fig. 1f).

Deformed and rolled specimens have strength characteristics higher than those found in annealed ones, which reduces the number of failed blisters and thus the erosion. Also, the pressure working produces a highly developed dislocation structure, with grain crushing, which results in numerous failed grain boundaries and subgrains. The dislocations and grain boundaries are vigorous traps for the helium atoms and the vacancies produced by irradiation, and they retard the formation of gas bubbles and therefore ultimately increase the critical dose for exfoliation.

Therefore, appropriate alloying and microalloying can be used with choice of the thermomechanical treatment conditions to reduce the erosion on irradiation by average doses of

Declassified and Approved For Release 2013/03/04 : CIA-RDP10-02196R000300010004-7

Declassified and Approved For Release 2013/03/04 : CIA-RDP10-02196R000300010004-7
helium ions. The austenitic chromium–nickel steels 18-10 and 16-15 are more resistant to erosion than high-nickel materials, which is of definite practical significance in selecting materials for a fusion reactor.

LITERATURE CITED

1. J. Davis and J. Kulcinski, Nucl. Fusion, 16, No. 2, 355 (1976).
2. I. V. Al'tovskii et al., NIIEFA Preprint A-0434, Leningrad (1979).
3. I. V. Gorynin et al., in: Reactor Materials Sciences. Proceedings of the Conference on Reactor Materials Science [in Russian], TsNIIatominform, Moscow (1978), p. 273.
4. A. M. Parshin, Atomic Science and Engineering. Series Physics of Radiation Damage and Radiation Materials Science [in Russian], Issue 3(14), p. 20 (1980).
5. G. I. Zabrev et al., in: Proceedings of the All-Union Conference on the Engineering Problems of Fusion Reactors [in Russian], NIIEFA, Leningrad (1977), p. 242.
6. V. M. Gusev et al., Preprint IAE-3145, Moscow (1979).
7. B. A. Kalin et al., [4], Issue 2(13), p. 72 (1980).
8. L. B. Bergambekov et al., in: Proceedings of the Fourth All-Union Conference on the Interactions of Atomic Particles with Solids [in Russian], Kharkov Physicotechnical Inst. (1976), p. 100.
9. V. M. Gusev et al., Prib. Tekh. Eksp., 4, 19 (1969).
10. P. Hirsch et al., Electron Microscopy of Thin Crystals [Russian translation], Mir, Moscow (1968).
11. A. A. Gusakov et al., Zavod. Lab., 44, No. 1, 37 (1978).
12. A. D. Gurov et al., At. Energ., 40, No. 3, 254 (1976).
13. D. M. Skorov et al., [4], Issue 1(6), 46 (1978).
14. B. A. Kalin et al., At. Energ., 49, No. 2, 132 (1980).
15. F. Garner et al., in: Proceedings of the International Conference on Radiation Effects and Tritium Technology for Fusion Reactors, Gatlinburg, CONF-750959 (1975), p. 474.
16. J. Evans, J. Nucl. Mater., 68, No. 2, 129 (1977).
17. A. P. Zakharov, Interaction of Hydrogen with Radiation Defects in Metals: Dissertation [in Russian], Inst. Fiz. Khim., Moscow (1980).
18. A. Van Veen and L. Caspers, Solid-State Commun., 30, 761 (1979).
19. R. Fastenau et al., Phys. Status Solidi (a), 47, 577 (1978).
20. L. Caspers et al., ibid., 52, K61 (1979).
21. D. Reed, Radiat. Effects, 31, 129 (1977).
22. J. Ellis et al., J. Trans. Am. Nucl. Soc., 21, 153 (1975).
23. D. Potter and P. Okamoto, in: Proceedings of the International Conference on Radiation Effects in Breeder Reactor Structural Materials. Progr. with Abstracts, Scottsdale (1977), p. 22.
24. J. Mansur and M. Yoo, J. Nucl. Mater., 74, No. 2, 228 (1978).
25. A. M. Parshin, Structure, Strength, and Plasticity of Stainless and Heat-Resisting Steels and Alloys used in Shipbuilding [in Russian], Sudostroenie, Leningrad (1972).

Declassified and Approved For Release 2013/03/04 : CIA-RDP10-02196R000300010004-7

Declassified and Approved For Release 2013/03/04 : CIA-RDP10-02196R000300010004-7

RESULTS WITH PILOT BITUMENING PLANTS

I. A. Sobolev, L. M. Khomchik,
V. V. Kulichenko, N. A. Rakov,
S. A. Dmitriev, and V. M. Chebyshev

UDC 621.039.73

To provide reliable final storage of low-level and medium-level wastes, a process of incorporating these into bitumen has been developed in the USSR. Research on this process was begun at the Central Radiation Safety Station in 1967. The initial product consisted of solutions remaining after the evaporation of low-concentration radioactive wastes. The average composition is given below (in some experiments borax was added to this, which is usually present in the wastes from nuclear power stations with boron control):

Concentration, g/liter:

salt residue	500-600
sodium nitrate	450-500
suspended particles	100-150
hydrated iron oxide	50-100
surfactants	20-30
pH	10-12
Specific β activity, MBq/liter	1.85-37
Main radionuclides	^{90}Sr, ^{134}Cs, ^{137}Cs, ^{60}Co
Density, kg/cm^3	1.3-1.4

In 1970, a batch-operation hot-mixing apparatus was built based on a BO-75 bitumenizer (vertical mixing vessel with blade stirrer). Heat was supplied to the mass by electric heaters of power 70 kW placed between the wall of the apparatus and the mixer. The working volume of the reactor was 0.3 m^3, while the throughput was up to 60 liter/h on the initial solution.

During the operation, studies were made to develop the bitumening process and to reveal the physicochemical features of the bitumen products [1]. Bitumens of various grades and asphalt from petroleum refining were used. A water-wet emulsion was used to remove the salt-bitumen deposits formed on the heating surfaces when local overheating occurred. At the same time, some serious disadvantages of apparatus of this type were identified, in particular the formation of foam on supplying liquid wastes to the surface of the molten bitumen, together with the low throughput and the possibility of the formation of chars on the heating surface when the heat flux was increased, and therefore such systems are undesirable for units of high throughput.

Technological studies in 1974-75 were used in a high-productivity system (the UBD-200) for continuous bitumening of liquid radioactive wastes [2].

The process was divided into two stages in order to provide an acceleration: in the first, the wastes were dewatered to give salts of a particular water content (heated roll dryers were used), while in the second the moist salts were mixed the molten bitumen and at the same time were finally dried, and the resulting bitumen compound was transported to the unloading section (a screw conveyer was used).

The apparatus (Fig. 1) consists of four dryers with a heated surface of 2.5 m^2 each, a two-screw mixer of throughput up to 1200 kg/h, units for transporting and dispensing the wastes in the bitumen, systems for purifying the steam–gas mixture, a salt-transportation unit, a system for heating the mixture, and a unit for removing the bitumen compound. The dryers were heated by spiral electric heaters placed within the rolls, while the mixer and the unloading unit were heated by a high-temperature organic material (ditolylmethane) with forced circulation (temperature 180°C).

Translated from Atomnaya Énergiya, Vol. 53, No. 4, pp. 250-255, October, 1982. Original article submitted December 7, 1981.

0038-531X/82/5304-0707$07.50 © 1983 Plenum Publishing Corporation

Declassified and Approved For Release 2013/03/04 : CIA-RDP10-02196R000300010004-7

Declassified and Approved For Release 2013/03/04 : CIA-RDP10-02196R000300010004-7

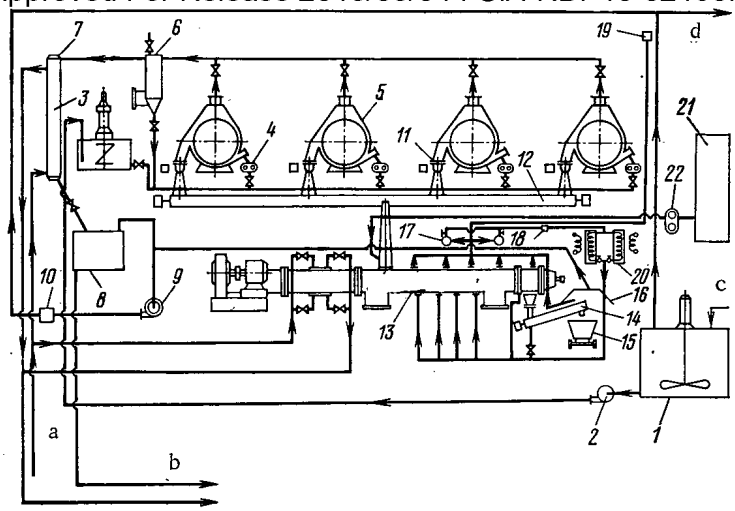

Fig. 1. Two-stage apparatus for bitumenizing liquid radioactive wastes type UBD-200: 1) waste collector; 2) centrifugal pump; 3) intermediate vessel; 4) pump feeding wastes to dryer; 5) dryer; 6) dust trap; 7) heat exchanger; 8) condensate collector; 9) fan; 10) fine-filtration unit; 11) worm for unloading salt from dryer; 12) worm feeding salt to mixer; 13) mixer; 14) worm for unloading compound; 15) shaping mold; 16) extraction hood; 17) pump for circulating heat carrier; 18) gas separator; 19) expansion tank; 20) heat generator; 21) bitumen store; 22) bitumen feed pump; a) cooling water; b) to station for handling low-activity wastes or to drain; c) liquid radioactive wastes; d) extraction ventilation.

The apparatus works continuously. The liquid wastes are pumped by gear pumps from the intermediate vessel into the dryer tanks. As the shafts rotate, a film of liquid waste is dried out in one rotation, and the salts crystallize. The steam-gas mixture leaving the dryer passes through a separator filter, a heat exchanger and condenser, and fine-filtration units. The salts from the rolls are transported by screws to the mixer, which is supplied by bitumen from the store at a temperature of 160°C by a gear pump. The water content of the salts entering the mixture is 15-17%, as against 4-5% at the exit from the mixture; the throughput of the mixture as regards evaporated water is ∿20 liter/h, while the time spent by the salts in it is ∿2 min. The choice of optimum salt water content provides with the above maximum throughput for minimum transfer of the salts into the steam-gas phase. The purification factor for the condensate is 3×10^3-5×10^4.

The amount of salt that can be mixed with the bitumen in this apparatus is almost unlimited. However, the mixture becomes inhomogeneous if the salt content is more than 80% and one can see salt crystals that are not enclosed in bitumen.

The salt–bitumen product is unloaded from the mixer at a temperature of 125-130°C into shaping vessels of volume 0.5 m^3. The matrix material is a BNK-2 bitumen (softening and boiling temperatures 38 and 240°C respectively, penetration 18.3 mm).

The mean daily throughput of the apparatus is 200 liter/h on the initial product with an energy consumption of 1500 $kW \cdot h/m^3$ of initial solution.

Operation of the UBD-200 for two years revealed the following deficiencies in the two-stage bitumening in this way:

1) the poor viability of some units, particularly those related to intermediate salt transfer;

2) complicated design and complicated servicing;

3) large specific energy consumption.

Declassified and Approved For Release 2013/03/04 : CIA-RDP10-02196R000300010004-7

Declassified and Approved For Release 2013/03/04 : CIA-RDP10-02196R000300010004-7

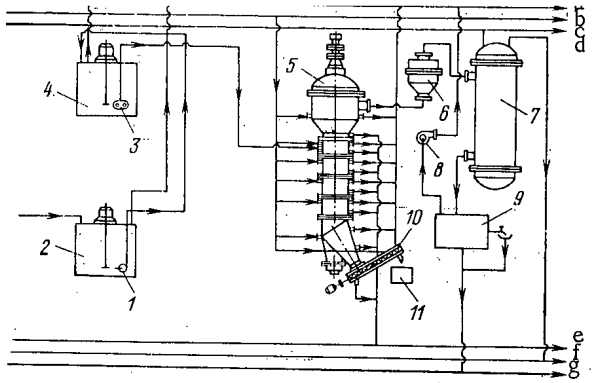

Fig. 2. Apparatus for bitumenizing liquid radioactive wastes type URB-8: 1) waste feed pump; 2) waste receiving vessel; 3) immersed dispensing pump; 4) intermediate vessel; 5) KRP-600-8S rotor film evaporator; 6) separator filter; 7) heat exchanger; 8) fan; 9) condensate-collection vessel; 10) screw transporter; 11) vessel for bitumen compound; a) blower; b) local extraction; c) steam; d) water; e) steam condensate; f) cooling water; g) special drain.

This gave interest to a one-stage continuous bitumening process using, in particular, rotor film evaporators, where the water evaporates from a thin film flowing down a heated vertical cylindrical wall of wastes and bitumen. A thin layer of solution and bitumen is mixed by blades attached to a rotating vertical rotor, which intensify the heat and mass transfer and at the same time clean the heating surface, which is heated by technical steam.

In 1978, the URB-8 apparatus was commissioned at the station (Fig. 2), which employed a standard KRP-600-8S film rotor evaporator used in deep watering chemical products. This apparatus includes equipment for temporary storage and dispensing of liquid wastes and bitumen, the rotor bitumenizer, a heat exchanger and condenser, apparatus for cleaning the steam—gas mixture, a system for unloading the bitumen—salt mixture (compound), and mobile vessels for solidifying it.

The KRP-600-85S is made of 12Kh18N10T steel and consists of a body, a rotor with drive, and sealing and bearing units. The body of the apparatus is a cylinder with a separator in the upper part and steam-heating jackets. According to the technical characteristics of the evaporator, the heat-transfer surface is 8 m^2, the speed of the rotor is 59 rpm, the height is 12 m, the internal diameter of the body is 0.6 m, and the pressure of the heating steam is up to 1621.2 kPa. The rotor takes the form of a shaft bearing disks, with hinged blades. In the upper part of the shaft there is a distribution ring, which provides for uniform supply of the components to the wall of the bitumenizer.

The technological scheme (Fig. 2) is as follows. The liquid wastes pass from a receiving vessel of volume 3.5 m^3 through a feed pump (up to 3 m^3/h) to another intermediate vessel, from which they are transferred by a gear pump (0.1-0.7 m^3/h) to the distribution ring. A gear pump supplies the molten bitumen (temperature 130°C) from a store. The wastes and the bitumen pass from the distribution ring over the internal heated surface, where they encounter the blades on the rotor, and they are mixed and distributed over the surface as a descending film. The water evaporates as the film moves downwards. The dehydrated bitumen compound is unloaded into vessels by a screw transporter. The internal surfaces of the vessels are lined with paper, and frames are fitted into them with projecting hooks for removing the solidified blocks.

The steam—gas mixture is partially freed from the condensed phase in a centrifugal separator in the upper part of the evaporator. Then the mixture passes to a gridded separator filter having several layers of filter grid made of 12Kh18N10T steel. The purified steam—gas mixture passes through a heat exchanger, where the water condenses and flows into a collector.

Declassified and Approved For Release 2013/03/04 : CIA-RDP10-02196R000300010004-7

Declassified and Approved For Release 2013/03/04 : CIA-RDP10-02196R000300010004-7

TABLE 1. Properties of Bitumens

Properties	BN-2 BNK-2	BN-3	BN-4
Penetration (using a needle at 25°C), 0.1 mm	81—180	41—80	21—40
Softening temperature	40	45	70
Boiling temperature in open crucible, °C (not less than)	240	200	230

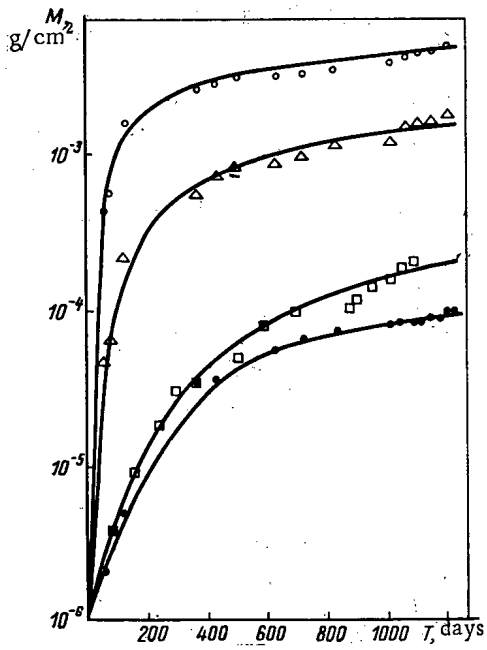

Fig. 3

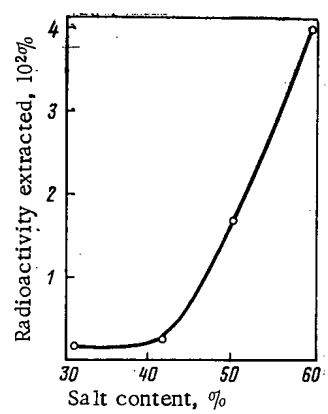

Fig. 4

Fig. 3. Dependence of escape of radionuclides from bitumenized wastes (bitumen BNK-2) on degree of filling: ○, △, □, ●) salt contents of 59, 50, 42.3, and 32%; specific radioactivities 2.59, 7.4, 0.41, and 5.18 mBq/m³, respectively.

Fig. 4. Effects of salt filling on relative radioactivity of nuclides escaping from bitumenized wastes (○ from experiment).

Then the gas flow passes through a system of fine-filtration units (the first stage is provided by Lavsan fiber and the second by FP cloth) and is discharged through a chimney into the atmosphere.

The apparatus was operated for 800 h during trials and routine working. The specific throughput from 1 m² of heating surface under optimum conditions was 60 liter/h (on the actual product) at a heating-steam pressure of 810.6 kPa. The mean daily throughput of the bitumenizer was 400-420 liter/h with a specific energy consumption of ∿1000 kWh/m³ of initial solution. The optimum salt incorporation was 60% from the viewpoint of the process (the unloading from the apparatus ceases at a higher salt content on account of the increase in viscosity). The water content of the compound does not exceed 5%, and the fall in temperature is 125-135°C, when the viscosity of the product is in the range 45-60 P (4.5-6 Pa·sec).

The purification factor on the β activity in the apparatus working with the steam-gas flow was 5-6 × 10^5, where the purification coefficient in the separator filter was 2.4-2.5 ×

Declassified and Approved For Release 2013/03/04 : CIA-RDP10-02196R000300010004-7

Declassified and Approved For Release 2013/03/04 : CIA-RDP10-02196R000300010004-7
10^2, and the specific radioactivity of the stack gas on average was 1.3 MBq/m^3; the oil content of the condensate was not more than 15-20 mg/liter, while the salt content was not more than 150 mg/liter. Experience with the URB-8 showed that the equipment was viable and simple to service and monitor, while the entire system was suitable for routing use.

In parallel with this development and testing, the station examined the migration of radionuclides from the bitumen blocks. The scope for storing radioactive wastes directly in the ground is largely determined by the geological and hydrological conditions.

Since 1968, we have performed experimental storage of bitumenized radioactive rocks in the ground and on an open area [1]. The experimental area was on a water-divide surface and had hindered surface runoff. The first aquifer with a pressure up to 10-15 m was associated with Upper Cretaceous beds. The depth of the top of the aquifer in the storage area was 74 m. This aquifer had infiltration supply without flow into rivers. The filtration coefficient for the water-bearing beds varied from 0.2 to 4.0 m/day. The rocks overlying the aquifer consisted of moraine beds composed of clays and loams of thickness up to 74 m. The filtration coefficients for the clays and bands of loam were 0.004 and 0.038 m/day, respectively.

Surface waters were fairly abundant, so the water content of the soil at a depth of 2-2.5 m was 27-30%. The soils covering the first aquifer were composed to 11-30% of clayey particles, and mineralogically these were represented by kaolinite, montmorillonite, and hydromicas, which were responsible for the low water permeability and good sorption. For example, the ion-exchange capacity of these beds ranges from 15 to 36 mg-eq/100 g, while the separation coefficients for ^{90}Sr and ^{137}Cs are, respectively, 140 and 800. On the whole, the geological and hydrological conditions are favorable and should rule out the entry of radionuclides to the first aquifer.

Experimental storage was performed with bitumen blocks obtained by processing radioactive wastes of specific activity 0.37-37 MBq/liter. We used bitumens of grades BNK-2, BN-2, BN-3, and BN-4 (Table 1). The radioactivity of the waste was due in the main to ^{137}Cs (up to 90%) and ^{90}Sr (up to 8%), while the salt composition of the wastes was 80% sodium nitrate.

In the experimental area, the specimens were in open racks made of stainless steel, which were installed on bases equipped to collect the precipitation that had been in contact with the bitumen. To examine the behavior of the bitumenized wastes in open ground, special experimental stores were built (trenches of depth 1-2 m) into which the bitumen products were loaded as blocks (1150 × 740 × 800 mm) in two ways: directly on the ground and on a metal base equipped to take samples of water. This monitoring of the water samples indicated the amount of radionuclide entering the water. The stores in which the blocks lay directly on the open soil were opened up to examine the contamination aureole.

Figures 3 and 4 show the dependence of the radionuclide leaching on the salt content. As in the case of laboratory experiments, most of the radionuclide leaching occurred during the initial period of storage, after which the leaching rate fell considerably. A product with a salt concentration of 32% released 17 kBq into the water in 1215 days (1.4×10^{-3}% of the initial radioactivity); at 42% salt, the release was 2.3 kBq in 1084 days (1.5×10^{-3}%), at 50% it was 407 kBq in 1215 days (1.7×10^{-2}%), and at 59% in the same time it was 407 kBq (4.0×10^{-2}%). The field studies thus confirmed that it is undesirable to increase the concentration of soluble salts in the bitumen above 40-45% (results obtained with BNK-2 bitumen). Figure 5 and Table 2 show the effects of bitumen type on the leaching.

TABLE 2. Escape of Radionuclides into Water in 1215 Days

Bitumen	Salt concentration, mass %	Total activity in the water, kBq	Radioactivity extracted
BN K-2	32	17	$1 \cdot 10^{-3}$
BN K-2	46	2,7	$1 \cdot 10^{-3}$
BN 2	44	6,8	$2 \cdot 10^{-4}$
BN-3	28	25	$4 \cdot 10^{-3}$
BN-4	27	520	$8 \cdot 10^{-2}$

Declassified and Approved For Release 2013/03/04 : CIA-RDP10-02196R000300010004-7

Declassified and Approved For Release 2013/03/04 : CIA-RDP10-02196R000300010004-7

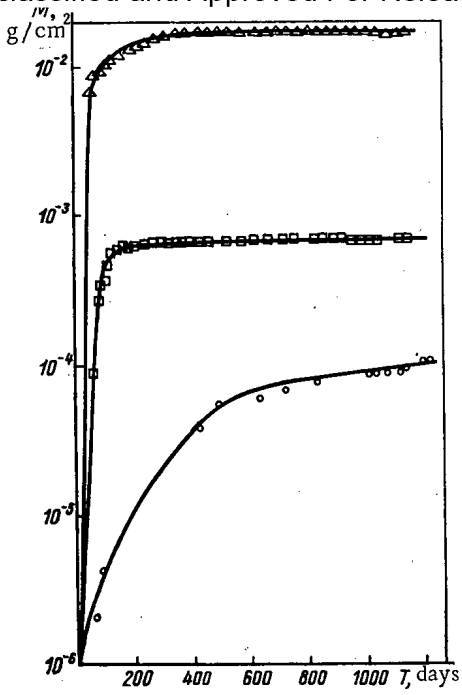

Fig. 5

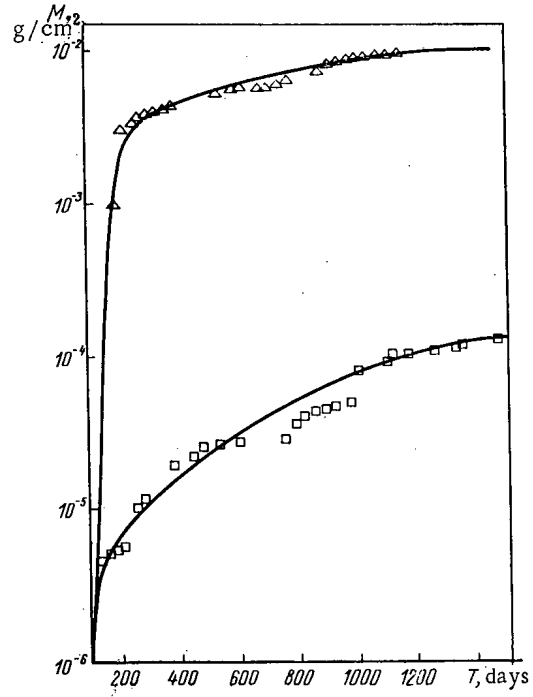

Fig. 6

Fig. 5. Dependence of escape of radionuclides from bitumenized wastes on type of bitumen: △, □, ○) bitumens BN-4, BN-3, and BN-2; salt contents 27.3, 27.7, and 32%, specific radioactivities 0.83, 0.89, and 5.13 mBq, respectively.

Fig. 6. Escape of radionuclides from bitumenized wastes using bitumen BNK-2 alone (Δ) with the addition of potassium–nickel ferrocyanide (□).

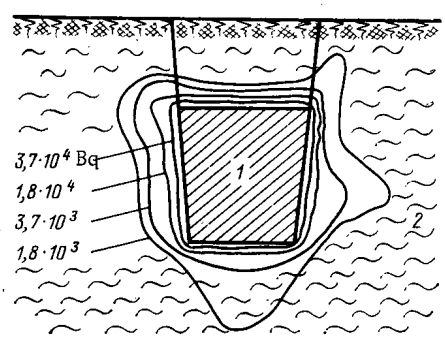

Fig. 7. Distribution of radioactivity (numbers on curves) in soil around bitumen block in store: 1) bitumen block; 2) surrounding soil.

It was difficult to evaluate the differential trapping of the radionuclides from water analysis for bitumen blocks stored in the ground because of the partial sorption of the radionuclides in the soil (laboratory tests have shown that the leaching rate for cesium is higher than that for strontium).

We determined the radionuclide contents in water that had been in contact with the bitumenized wastes on storage in the ground and found that after 1215 days the yields of ^{90}Sr, ^{60}Co, and ^{137}Cs were 2.4×10^{-2}, 7.0×10^{-3}, and 2.3×10^{-3} g/cm². The proportions of the radioactivity due to ^{90}Sr and ^{60}Co decreased with the passage of time, while therefore ^{137}Cs tended to increase, evidently because the cesium is taken up more vigorously by the soil than

Declassified and Approved For Release 2013/03/04 : CIA-RDP10-02196R000300010004-7

Declassified and Approved For Release 2013/03/04 : CIA-RDP10-02196R000300010004-7
are strontium and cobalt. With the passage of time however, the ground becomes saturated on account of the sorption of sodium, which is eluted from the block, and therefore the uptake of cesium decreases, while the content in the water increases. If the wastes contain borax (>10 g/liter), the bitumen blocks have low water stability. In that case, the properties of the blocks are considerably improved by introducing a small amount of potassium–nickel ferrocyanide (Fig. 6).

There is considerable interest in the distribution of the radionuclides around bitumen blocks stored in the open soil for 11 years (thickness of soil over a block 0.6 m). We examined soil specimens taken at various distances from a block. Figure 7 shows that the maximum radioactivity occurs directly under a block (36 kBq/kg). The maximum distance at which the radioactivity of the soil exceeded the background value (the background specific radioactivity of the loam 1.71 kBq/kg) range from 40 to 26 cm, i.e., the migration speed was 3.6–2.5 cm/yr, which is less by a factor 10–15 than the rate of propagation of radionuclides from cement blocks stored in the same soil [3]. Also, the bitumen blocks were well preserved after 11 years storage in the open soil, in spite of the long-term action of the moist soil, and the freezing and thawing that occurred because of the shallow depth. The boundary between the bitumen and the soil was sharp, and the bitumen was plastic and lustrous in section.

It has thus been found that liquid radioactive wastes can be incorporated into bitumen in equipments of various designs. The rotor film evaporator is the most promising. The reliable trapping of the radionuclides in the bitumen compound is confirmed by observations on bitumen blocks from prolonged storage in open soil.

LITERATURE CITED

1. O. I. Volkova et al., in: Management of Low and Intermediate-Level Radioactive Wastes. IAEA, Vienna (1970), p. 725.
2. I. A. Sobolev, in: Researches on the Management of Liquid, Solid, and Gaseous Radioactive Wastes and Decontamination of Contaminated Surfaces [in Russian], Issue 2, Atomizdat, Moscow (1978), p. 67.
3. I. A. Sobolev et al., in: Proceedings of the Conference IAEA on Disposal of Radioactive Wastes in the Ground. IAEA, Vienna (1967), p. 37.

Declassified and Approved For Release 2013/03/04 : CIA-RDP10-02196R000300010004-7

Declassified and Approved For Release 2013/03/04 : CIA-RDP10-02196R000300010004-7

PROSPECTS FOR THE DEVELOPMENT OF NEUTRON-ACTIVATION ANALYTICAL FACILITIES BASED ON POWERFUL ANTIMONY—BERYLLIUM SOURCES

G. N. Flerov, Yu. N. Burmistenko,
Yu. V. Dyadin, Yu. S. Zamyatnin,
A. A. Medvedev, A. A. Sal'nikov,
and Yu. G. Teterev

UDC 550.835

During the last decade, both in the Soviet Union and abroad, work on the construction of neutron-activation analytical facilities with nuclide neutron sources has been widely developed [1-3]. This is because these facilities, in which the content of the elements being analyzed amounts to 10^{-3}-10^{-5} mass %, are of the greatest importance for analytical monitoring. In this case, fot the activation of samples a neutron flux density of 10^6-10^8 neutrons/($cm^2 \cdot sec$) is sufficient, which can be provided by means of neutron sources giving a yield of 10^8-10^{10} neutrons/sec: sources based on spontaneously fissile ^{252}Cf have acquired the greatest popularity [4, 5]. Based on these sources with a yield of 10^8-10^{10} neutrons/sec, several experimental facilities have been constructed by the Institute of Nuclear Physics of the Academy of Sciences of the Uzbek SSR, the Institute of Chemistry Far-Eastern Research Center, the All-Union Scientific-Research Institute of Nuclear Geophysics and Geochemistry, the Yansk Geological Exploration Expedition, and the North-Eastern Industrial Society [6, 7].

Together with these sources, there is great practical interest in the problem of the use for these same purposes of powerful antomony—beryllium neutron sources, the most important advantages of which are the "soft" neutron spectrum, providing a high contribution in the resonance region of energy; the absence of fast neutrons, excluding the possibility of interfering reactions taking place; a low cost of the source [8]; and simplicity of transportation (after removal of the antimony-124 source from the beryllium block, only shielding from γ-radiation is required).

The wide application of ^{124}Sb sources is limited by the short half-life ($T_{1/2}$ = 60 days) and the high specific γ-activity, requiring heavy shielding. However, with the modern level of development of shielding technology, operations with these sources do not cause difficulties, and the present-day network of research and power nuclear reactors can ensure the production and regeneration of the activity of a large number ^{124}Sb sources.

Many works [8-11] have deen devoted to the study of the feasibility of ^{124}Sb—Be neutron sources for activation analysis. The antimony—beryllium sources used in them for the most part were ampuled rods of activated metallic antimony, surrounded by converter of metallic beryllium with a mass of 50-100 g [8]. With this design of source, the utilization factor of the ^{124}Sb is small, since the major part of the quanta passes through the layer of beryllium without interaction. Moreover, in these experiments, hydrogen-containing moderators were used (water, paraffin), which leads to a high neutron flux gradient in the region of location of the samples and to a low contribution in the resonance region of the neutron energy.

The authors of the present paper during 1979-1981 conducted a cycle of investigations directed at an assessment of the applicability of powerful antimony—beryllium neutron sources for activation analysis, the optimization of moderating compositions, a study of the conditions of manufacture of powerful ^{124}Sb sources, the construction of experimental facilities, and the conduct on them of experimental work on the development of activation analysis procedures [12-14]. Staff of the Laboratory of Nuclear Reactions of the Joint Institute for Nuclear Research, the Faculty of Nuclear-Radiometric Methods of the S. Ordzhonikidze Geologi-

Translated from Atomnaya Énergiya, Vol. 53, No. 4, pp. 255-260, October, 1982. Original article submitted March 9, 1982.

 0038-531X/82/5304-0714$07.50 © 1983 Plenum Publishing Corporation

Declassified and Approved For Release 2013/03/04 : CIA-RDP10-02196R000300010004-7

Declassified and Approved For Release 2013/03/04 : CIA-RDP10-02196R000300010004-7

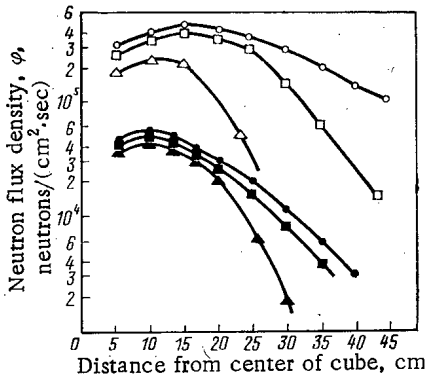

Fig. 1

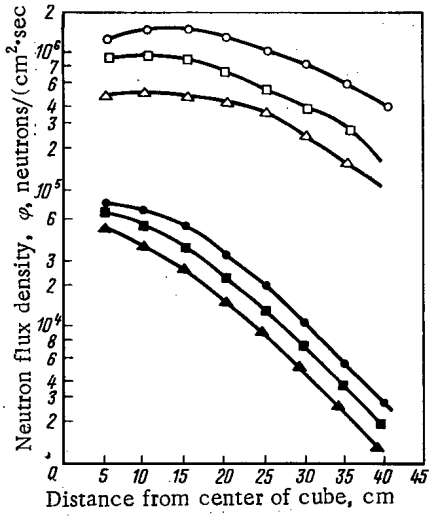

Fig. 2

Fig. 1. Spatial distribution of the flux density of thermal (●, □, △) and resonance (●, ■, ▲) neutrons in graphite cubes of different dimensions. Beryllium block 28 × 28 × 20 cm. Activity of ^{124}Sb, 50 Ci: ○, ●) side of cube 90 cm; □, ■) 70 cm; △, ▲) 50 cm.

Fig. 2. Spatial distribution of the flux density of thermal and resonance neutrons in beryllium blocks of different dimensions. Graphite cube 70 × 70 × 70 cm. Activity of ^{124}Sb, 50 Ci: ○, ●) dimensions of block 48 × 48 × 20 cm; □, ■) 28 × 28 × 20 cm; △, ▲) 18 × 18 × 10 cm.

cal Prospecting Institute, Moscow, and the Institute of Theoretical and Experimental Physics participated in the work.

The main difference between our work and the previous ones, is the use of beryllium converters of large mass (in this case the beryllium is used simultaneously as the material generating the neutrons and also as part of the moderating composition) and also neutron moderators and reflectors not containing hydrogen. This has led to a new quality of the irradiation facility: The gradient of the neutron flux density has been reduced significantly; it has allowed large batches of samples to be irradiated simultaneously, and the flux density of resonance neutrons has been increased significantly.

Neutrons Fields of an Antimony–Beryllium Source in a Beryllium–Graphite Composition. The dependence of the spatial distribution of the neutron flux density on the dimensions of the beryllium block and the graphite reflector was studied experimentally by means of the activation of gold foils [13]. The results, which are shown in Figs. 1 and 2, allow the following conclusions to be drawn:

1) The flux density of resonance and epicadmium neutrons, right up to a distance of 20 cm from the center of the cube, is almost constant with increase of the thickness of graphite;

2) the thermal neutron flux density is almost identical for graphite cubes with sides of 70 and 90 cm;

3) with increase of volume of the beryllium block from 3.2 to 4.6 dm^3, the thermal neutron flux density increases by a factor of 3, and the epicadmium and resonance neutrons by a factor of 1.5. This confirms the "softened" spectrum of the neutrons with increase of the amount of beryllium, which is a much better moderator than graphite.

For the purpose of comparison of the ^{124}Sb–Be-source with a spontaneous fission source of ^{252}Cf, the spatial distribution of the neutrons also was measured for the latter. The results of the comparison allowed us to conclude that because of the lower initial energy of the neutrons, the ^{124}Sb–Be source generates a flux density of thermal and resonance neutrons greater by a factor of 2 than the californium source with the same yield [13].

Declassified and Approved For Release 2013/03/04 : CIA-RDP10-02196R000300010004-7

Declassified and Approved For Release 2013/03/04 : CIA-RDP10-02196R000300010004-7

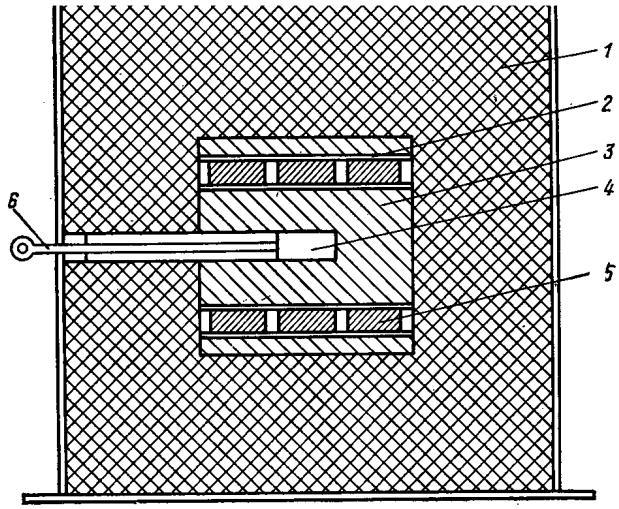

Fig. 3. Antimony–beryllium–graphite assembly in section: 1) graphite 2) cadmium filter; 3) beryllium; 4) container with ^{124}Sb source; 5) samples to be activated; 6) rod.

The data obtained concerning the neutron fields of the antimony–beryllium source in different moderators can be used for the optimization of the moderating assemblies, designed for the neutron-activation analysis of samples. The optimum size of the graphite moderator is a cube with a side of ∿70 cm, and further increase of its dimensions does not lead to an increase of the neutron flux density. It is more complicated to draw and unambiguous conclusion about the optimum dimensions of the beryllium block, because with increase of the mass of beryllium, the flux density of thermal neutrons mainly increases. The choice of dimensions of the beryllium block depends also on the designation of the facility. When using a beryllium block with a mass of ∿30 kg, the thermal neutron flux density per 1 Ci near the center of the cube amounts to $\sim 2 \cdot 10^4$ neutrons/(cm^2·sec), and the resonance neutron flux density is $1.5 \cdot 10^3$ neutrons/(cm^2·sec) per unit interval of lethargy (1 Ci = $3.700 \cdot 10^{10}$ Bq).

Assessment of the Feasibilities of Neutron-Activation Analysis on a Facility with an Antimony–Beryllium Neutron Source. We had previously used an antimony–beryllium source of low activity [12, 13]. The results of these experiments allowed us to estimate the required initial activity of the ^{124}Sb source, to choose the point of location of the samples in the moderating medium and the necessary dimensions of the beryllium block and the graphite moderator. Undoubted promise was shown for the use of antimony–beryllium neutron sources for the activation analysis of the composition of a substance, in particular, geological samples. The main cycle of the experimental work was conducted on a neutron-activation facility with a powerful antimony–beryllium source with an activity of up to 1200 Ci. When constructing the assembly, account was taken of the experimental data concerning the neutron fields of antimony–beryllium sources in different moderators. As the transportation of powerful ^{124}Sb sources has not yet been resolved organizationally, it was advantageous to install the neutron-activation antimony–beryllium–graphite assembly (Fig. 3) in the shielded chamber of a hot laboratory for a nuclear reactor [14]. The assembly consisted of a graphite cube with dimensions of 700 × 700 × 700 mm, inside of which was installed the beryllium block with dimensions of 300 × 300 × 300 mm and with a horizontal channel of 40 × 40-mm cross section. At the center of the beryllium block the container with the ^{124}Sb source was placed, to which was attached a rod for withdrawing the source from the assembly. Inside the beryllium block there were two horizontal slits with a height of 25 mm for placing the samples to be activated.

Figure 4 shows the construction of the ^{124}Sb sources used. The container and cover are made of aluminum. The source is composite, assembled from five separate blocks, each being a cylindrical hermetically sealed aluminum capsule with a diameter of 33 mm and a height of 31.5 mm; inside it is placed a casting of metallic antimony with a mass of 100 g. Each block is irradiated in the reactor in its individual container and then all the blocks are delivered to the hot box and, by means of a remote handler, they are packed into a single container

Declassified and Approved For Release 2013/03/04 : CIA-RDP10-02196R000300010004-7

Declassified and Approved For Release 2013/03/04 : CIA-RDP10-02196R000300010004-7

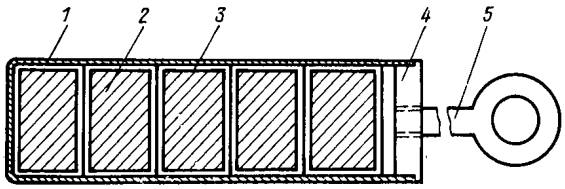

Fig. 4

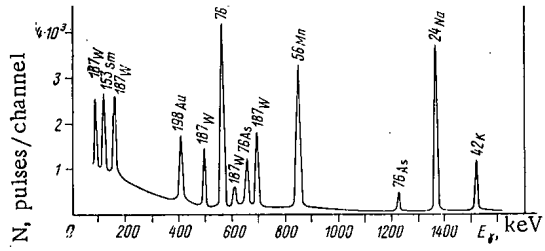

Fig. 5

Fig. 4. Diagram of the construction of the ^{124}Sb source: 1) container body; 2) block of metallic antimony; 3) casing of block; 4) container lid; 5) rod.

Fig. 5. γ-Emission spectrum of the induced activity of a sample of gold-bearing ore irradiated in the antimony–beryllium-graphite assembly. Activity of the ^{124}Sb source ∿400 Ci.

(see Fig. 4). The cells with a diameter of 70 mm and a height of 15 mm, into which the samples to be activated are placed, are made of polyethylene. The mass of the powdered material packed into the cell is 50-80 g. Before being placed in the assembly, the samples are arranged on trays which, if necessary can be screened with a cadmium sheet. At the time of interchanging the samples, the source is withdrawn from the assembly and by means of a conveyer is transferred to an adjoining shielded chamber.

Experiments were conducted on the activation analysis of samples of gold-containing ores from different locations of the Soviet Union; the initial activity of the sources was from 300 to 1200 Ci. A sample of RZS-1, with a gold content of (52.1 ± 1) g/ton was used as a standard sample; the samples were irradiated during 1-3 days and the γ-emission of the induced activity was measured on semiconductor spectrometers with Ge(Li)-detectors with a volume of 80-120 cm^3. In order to take account of the nonuniformity of the neutron flux density in the zone of location of the samples, each sample was irradiated together with a monitor. Figure 5 shows one of the γ-emission spectra of a sample of gold-containing rock with a gold content of 2.1 g/ton. Photopeaks of the radionuclides of various elements can be distinguished in the spectrum. With a ^{124}Sb activity of 400 Ci and defined time conditions of analysis (irradiation 24 h, holding 1 h, measurement 0.25 h), a limit of determination of gold of 0.2 g/ton ($2\cdot10^{-5}$%) is ensured. The minimum value of the limit of determination of gold is 0.06 g/ton ($6\cdot10^{-6}$%) and is obtained with a time of irradiation, holding, and measurement of 3 days, 1 day, and 1 h, respectively. The results of the analysis of certificated specimens showed good agreement with the data of the assay analysis.

The following values of the limit of determination of different elements with the antimony–beryllium neutron source with an activity of 400 Ci were obtained on synthetically prepared samples (a mixture of quartz sand with oxides and salts of the elements to be determined):

Na, K, Ga, Ce, Tu, Se, Rb, Ag, Cd	$5\cdot10^{-3}$–$1\cdot10^{-3}$
Co, Dy, Ho, Lu, Hf, Cs, U	10^{-3}–$5\cdot10^{-4}$
Mn, As, Ta, Sb, La, W, Pd	$5\cdot10^{-4}$–$1\cdot10^{-4}$
Sm, Eu, Au	$1\cdot10^{-4}$–$1\cdot10^{-5}$

Preparation of the ^{124}Sb Sources. In order to ensure a sufficiently high sensitivity of the neutron-activation analysis, it is necessary to use sources with a yield of 10^9-10^{10} neutrons/sec. According to the data of [12, 13], this yield is provided by an activity of the ^{124}Sb source of ∿10^2-10^3 Ci.

Figure 6 shows the calculated curves of the buildup and decay of the isotopes of arsenic for a neutron flux density of the reactor of $3\cdot10^{13}$ neutrons/(cm^2·sec) and a mass of metallic antimony of 500 g. The curves are calculated for a continuous operating cycle of the reactor. It can be seen that in addition to ^{124}Sb the short-lived nuclide ^{122}Sb ($T_{1/2}$ = 2.8 days) is formed, for which the saturation activity amounts to 8 kCi. Therefore, in order to reduce the radiation hazard after completion of the irradiation of the antimony in the reactor, it is necessary to cool for 15-20 days. It follows from the data shown in Fig. 6 that activation of the antimony should be carried out over 30-50 days. On completion of this period, the activity of the source amounts to 1100-1700 Ci. After cooling for two weeks (in order to reduce the ^{122}Sb activity), the activity of the ^{124}Sb is reduced to 1000-1500 Ci.

Declassified and Approved For Release 2013/03/04 : CIA-RDP10-02196R000300010004-7

Declassified and Approved For Release 2013/03/04 : CIA-RDP10-02196R000300010004-7

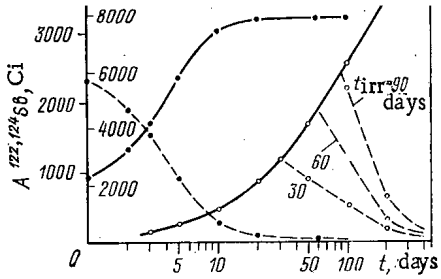

Fig. 6. Buildup and decay of ^{122}Sb (●) and ^{124}Sb (○).

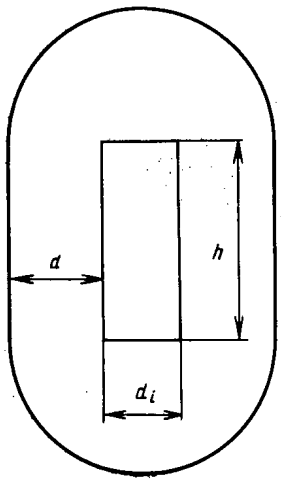

Fig. 7

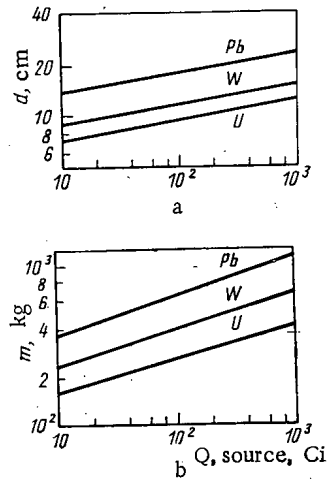

Fig. 8

Fig. 7. Diagram of a shielded transportation container for a ^{124}Sb source.

Fig. 8. Thickness of shielding (a) and mass of container (b) for the transportation of ^{124}Sb sources in accordance with the third transport category.

This source, installed in the beryllium converter, provides a yield of neutrons of $\sim(2\text{-}3)\cdot10^{10}$ neutrons/sec. After a half-year of operation, the activity of the source is reduced to 120-200 Ci, which provides a neutron yield of $\sim(2.5\text{-}4)\cdot10^{9}$ neutrons/sec. Thus, by replacing the source once during the half-year, a neutron flux density can be obtained in the activation facility within the required limits. Over the period of the experimental work, 6 sources of ^{124}Sb were prepared with an activity of 300 up to 1200 Ci. One of the sources was three times subjected to regeneration of its activity in the reactor.

Estimate of the Parameters of a Transportable Container. The bulk use of antimony—beryllium sources for neutron-activation analysis in the first place raises the problem of transportation of the sources from the reactors to the customers. A numerical estimate of the dimensions and mass of a shielded container was performed (Fig. 7) in order to transport ^{124}Sb sources according to the third transportation category [15]. Starting from our experience in the construction of ^{124}Sb sources, it was assumed in the calculations that the height of the source h is equal to 170 mm and its diameter d_i is 40 mm. The calculation was performed by the method of "competitive lines" [16] for the shielding materials lead, tungsten, and uranium (see Fig. 8a). The data obtained allowed the mass of the transportation container to be estimated, calculated for ^{124}Sb sources of different initial activity (see Fig. 8b).

Thus, for a source of ^{124}Sb with an activity of 1000 Ci, the diameter and height of the lead container should be 500 and 610 mm with a mass of 1100 kg, and those of a uranium container — 280 and 410 mm, with a mass of 470 kg.

Declassified and Approved For Release 2013/03/04 : CIA-RDP10-02196R000300010004-7

Declassified and Approved For Release 2013/03/04 : CIA-RDP10-02196R000300010004-7

Course of Future Work. The next step in the development of neutron-activation analysis with ^{124}Sb–Be neutron sources is the construction of industrial facilities. The most important challenges in the solution of this problem are: the construction of a transportation container with a system for admitting the source into the activator; the development of a system for loading and discharging the samples; provision of possibilities of analysis for both short-lived and long-lived radionuclides; standardization of powerful ^{124}Sb sources, and the organization of their production in research and power-generating nuclear reactors. In order to ensure uniformity of the neutron flux in the region of location of the samples being activated, it is advantageous to use a cylindrical geometry for the activator. Calculations show that in a single activator 70-150 samples can be irradiated simultaneously.

CONCLUSIONS

When using antimony–beryllium neutron sources for activation analysis of the composition of a substance, the problem of the analytical monitoring of many elements can be solved with a limit of determination of 10^{-3}-10^{-5}%. Based on the data obtained by the authors concerning the spatial distribution of the neutrons from a ^{124}Sb–Be-source in different moderators, a beryllium–graphite assembly with a powerful ^{124}Sb source has been designed, manufactured, and introduced into operation, for neutron-activation analysis.

As applicable to the ^{124}Sb–Be–graphite assembly, a procedure has been developed for the neutron-activation determination of gold, with a limit of determination of $2 \cdot 10^{-5}$%. The possible limits of the neutron-activation determination of certain other elements have been estimated. In order to ensure operation of the facility with recharging of the source once in 6 months, it is advisable to carry out the preparation of a source in a neutron flux with a density of $3 \cdot 10^{-13}$ neutrons/(cm^2·sec) during 30-50 days (for a mass of metallic antimony of 500 g) with subsequent two-week cooling in order to reduce the ^{122}Sb activity. Initial data have been obtained for the design of a transportation container for powerful ^{124}Sb sources.

LITERATURE CITED

1. Neutron Sources and Application. Proceedings of the American Nuclear Society. National Topical Meeting, USAEC Conference N-710402, Augusta (1971).
2. J. Kuusi, Nucl. Appl. Technol., 8, 465 (1970).
3. G. N. Flerov and V. Ya. Vyropaev, in: Proceedings of the Third Conference on the Use of Nuclear-Physics Methods for the Solution of Scientific–Technical and National Economic Problems [in Russian], JINR, Dubna, P. 18-12147 (1979).
4. Proceedings of an Internal Symposium on Californium-252 Utilization, Paris, 26-28 April (1976).
5. K. MacMurdo and W. Bowman, Automated Absolute Activation Analysis with Californium-252 Sources, DP-1457 (1978).
6. V. V. Ivanenko et al., in: Thesis of the Fourth All-Union Conference on Activation Analysis [in Russian], Tiflis (1977), p. 200.
7. T. S. Saidmuradov and Kh. Sirazhet, ibid., p. 185.
8. M. A. Bak and N. S. Shimanskaya, Neutron Sources [in Russian], Atomizdat, Moscow, p. 82.
9. T. Churchill, Production of Short-lived Radioisotope Tracers in a Sb–Be Source. Radioisotope Tracers in Industry and Geophysics. IAEA, Vienna, p. 271 (1967).
10. É. G. Ashirov, et al., in: Activation Analysis in the National Economy [in Russian], Fan, Tashkent (1974).
11. R. Tolmie and C. Thompson, Field Equipment for Neutron Activation Analysis, Nuclear Techniques and Mineral Resources, IAEA, Vienna (1969), p. 489.
12. V. Ya. Vyropaev and Yu. N. Burmistenko, Preprint JINR 18-80-584, Dubna (1980).
13. Yu. G. Teterev, Yu. S. Zamyatnin, and A. M. Kucher, Preprint JINR 18-80-559, Dubna (1980).
14. Yu. N. Burmistenko, Yu. S. Zamyatnin, and Yu. G. Teterev, Preprint JINR 18-81-171, Dubna (1981).
15. Regulations for the Safety and Transportation of Radioactive Substances [in Russian], (PBTRV-73), Atomizdat, Moscow (1974).
16. L. R. Kimel' and V. P. Mashkovich, Protection from Ionizing Radiations (Reference Book) [in Russian], Atomizdat, Moscow (1966).

Declassified and Approved For Release 2013/03/04 : CIA-RDP10-02196R000300010004-7

Declassified and Approved For Release 2013/03/04 : CIA-RDP10-02196R000300010004-7

STABILITY OF A NUCLEAR REACTOR WITH NATURAL CIRCULATION OF A LIQUID FUEL

V. A. Blinkin and E. I. Emel'yanov

UDC 621.039.512.4

Reactors with circulating liquid nuclear fuel, which is simultaneously also the coolant, have been studied since the mid-1950's [1]. Reactors operating on aqueous solutions of uranium, liquid-metal reactors, and liquid-salt reactors [2] belong to this type. These reactors, in principle, can operate in natural circulation conditions of the fuel coolant [3] (Fig. 1). The stability of the steady-state regime of this system is determined by the nature of the power feedbacks, which are effected through the reactivity temperature coefficients (RTC) and the characteristic time of response of the system parameters to a change of reactor power.

Let us consider a thermal reactor, in the core of which a stream of liquid fuel flows in channels surrounded by the moderator. We shall describe the physical model of the dynamics as a multipoint system with lumped parameters in each section. The temperature feedbacks are characterized by two RTC: ε_T with respect to the temperature of the liquid fuel T_1 and ε_M with respect to the temperature of the moderator in the core T_M. The effect of delayed neutrons is described in the approximation of a single equivalent group. We shall assume the heat-transfer coefficients and the specific heat of the fuel and moderator to be constant, and we shall write the dependence of the fuel density on the temperature in the approximation

$$\gamma(T)=\gamma_0[1-\alpha(T-T_0)],\ \alpha=\text{const}, \tag{1}$$

with $\alpha(T - T_0) \ll 1$, so that the difference of $\gamma(T)$ from γ_0 can be neglected everywhere, with the exception of the term describing the driving pressure head of the natural circulation.

On this assumption, the system of equations for the dynamics can be represented in the following way:

A. Neutron kinetic equations:

$$\frac{dN}{dt}=\frac{k-\beta}{l}N+\lambda C; \tag{2}$$

$$\frac{dC}{dt}=\frac{\beta}{l}N-\lambda C+\frac{1}{\tau_1}(C_{\text{i.c}}-C); \tag{3}$$

$$k=k_0+\varepsilon_T(T_1-T_0)+\varepsilon_M(T_M-T_{M0}), \tag{4}$$

where $C_{i.c} = C(t - \tau_B)e^{-\lambda\tau_0}$ [4]; N is the reactor power; C, the concentration of delayed neutron emitters; $\tau_B = \sum_{i=2}^{n} \tau_i$; $\tau_i = \tau_{i0}/\xi$ is the time of transit of the fuel through the i-th section of the circuit (see Fig. 1); k is the reactivity; l, average lifetime of the prompt neutrons; β, delayed neutron fraction; $\tau_{i0} = m_i G_{nom}$, where m_i is the mass of fuel in the i-th section of the circuit; $\xi = G(t)/G_{nom}$, where $G(t)$ and G_{nom} are the mass flow rate of the fuel at the instant t, and its value in the nominal regime. The subscripts "i.c" and "i.h.e" denote variables at the inlet to the core and heat exchanger, respectively, and the subscript "0" denotes the values of the variables in the steady-state regime.

B. Heat-exchange equations:

Translated from Atomnaya Énergiya, Vol. 53, No. 4, pp. 261-263, October, 1982. Original article submitted May 4, 1982.

 0038-531X/82/5304-0720$07.50 © 1983 Plenum Publishing Corporation

Declassified and Approved For Release 2013/03/04 : CIA-RDP10-02196R000300010004-7

Declassified and Approved For Release 2013/03/04 : CIA-RDP10-02196R000300010004-7

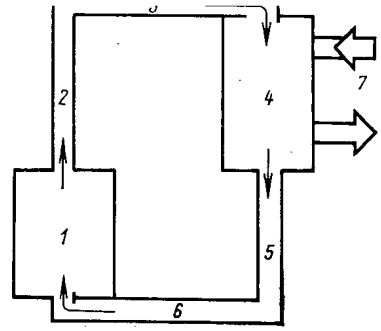

Fig. 1. Diagram of the fuel circulation in a reactor with liquid metal fuel circulation: 1) core; 2) tractive section; 3) upper horizontal section; 4) heat exchanger; 5) descending section; 6) lower horizontal section; 7) secondary coolant circuit.

$$\tau_1 \frac{dT_1}{dt} = \xi (T_{\text{i.c}} - T_1) + A_1 N + A_2 (T_{\text{M}} - T_1); \tag{5}$$

$$\tau_{\text{M}} \frac{dT_{\text{M}}}{dt} = T_1 - T_{\text{M}} + A_3 N; \tag{6}$$

$$\tau_4 \frac{dT_4}{dt} = \xi (T_{\text{i.c}} - T_4) + A_4 (T_{\text{W}} - T_4); \tag{7}$$

$$T_{\text{i.c}}(t) = T_4 (t - \tau_5 - \tau_6), \quad T_{\text{i.h.e}}(t) = T_1 (t - \tau_2 - \tau_3), \tag{8}$$

where T_i and T_W are, respectively, the average temperature of the fuel in the i-th section and the temperature of the heat-exchanger wall;

$$A_1 = \frac{1-a}{c_1 G_{\text{nom}}}, \quad A_1 = \frac{k_1 S_{\text{T0}}^{(1)}}{c_1 G_{\text{nom}}}, \quad A_3 = \frac{a}{k_1 S_{\text{T0}}^{(1)}};$$

$$A_4 = \frac{k_4 S_{\text{T0}}^{(4)}}{c_1 G_{\text{nom}}};$$

a is the fraction of the bulk energy release in the moderator; $S_{c_o}^{(i)}$, surface area of the heat-exchanger in the i-th section; c_1 and c_M, specific heats of the fuel and moderator; $\tau_M = m_M c_M / k_i S_{T0}^{(i)}$, where m_M is mass of the moderator in the core; k_i, heat-transfer coefficient in the i-th section.

C. Heat-transfer equations:

The driving pressure head of the natural circulation is determined by the expression

$$\Delta p_{\text{d}} = \alpha \gamma_0 g \, (h_1 T_1 + h_2 T_2 - h_4 T_4 - h_5 T_5); \tag{9}$$

$$T_2 = \begin{cases} \frac{t}{\tau_2} (T_1 - T_{1\,0}) + T_{1\,0}, & t \leqslant \tau_2; \\ T_1, & t > \tau_2; \end{cases}$$

$$T_5 = \begin{cases} \frac{t}{\tau_5} (T_4 - T_{1\,0}) + T_{4\,0}, & t \leqslant \tau_5; \\ T_4, & t > \tau_5, \end{cases}$$

where g is the acceleration due to gravity; h_i is the height of the i-th section of the circuit. The hydraulic losses in the circuit are determined by the frictional drag and the fuel acceleration losses, i.e.,

$$\Delta p_{\text{c}} = K_{1\text{c}} \frac{d\xi}{dt} + K_{2\text{c}} \xi^2, \tag{10}$$

where

Declassified and Approved For Release 2013/03/04 : CIA-RDP10-02196R000300010004-7

Declassified and Approved For Release 2013/03/04 : CIA-RDP10-02196R000300010004-7

$$K_{1c}=\frac{G\text{nom}}{\gamma_0}\sum_{i=1}^{6}\frac{m_i}{S_1};\quad K_{2c}=\frac{G_{\text{nom}}^2}{\gamma_0^2}\sum_{i=1}^{6}\frac{\alpha_i}{S_i^3};$$

S_i and α_i are the cross-section of the circuit and the hydraulic drag coefficient in the i-th section.

The natural circulation regime is determined by the condition $\Delta P_d = \Delta P_c$, which gives

$$K_{1c}\frac{d\xi}{dt}+K_{2c}\xi^2=\alpha\gamma_0 g\,(h_1T_1+h_2T_2-h_4T_4-h_5T_5) \tag{11}$$

and in the steady-state regime $K_{2c}\xi_0^2 = \alpha\gamma_0 g_0 H(T_{10} - T_{40})$, where $H = h_1 + h_2 = h_4 + h_5$.

The stability in a small dynamic system was investigated by the method of D-partition [5] with respect to two parameters — ε_T and ε_M. In order to conduct the investigation, the system of equations (1)-(11) was linearized and Laplace-transformed with the parameter p; $p = j\omega$ was put in the characteristic equation, formulated in this way and, after separation of the real and imaginary part, the D-curve equation was obtained in parametric form. This curve, in the plane of the parameters (ε_T, ε_M) defines the boundary of the region of stability of different orders. With p = 0, the characteristic equation is described by a singular straight line, by crossing through which the sign of one real root is changed. The equation of the straight line has the form

$$F(\varepsilon_T,\varepsilon_M)=\varepsilon_T+\varepsilon_M\left[1+a\left(1+\frac{2}{3}\frac{A_4}{\xi_0}\right)\frac{k_4S_{T0}^{(4)}}{k_1S_{T0}^{(1)}}\right]-\frac{1}{3}\frac{\beta\varphi_0}{\Delta T\text{nom}}\frac{A_4}{\xi_0}\left(1+\frac{2}{3}\frac{A_4}{\xi_0}\right)^{-1}\cdot\frac{1-(1+\lambda\tau_{B0}/\xi_0)\exp(-\lambda\tau_{B0}/\xi_0)}{1+\lambda\tau_{10}/\xi_0-\exp(-\lambda\tau_{B0}/\xi_0)}=0, \tag{12}$$

where ΔT_{nom} is the temperature drop of the fuel in the core in the nominal regime; $\varphi=\frac{\lambda\tau_{10}}{\xi_0}\times\{1+\lambda\tau_{10}/\xi_0-\exp(-\lambda\tau_{B0}/\xi_0)\}^{-1}$; $\tau_{B0}=\sum_{i=2}^{6}\tau_{i0}$. The function $F(\varepsilon_T, \varepsilon_M)$ has the physical meaning of the steady-state reactivity coefficients, for which the condition of negativity is an essential condition of the reactor stability.

We note that with a sufficiently good heat exchanger ($A_4 >> 1$), the delay due to the time of transit of the fuel in sections 2, 3, 5 and 6 (see Fig. 1), will not appreciably affect the behavior of the system, since in this case T_4 will be only slightly sensitive to the reactor power. Therefore, only τ_1, τ_4 and τ_M remain the essential characteristic times of the system.

An analysis of the equations obtained for the D-curve indicates that in the plane of the parameters (τ_{10}/τ_M and τ_{40}/τ_M) three characteristic regions exist, in each of which the number of D-partition zones with a different order of stability is different. As an example, Fig. 2 shows the D-partition for these regions of a high-temperature, liquid-salt reactor (HTLSR) with the following parameters:

$$\begin{gathered}T_{10}=1300^\circ\text{C};\ T_{40}=1100^\circ\text{C};\ T_{M0}=1400^\circ\text{C};\ T_{CT}=1000^\circ\text{C};\\ A_1=194;\ A_2=0.12;\ A_3=50;\ A_4=5;\ \beta=0.0032;\\ \lambda=0.1\,\text{sec}^{-1}\ \tau_M=33\,\text{sec}.\end{gathered} \tag{13}$$

For this reactor, $\varepsilon_T < 0$ and $\varepsilon_M > 0$, i.e., its working point is found in quadrant II of the plane (ε_T, ε_M).

Figure 2a shows the boundaries of the D-partition for a system with the parameters of (13) for $\tau_{10}/\tau_M = 0.41$ and $\tau_{40}/\tau_M = 0.52$. It can be seen that quadrant II is divided by the straight line into two regions; the lower is the region of stability and the upper is the region of aperiodic instability. The working point of reactor being considered ($\varepsilon_T = -1.1\cdot10^{-5}\,^\circ\text{C}^{-1}$ and $\varepsilon_M = 1.4\cdot10^{-6}\,^\circ\text{C}^{-1}$) is located for this in the region of stability, whereas the working point of the MSBR-1000 [2] ($\varepsilon_T = -3.3\cdot10^{-5}\,^\circ\text{C}^{-1}$ and $\varepsilon_M = 2.4\cdot10^{-5}\,^\circ\text{C}^{-1}$) is in the region of instability. It can be seen from this same figure that taking account of the actual values of the times τ_2, τ_3, τ_5, and τ_6 (curve 2) does not lead to a significant change of

Declassified and Approved For Release 2013/03/04 : CIA-RDP10-02196R000300010004-7

Declassified and Approved For Release 2013/03/04 : CIA-RDP10-02196R000300010004-7

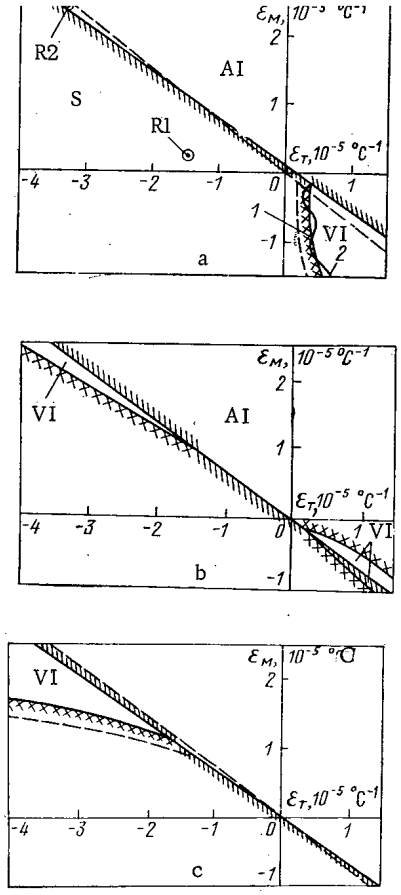

Fig. 2. D-partition in the plane of the TRC (ε_T, ε_M) for $\tau_{10}/\tau_M = 0.41$, $\tau_{40}/\tau_M = 0.50$ (a); 2.9 and 3.6 (b); 8.2 and 10.4 (c); S is the region of stability, and AI and VI are the regions of aperiodic and vibrational instability; ——— and — — — — denote natural and forced circulation; R1 and R2 are the working points of the HTLSR and MSBR reactors.

disposition of the D-curve, obtained for the case $\tau_2 = \tau_3 = \tau_5 = \tau_6 = 0$ (curve 1), as was also suggested above.

With increase of the values of τ_{10}/τ_M and τ_{40}/τ_M (e.g., with increase of the system dimensions or reduction of the dimensions of the moderator blocks), these parameters can transfer to another characteristic region of the D-partition (see Fig. 2b) in which two branches of the D-curve appear; one is located in quadrant II, where the region of vibrational instability appears. With even larger values of τ_{10}/τ_M, the D-curve has a single branch, but still in quadrant II. In this case, the region of stability with increase of τ_{10}/τ_M is reduced (see Fig. 2c).

From the analysis of the characteristic equation for the D-curve, it follows that a region of asymptotic instability exists even for $\varepsilon_T > 0$ and $\varepsilon_M > 0$, i.e., in quadrant I of the plane of D-partition [see Eq. (12) and Fig. 2]. This is due to the stabilizing effect of the delayed neutrons, since with increase of the reactor power the flow rate of the liquid fuel is increased, which leads to an increase of the rate of removal of delayed neutron emitters from the core, and thereby to a reduction of reactivity. This effect becomes less with increase of the fuel circulation velocity, since in this case the fraction of delayed neutrons is characteristic only for a reactor with natural fuel circulation.

Declassified and Approved For Release 2013/03/04 : CIA-RDP10-02196R000300010004-7

Declassified and Approved For Release 2013/03/04 : CIA-RDP10-02196R000300010004-7

The D-partition, for a system with forced fuel circulation (G = const), is shown by broken lines in Fig. 2. In this case, the singular straight line passes through the coordinate origin, i.e., when $\varepsilon_T > 0$ and $\varepsilon_M > 0$, the system is always unstable. Moreover, this straight line is disposed more steeply to the axis of abcissa than the singular straight line in the case of natural fuel circulation since, with G = const, the fuel temperature in the core varies proportionally with the reactor power N, and in the case of natural circulation a change of N leads to a change of G; in view of this, the temperature varies according to a $N^{2/3}$ law. It can also be shown that with a reduction of the steady power of the reactor N_0 in the case of natural fuel circulation, the region of stability in quadrant II of the plane $(\varepsilon_T, \varepsilon_M)$ is increased.

We note that for a liquid-salt reactor with a graphite moderator, when $\varepsilon_T > 0$ instability does not present a great hazard, since the inertia of $\varepsilon_M > 0$ is greater than the inertia of ε_T at the time τ_M = 30-50 sec, and a reactor excursion is started only several tens of seconds after injection of the perturbation. This excursion can be suppressed easily by the control system.

LITERATURE CITED

1. J. Lane, M. Macpherson, and E. Maslan, Fluid Fuel Reactors, Addison-Wesley, New York (1958).
2. V. L. Blinkin and V. M. Novikov, Liquid-Salt Nuclear Reactors [in Russian], Atomizdat, Moscow (1978).
3. S. S. Abalin et al., Problems of Nuclear Science and Technology. Series Atomic-Hydrogen Power Generation and Technology [in Russian], 1(6) (1980), p. 42.
4. V. D. Goryachenko, At. Energ., 21, No. 1, 3 (1966).
5, Yu. I. Neimark, Dynamic Systems and Controlled Processes [in Russian], Nauka, Moscow (1978).

INDICATOR OF THE ENERGY DISTRIBUTION IN THE RBMK-1000 FIELD

G. N. Aleksakov, S. A. Gavrilyuk,
A. V. Kudryavtsev, and G. P. Terekhov

UDC 681.518:53.083.94

Indicators which sense the contact with the object to be controlled facilitate the work of an operator and increase the reliability of the entire man—machine system. Luminous modeling provides the operator with a pattern of the distribution of the quantity to be controlled, e.g., of the energy distribution in the reactor core, in the form of a brightness field obtained by reconstructing a continuous field from the data of discrete sensors [G. N. Aleksakov and G. P. Terekhov, At. Energ., 48, No. 2, 103 (1980)].

A field of light sources can be produced on the screen of a cathode-ray tube by connecting its grid to sensors through a switching circuit in synchronism with the beam sweep over the screen and in accordance with the position of a sensor selected. In modeling without a lens, the optimum reconstruction of the field of the energy distribution in the RBMK-1000 is obtained with light sources in the form of plane rectangular areas. This or any other pattern of light sources can be easily generated by deflecting the beam of the cathode-ray tube. When a cathode-ray tube is employed, the field is generated in successive steps in distinction from the field of "parallel" sources (see the cited paper by Aleksakov and Terekhov). Owing to the inertia of vision, the results of the modeling on a display screen are perceived in both cases in the same fashion at high scanning frequencies. In the television display of a brightness pattern the problem is solved by using a cathode-ray tube with long afterglow or a photodetector with charge storage. Television standards prescribe a specified rate of image formation; television kinescopes can provide high brightness.

Translated from Atomnaya Énergiya, Vol. 53, No. 4, pp. 263-265, October, 1982. Original article submitted June 2, 1981.

 0038-531X/82/5304-0724$07.50 © 1983 Plenum Publishing Corporation

Declassified and Approved For Release 2013/03/04 : CIA-RDP10-02196R000300010004-7

Declassified and Approved For Release 2013/03/04 : CIA-RDP10-02196R000300010004-7

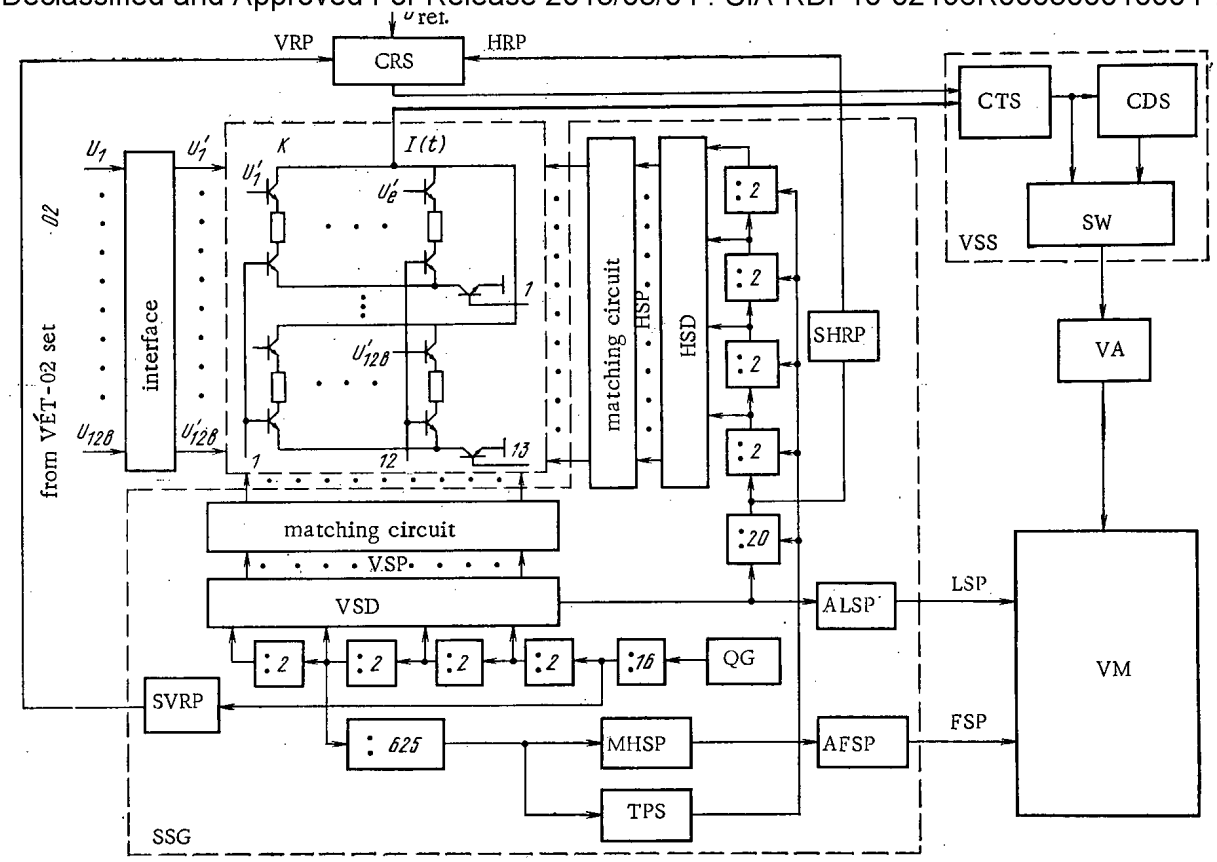

Fig. 1. Structure scheme of the "Poleskop-5" field indicator: VSD) vertical strip decoder; HSD) horizontal strip decoder; MHSP) monovibrator of the semiframe synchronization pulses; AFSP) amplifier of the semiframe synchronzation pulses; TPS) trigger pulse shaping circuit; SHRP) stage shaping the horizontal reference pulses; SVRP) stage shaping the vertical reference pulses; ALSP) amplifier of line synchronization pulses.

In the "Poleskop-5" indicator of physical fields a field of luminous sources is formed in the standard television manner on the screen of a kinescope in accordance with the position pattern of sensors detecting the energy distribution in the core of the RBMK-1000 reactor. The sensors of the energy distribution are placed at equidistant points of a 13 × 12 mesh. The television scanning field is accordingly divided into 13 horizontal and 12 vertical strips. A rectangle at the intersection of the i-th horizontal strip with the j-th vertical strip is modeled by the signal of the sensor situated at the point with the coordinates y_i and x_j in the core.

Figure 1 shows schematically the structure of the luminous field generation in the "Poleskop-5." Data on the energy distribution are derived from signals arriving from the amplifiers correcting the field shape of the VÉT-02 instrument via an interface to switch S which connects the signals U_1', ..., U_{128}' in synchronism with the beam sweep over the screen and in accordance with the sensor position. In this form of the interrogation a 13 × 12 matrix is conveniently used as switch. A channel is selected by calling a line and column in accordance with the sensor position at a minimum number of controlling signals. A sequence of currents I(t) is obtained at the output of the switch. The signals currents are passed through video-signal shaping stages (VSS) and a video amplifier (VA) and applied to the modulator of the kinescope in a video monitor (VM).

The video-signal shaping stages convert the signal currents into a video signal. The video-signal stages comprise circuits forming the total signal (CTS) and circuits forming the deflection signal (CDS). The output of the circuits of the first type is the total signal (TS), the amplitude of which is proportional to the absolute values of the parameter to be monitored; the output of the circuits of the second type is the deflection signal which is proportional to the deflection of the parameter to be monitored from the control point U_{ref}. The signal is selected with a switch (SW).

Declassified and Approved For Release 2013/03/04 : CIA-RDP10-02196R000300010004-7

Declassified and Approved For Release 2013/03/04 : CIA-RDP10-02196R000300010004-7

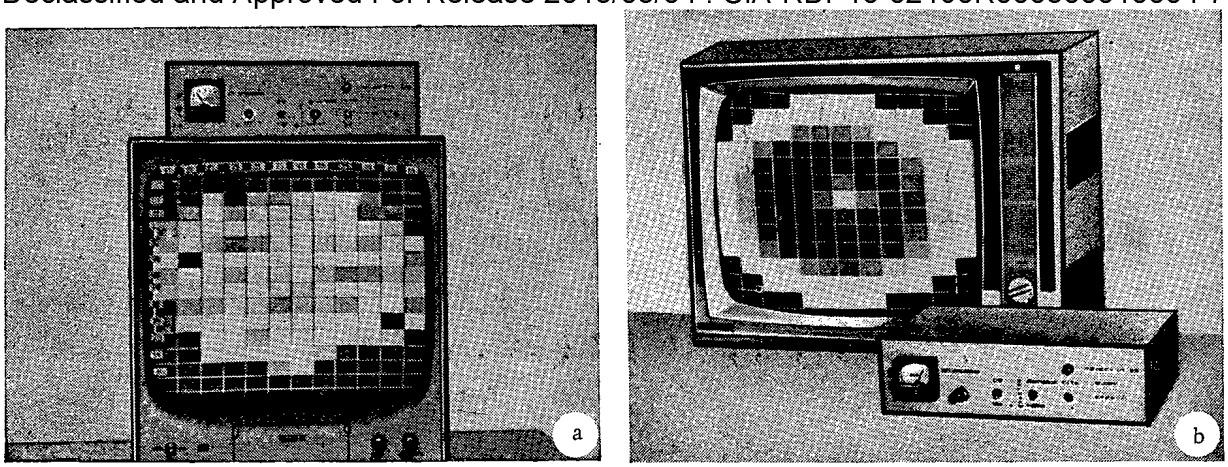

Fig. 2. Overall view of the "Poleskop-5" field indicator.

In order to determine the characteristics of the signal forming circuits of the luminous field, on the screen a reference grid is generated along with the field pattern. The reference grid consists of narrow vertical and horizontal strips defining rectangular areas on the screen. The brightness of all reference fields is identical and can be adjusted within 0 and 100% of the maximum screen brightness by changing the U_{ref} voltage. The circuit in which the signal of the reference strips is generated (CRS) is identical with the other switch channels.

A signal-system generator (SSG) generates a system of synchronous signals for controlling the blocks of the signal-shaping stages. The system comprises line (LSP) and semiframe (FSP) synchronization pulses (SP) for the videl monitor (VM), control pulses for the lines of the vertical strip (VSP) and control pulses for the columns of the horizontal strips (VRP) and horizontal reference strips (HRP). The control signals are obtained by successive division of the frequency (4 MHz) of a quartz generator (QG).

The frequency and the duration of the controlling pulses are defined by the structure of the image. In horizontal direction the size of the area is 4 μsec and 20 lines in the vertical direction of a semiframe; the width of the vertical reference strips is 0.5 μsec; the horizontal reference strip has a width of one line in a half-frame.

In order to measure the modulation characteristics of the channels, a particular adjustable voltage was applied to all inputs. By equalizing the brightness of the reference grid with each of the areas on the screen, the modulation characteristics $U_{ref.i} = f(U_{in})$ are measured. The accuracy of the measurements depends upon the brightness discrimination threshold of neighboring image sections and is better than 0.5%. For the assumptions made, the modulation characteristics are not identical with an error of less than 3%.

The television indicator was tested when fields were modeled with a resistive grid. One of the examples of field images is shown in Fig. 2a. In April of 1981 the Poleskop field indicator entered into test operation in the Kursk Atomic Power Station. An example of the field pattern in the second block of the Kursk Atomic Power Station is shown in Figure 2b.

The authors thank the representatives of the Kursk Atomic Power Station, Yu. N. Filimontsev, O. F. Safronov, and V. A. Shchigolev, for their support and practical help in building and testing the "Poleskop-5" field indicator.

Declassified and Approved For Release 2013/03/04 : CIA-RDP10-02196R000300010004-7

Declassified and Approved For Release 2013/03/04 : CIA-RDP10-02196R000300010004-7

DIFFUSION OF ^{131}I AND ^{103}Ru IN SINGLE-CRYSTAL TUNGSTEN

E. S. Bekmukhambetov, D. K. Daukeev,
Zh. R. Zhotabaev, and R. T. Musurmankulov

UDC 539.219.3

There has recently been a considerable increase in interest in diffusion and segregation of impurity atoms in irradiated metals [1]. Segregation of alloy elements to defect sinks (outer surfaces, grain boundaries, dislocations, pores, and so on) has been observed in a wide range of alloys after irradiation by neutrons or charged particles at moderate temperatures. Segregation has also been observed in experiments on quenching [2].

The possible segregation mechanisms include [3-5] the formation of mobile binary complexes of vacancy-impurity atom type and interstitial atom-impurity atom type, as well as fluxes of impurity atoms produced by the migration of free point defects to sinks. Considerable significance is attached to the accumulation of data on impurity redistribution in metals when there is a superequilibrium point-defect concentration.

Unique scope is offered by the diffusion of implanted fission products. The specimen is irradiated in a reactor in contact with a fissile material, which can introduce various fission products simultaneously. With this method, one has absolutely identical diffusion conditions for all the fission-product atoms, while the specimen acquires a defect structure that on subsequent high-temperature annealing very rapidly goes over to a comparatively stable system of pores surrounded by regions with an excess vacancy concentration. The concentration gradients for the fission products, pores, and excess vacancies then give rise to the corresponding fluxes on diffusion annealing.

Measurements have been made by this method on the diffusion of ^{133}Xe, ^{140}Ba, and ^{132}Te in polycrystalline molybdenum [6, 7], which have shown that the concentration gradients of these elements diminish during annealing, but that the diffusion is retarded as the radiation dose increases, evidently because the fission products are trapped by traps of radiation origin. Here we report results on the diffusion of ^{131}I and ^{103}Ru in tungsten single crystals of purity 99.99%. Circular plates of diameter 5 mm and thickness 2 mm were cut by electrospark means from a tungsten rod. The damaged layer was removed by grinding with diamond paste and electropolishing in an aqueous NaOH solution. Then the specimens were annealed at a vacuum of 4×10^{-5} Pa at 2200°C for 3 h in order to eliminate the internal stresses and were again electropolished. X-ray examination showed that the specimens made in this way were perfect. The fission products were implanted at a temperature not above 100°C by irradiating the specimens in contact with a layer of enriched uranium in a VVR-K reactor by the previous method [6, 7].

The fission-product dose was 1.2×10^{13} fragment/cm^2. The specimens after irradiation were kept for 20 days. Distributions of the implanted products before and after diffusion annealing were determined by removing thin layers by electropolishing. The relative concentrations of the fission products in the remaining part of the specimen were determined by γ spectrometry. The diffusion annealing was performed in a vacuum of 4×10^{-5} Pa at 2000°C for 20 h for tungsten or at 1680°C for 10 h for molybdenum.

The integral distribution curves for ^{131}I and ^{103}Ru in molybdenum and tungsten before and after diffusion annealing (Figs. 1 and 2) show that ^{103}Ru diffuses in the same way in these metals. On the other hand, the diffusion of ^{131}I in tungsten is directed against the concentration gradient, i.e., there is a process analogous to segregation of iodine at the surface. This can hardly be due to diffusion of complexes of vacancy-impurity type by the Johnson–Lam mechanism on account of the high annealing temperature, but rather it is caused by the inverse Kirkendall effect, i.e., displacement of the ^{131}I atoms in the opposite direction to the flow of excess vacancies due to the presence of pores. We examined molybdenum

Translated from Atomnaya Énergiya, Vol. 53, No. 4, pp. 265-266, October, 1982. Original article submitted July 23, 1981.

0038-531X/82/5304-0727$07.50 © 1983 Plenum Publishing Corporation

Declassified and Approved For Release 2013/03/04 : CIA-RDP10-02196R000300010004-7

Declassified and Approved For Release 2013/03/04 : CIA-RDP10-02196R000300010004-7

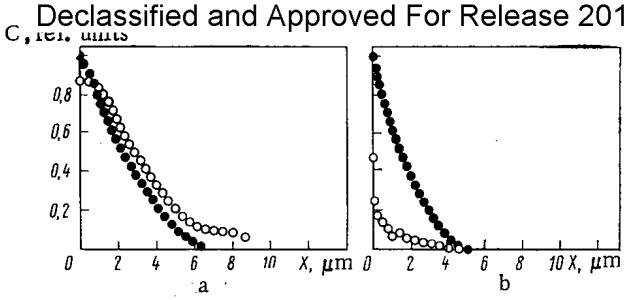

Fig. 1

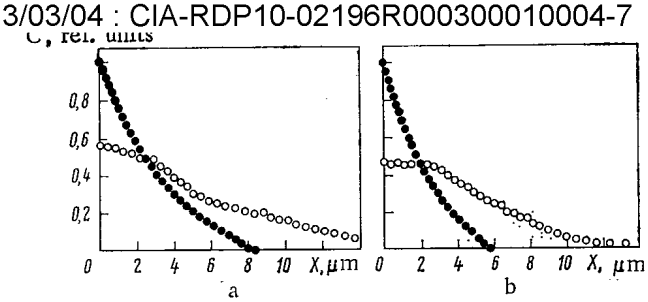

Fig. 2

Fig. 1. Integral distribution profiles for ^{131}I in molybdenum (a) and tungsten (b): ●) initial; ○) after diffusion annealing.

Fig. 2. Integral distribution profiles for ^{103}Ru in molybdenum (a) and tungsten (b): ●) initial; ○) after diffusion annealing.

specimens containing fission fragments in a transmission electron microscope and found that the average concentration of pores of size 14-19 nm in the diffusion zone was 10^{14} cm^{-3}. Therefore, in diffusion annealing at a high temperature there must be of excess vacancies into the specimen, which can cause a flux of impurity atoms to the surface, which is [3]:

$$j = \sigma_v C D_v \nabla^2 C_v,$$

where C is the impurity concentration; D_V, vacancy diffusion coefficient; C_V, vacancy concentration; and σ_V, a coefficient characterizing the effects of vacancies on the diffusion mobility of the atoms [8].

Also, the reason for the segregation may be the considerable ascending diffusion of iodine to the surface of the tungsten caused by the formation of a compound and corresponding reduction in the chemical potential [9].

LITERATURE CITED

1. P. Okamoto, S. Harkness, and J. Laidler, Trans. ANS, 16, 70 (1973).
2. D. Potter et al., Scripta Meth., 11, 1095 (1977).
3. R. Johnson and N. Lam, Phys. Rev., B13, 4364 (1976).
4. H. Wiedersich, R. Okamoto, and N. Lam, J. Nucl. Mater., 83, 98 (1979).
5. G. M. Kudinov, B. Ya. Lyubov, and V. A. Shmakov, Fiz. Met. Metalloved., 48, 1245 (1979).
6. E. S. Bekmukhambetov, Atomic Science and Engineering, Series Physics of Radiation Damage and Radiation Materials Science [in Russian], Issue 1/4, (1977), p. 40.
7. E. S. Bekmukhambetov, Fiz. Met. Metalloved., 46, No. 1, 192 (1978).
8. R. Howard and A. Lidiard, Philos. Mag., 11, 1179 (1965).
9. Handbook of Physicochemical Properties of the Elements [in Russian], Naukova Dumka, Kiev (1965).

Declassified and Approved For Release 2013/03/04 : CIA-RDP10-02196R000300010004-7

Declassified and Approved For Release 2013/03/04 : CIA-RDP10-02196R000300010004-7

CHARACTERISTICS OF REFLECTED γ RAYS WITH A SHORT DISTANCE BETWEEN THE DETECTOR AND THE SCATTERING SURFACE

V. I. Kulikov, K. K. Popkov, and V. I. Titov

UDC 539.166.3

In order to ascertain the laws governing the formation of the scattered γ-ray field with a small distance between the detector and the scattering surface, an attempt has been made to generalize the concept of albedo, which is used extensively in shielding calculations (see, e.g., [1]).

Suppose that a pencil monodirectional beam of γ-rays of energy E_0 is incident on a flat reflector at an angle θ_0 at a point with the coordinates, R, θ, φ, specified in a spherical coordinate system whose origin coincides with the incidence point of the primary beam, and the flux density of the reflected γ rays of energy E is Φ (R, θ, φ, E). The effective albedo can then be introduced with the aid of the relation

$$a(R, \theta, \varphi, E, \theta_0, E_0) = \frac{R^2 \cos\theta \Phi(R, \theta, \varphi, E)}{Q(\theta_0, E_0)}, \quad (1)$$

where Q (θ_0, E_0) is the total number of γ-ray quanta incident on the reflector per unit time. For values of the distance R commensurate with the linear size of the scattering region, a(R, θ, φ, E, θ_0, E_0) determines a reflection characteristic similar to the differential current albedo of γ rays as far as sense and dimension are concerned. In this case,

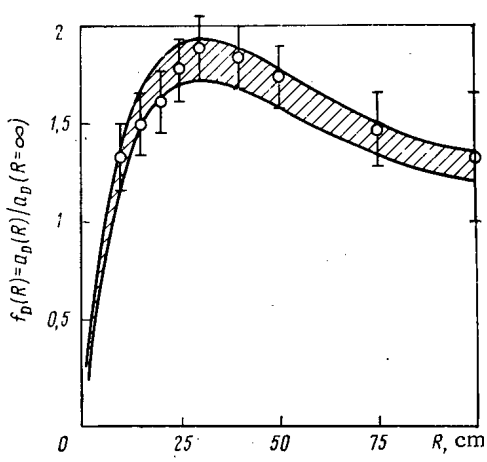

Fig. 1. The f_D(R) curve for the dose albedo of a plane paraffin scatterer: The points denote the results of measurements; the shaded region denotes the results of calculations by the Monte Carlo method; ^{137}Cs was the radiation source; the incidence angle was Θ_0 = 45°; the reflection angle was Θ = 75; φ = 0°; E_0 = 0.66 MeV.

Translated from Atomnaya Énergiya, Vol. 53, No. 4, pp. 266-268, October, 1982. Original article submitted December 1, 1981.

0038-531X/82/5304-0729$07.50 © 1983 Plenum Publishing Corporation

Declassified and Approved For Release 2013/03/04 : CIA-RDP10-02196R000300010004-7

Declassified and Approved For Release 2013/03/04 : CIA-RDP10-02196R000300010004-7

TABLE 1. Energy Coefficients for Calculating Dose and Energy Albedos from Eq. (7)

Substance	Albedo	φ^0	b_0	b_1	b_2	b_3	c_1	c_2	d_1	d_2
Water	Dose	0	0,0053	5,1	3,06	0,0260	1,205	0,0333	14,98	0,0136
		180	0,0056	21,5	0,505	0,0356	1,050	0,0313	17,42	0,0464
	Energy	0	0,0051	7,58	2,97	0,025	1,214	0,0333	14,23	0,0125
		180	0,0055	22,5	0,505	0,0356	1,053	0,0313	17,76	0,0457
Iron	Dose	0	0,050	0,761	0,361	0,307	1,008	0,047	1,155	0,467
		180	0,049	1,253	0,0112	0,398	0,879	0,0464	1,417	1,033
	Energy	0	0,048	0,829	0,343	0,291	1,018	0,0469	1,127	0,430
		180	0,049	1,277	0,0117	0,397	0,880	0,0464	1,440	1,031
Lead	Dose	0	0,143	1,650	0,223	0,726	0,908	0,0462	2,18	1,633
		180	0,023	4,28	0,0099	0,768	0,856	0,0391	5,43	1,987
	Energy	0	0,136	1,800	0,182	0,649	0,915	0,446	2,24	1,43
		180	0,0185	4,42	0,0089	0,765	0,858	0,0387	5,57	1,97

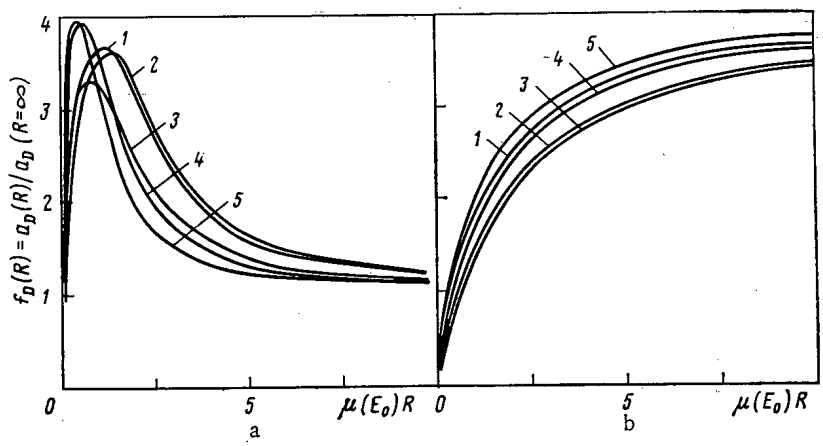

Fig. 2. Function $f_D(R)$ for dose albedo of plane iron scatterer for different values of initial γ-ray energy E_0, MeV: 1) 0.25; 2) 1.0; 3) 2.0; 4) 4.0; 5) 8.0 [a) $\theta_0 = 0°$, $\theta = 85°$, $\varphi = 0°$; b) $\theta_0 = 85°$, $\theta = 0°$, $\varphi = 0°$].

$$a(R, \theta, \varphi, \theta_0, E_0)|_{R\to\infty} \to a(\theta, \varphi, E, \theta_0, E_0), \tag{2}$$

where $a(\theta, \varphi, E, \theta_0, E_0)$ is the differential current albedo.

The dependence of the effective albedo on the distance has been studied by the Monte Carlo method, using a special program. The effectiveness of the program was checked by comparing the calculated results with published data [1-4] as well as with the data of experiments in which measurements were made of the dose effective albedo of a plane paraffin scatterer with dimensions of 100 × 100 × 150 cm for ^{137}Cs and ^{60}Co photons. The reflected γ rays were detected by small SBM-10 counters with filters for correcting the energy dependence. During the measurements the detector was moved along the direction (θ, φ) of the reflected radiation. Figure 1 presents the measured and calculated effective dose albedo of paraffin for various detector—reflector distances.

The computational program mentioned above was used for investigations to substantiate the method of economical investigations [1] in calculations using the effective albedo. For this purpose, in the range 0.28-8.0 MeV a series of calculations were carired out for water, aluminum, iron, and lead scatterers. It was established that this method can be extended to the case of finite distances R between the detector and the incidence point of the primary beam, provided that R remains constant on passing to equivalent incidence and reflection angles. In most of the cases considered, for R < 100 cm when the method of economical investigations is used, the error does not exceed 15-20% for angular characteristics and 25-30% for spectral-angular characteristics. In cases when the real and equivalent angles differ by

Declassified and Approved For Release 2013/03/04 : CIA-RDP10-02196R000300010004-7

Declassified and Approved For Release 2013/03/04 : CIA-RDP10-02196R000300010004-7

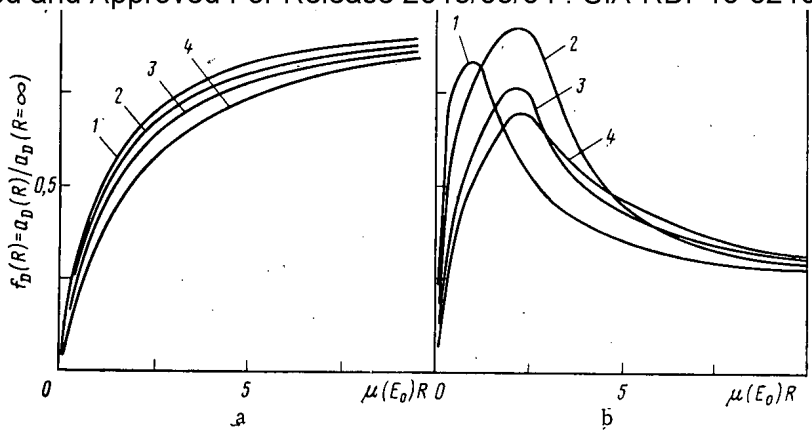

Fig. 3. Function $f_D(R)$ for dose albedo of plane iron scatterer for different values of the incidence angle θ_0: 1) 0°; 2) 30°; 3) 60°; 4) 85° [initial γ-ray energy E_0 = 2.0 MeV; a) θ = 0°, φ = 0°; b) θ = 85°, φ = 0°].

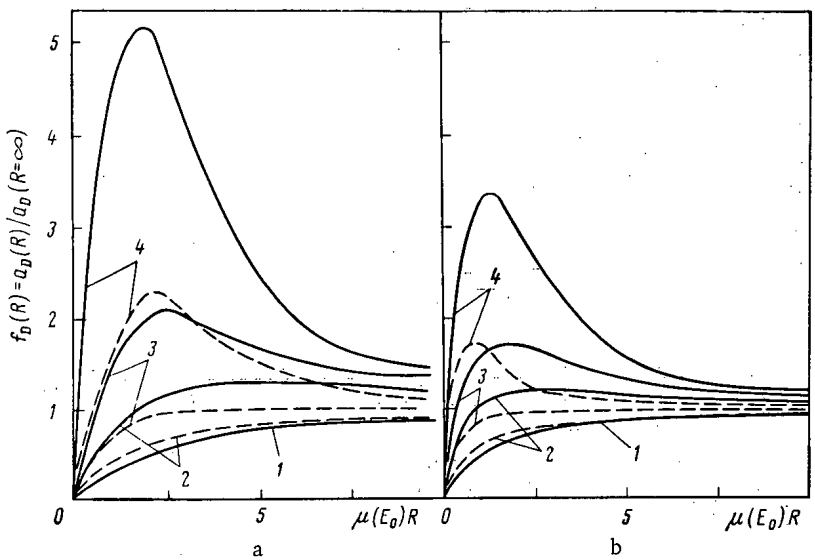

Fig. 4. Function $f_D(R)$ for dose albedo of plane scatterers of water (a) at E_0 = 0.25 MeV and θ_0 = 60° and iron (b) at E_0 = 8.0 MeV and θ_0 = 60° for different reflection angles θ [1) 0°; 2) 60°; 3) 75°; 4) 85°] and φ [the solid line represents 0° and the dashed line, 180°].

more than 50°, the error of albedo determination grows to 70% for angular characteristics and to 200-300% for spectral-angular characteristics. In this case, we observe a general tenency for the error to increase as E_0 and the atomic number Z of the element decrease.

Examination of the dependence of the effective albedo on the distance R showed that for R > 10-15 $\mu^{-1}(E_0)$ we have

$$\left|\frac{a(R,\theta,\varphi,E,\theta,E_0)-a(\theta,\varphi,E,\theta_0,E_0)}{a(\theta,\varphi,E,\theta_0,E_0)}\right|<0.1, \tag{3}$$

where $\mu(E_0)$ is the linear attenuation factor for primary γ rays of energy E_0 for the material of the reflector.

During the work, we studied the dependence of $\frac{a(R,\theta,\varphi,\theta_0,E_0)}{a(\theta,\varphi,\theta_0,E_0)}=f(R,\theta,\varphi,\theta_0,E_0)$ on the distance R as applied to the numerical, energy, and dose albedos. Figures 2-4 give some re-

Declassified and Approved For Release 2013/03/04 : CIA-RDP10-02196R000300010004-7

Declassified and Approved For Release 2013/03/04 : CIA-RDP10-02196R000300010004-7

sults of these calculations, carried out by the Monte Carlo method. Analysis of the data obtained revealed that the character of the dependence of the effective albedo on the distance R is preserved for substances with different Z, but the range over which f(R) varies decreases as Z grows.

In the region $\mu(E_0)R \leqslant 10$ the function $f(R, \theta, \varphi, \theta_0, E_0)$ can be represented as an empirical formula

$$f(R,\theta,\varphi,\theta_0,E_0)=\frac{\left[b_0+b_1\mu^3(E_0)+b^2\frac{\mu^2(E_0)}{\cos\theta}+b_3\frac{\cos\theta_0}{\cos\theta}\right]R}{1+[d_1\mu^3(E_0)+d_2\cos\theta_0]R^{\left(c_1+\frac{c_2}{\cos\theta}\right)}}, \quad (4)$$

where b_0, b_1, b_2, b_3, c_1, c_2, d_1, and d_2 are empirical constants whose values are given in Table 1 for $\mu(E_0)R > 10$ we can assume that $f(R) \approx 1$ with an error not exceeding 20% in most cases.

The results of the calculations from Eq. (4) differ from those obtained by the Monte Carlo method by no more than 20-25%, the maximum divergence being 60%. The statistical error of Monte Carlo calculations is 5-20%.

In conclusions, the authors thank A. N. Barkovskii and Yu. V. Kiselev for assistance with the work.

LITERATURE CITED

1. N. G. Gusev et al., Physical Foundations of Radiation Protection [in Russian], Atomizdat, Moscow (1980).
2. V. I. Bulatov et al., Gamma-Ray Albedo [in Russian], Atomizdat, Moscow (1968).
3. V. I. Kulikov et al., At. Energ., 44, No. 1, 85 (1978).
4. V. I. Kulikov et al., At. Energ., 51, No. 1, 59 (1981).

CREEP IN A CARBON—CARBON MATERIAL

Yu. A. Kalinkin, Yu. N. Podladchikov,
O. P. Popov, V. N. Stetsyuk,
and A. R. Khenven

UDC 621.039.532.2

There is now an extensive discussion of the scope for using materials of carbon—carbon type with high-tensile fibers (KUP-VM) as constructional materials for high-temperature systems [1-3] including high-temperature gas-cooled reactors [4, 5]. The high strength performance of such materials is particularly pronounced for compressive loads.

The creep is considerably dependent on the structure [3, 6], so it is of interest to determine the creep kinetics for material of KUP-VM type at high temperature under compressive axial loads.

We tested cylindrical sleeve specimens made of KUP-VMSKM material* with a coke matrix of diameter 60 mm, height ∿100 mm, and wall thickness 5 mm. The density of the material was ∿1.3 g/cm³. The specimens were placed in a rigid graphite holder and loaded with a graphite plunger. The tests were performed for 1 h at 1800, 2200, and 2300°K at loads of 5 and 8 MPa. A specimen was heated to the required temperature under vacuum, after which an excess pressure of argon was set up in the apparatus (0.02 MPa). After the set temperature had been

*This material was developed by G. I. Babayants, V. I. Artem'ev, and O. V. Bokov; it is a material of carbon—carbon type based on a coke matrix.

Translated from Atomnaya Énergiya, Vol. 53, No. 4, pp. 268-269, October, 1982. Original article submitted November 3, 1981.

 0038-531X/82/5304-0732$07.50 © 1983 Plenum Publishing Corporation

Declassified and Approved For Release 2013/03/04 : CIA-RDP10-02196R000300010004-7

Declassified and Approved For Release 2013/03/04 : CIA-RDP10-02196R000300010004-7

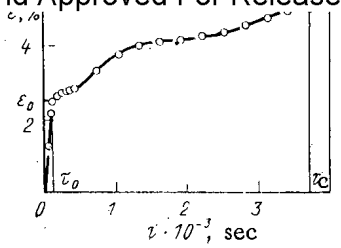

Fig. 1

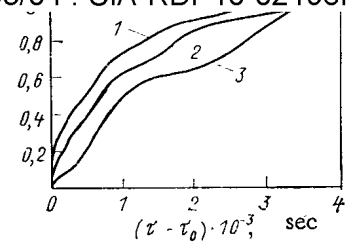

Fig. 2

Fig. 1. Axial deformation as a function of time for T = 2300°K and σ = 8 MPa.

Fig. 2. Dependence of the axial strain on time for T = 1800°K and σ = 8 MPa (1); 2200°K and 5 MPa (2); 2300°K and 8 MPa (3).

attained, the specimen was loaded by an axial force with a rate of ∿50 N/sec. The time recorder was started at the instant of application of the load and the axial strain was measured. The limiting errors in determining the parameters were not more than ±0.4% for temperature, ±5% for force, and ±2% for axial strain.

Figure 1 shows a typical strain–time relationship, where $\varepsilon = \Delta H/H_0$ is the relative axial deformation (H_0 is the initial height of the specimen, while ΔH is the measured axial deformation), while τ is time. These creep curves show the elastic-strain part clearly together with a transitional stage, after which the creep does not vary linearly, as for most constructional materials, but with characteristic fluctuations.

This feature is clearly illustrated if the strain is represented in relative coordinates (Fig. 2), where $\delta = (\varepsilon - \varepsilon_0)/(\varepsilon_c - \varepsilon_0)$ and ε_0 is the strain at the end of the elastic-strain zone τ_0, with ε_c the strain throughout the test time τ_c.

Each curve in Fig. 2 has been constructed from the results for several (two or three) specimens, and the spread in ε for the individual specimens at a given τ was not more than ±6% of the mean value. A similar picture was observed under all test conditions, which indicates that the KUP-VMSKM material does not have a stage of steady-state creep. This feature must be borne in mind in developing designs to work at high temperature under compressive load.

LITERATURE CITED

1. D. M. Karpinos, L. I. Tuchinskii, and L. R. Vishnyakov, New Composite Materials [in Russian], Vysshaya Shkola, Kiev (1977).
2. C. Chamis (ed.), Composite Materials [Russian translation], Vol. 8, Mashinostroenie, Moscow (1978).
3. Handbook on the Properties of Constructional Materials Based on Carbon [in Russian], Metallurgiya, Moscow (1975).
4. K. A. Andrianov et al., At. Energ., 46, No. 6, 406 (1979).
5. T. B. Ashrapov et al., Atomic Science and Engineering, Physics of Radiation Damage and Radiation Materials Science [in Russian], Issue 2(13) (1980), p. 26.
6. L. Brantman (ed.)., Composite Materials [Russian translation], Vol. 5, Mir, Moscow (1978).

Declassified and Approved For Release 2013/03/04 : CIA-RDP10-02196R000300010004-7

Declassified and Approved For Release 2013/03/04 : CIA-RDP10-02196R000300010004-7

FORMATION OF BUBBLES OF RADIOLYTIC GAS IN POLYETHYLENE

N. N. Alekseenko, P. V. Volobuev, and S. B. Trubin

UDC 621.039.538:541.28

The radiolysis of polyethylene (PE) is accompanied by intense gas release [1], which can lead to the formation of internal bubbles and bulges [2]. It has been established experimentally that the stress—strain curves for crystalline polymers, including PE, consist of three parts. Each of these parts represents a definite physical process in deformable PE [3]. The largest deformation corresponds to the recrystallization process, and the stress at which orientation of PE crystallites occurs is known as the recrystallization stress σ_{rec}.

During the radiolysis of PE the gas pressure in a bubble may become equal to the stress σ_{rec}. Further gas formation causes an increase in bubble volume at the constant pressure $P = \sigma_{rec}$. We assume that an increase in the gas concentration per unit volume in a sample during the radiolysis of PE is related to the growth of gas bubbles.

Let us consider the formation of a gas bubble in a spherical microcavity. Elasticity theory [4] gives the following expression for the components of the stress tensor in an infinite medium with a gas bubble of radius R and an excess internal pressure P:

$$\sigma_{rr} = \sigma_{\theta\theta} = \sigma_{\varphi\varphi} = \frac{PR^3}{\rho^3}, \tag{1}$$

where ρ is the distance from the center of the bubble to the point where the stress is determined. It is clear from Eq. (1) that the stress is independent of the radius of the bubble, and will be maximum at the gas—solid interface. Under these conditions the concentration of the dissolved gas in a sample in which bubble growth occurs is described by the relation

$$n_G = SP = S\,\sigma_{rec} = \text{const},$$

where S is the solubility constant of the radiolytic gas in the sample.

Let us consider the steady-state diffusion of radiolytic gas from a sample into a vacuum when gas bubbles grow in an infinite plate of thickness l. The diffusion equation describing this process has the form

$$D\frac{d^2n(x)}{dx^2} = -\nu(t, x), \tag{2}$$

where D is the diffusion coefficient of the radiolytic gas in PE, and ν is the rate of gas release. Since we are considering a steady-state process, in the first approximation we can assume that for a finite time $\nu \neq f(t)$. We assume that in the region of gas bubble formation where the concentration of the gas is constant, and consequently the rate of recombination of molecules of the radiolytic gas is also constant, the source function does not depend on coordinates.

We write the boundary conditions for Eq. (2) in the form

$$n(0) = n(l) = 0. \tag{3}$$

For $x = \delta$ and $x = l - \delta$, $n = n_G = \text{const}$. Here δ is the thickness of the surface layer of the plate from which radiolytic gas can reach the surface without the formation of bubbles. The value of δ can be found from the condition

Translated from Atomnaya Énergiya, Vol. 53, No. 4, pp. 269-270, October, 1982. Original article submitted December 25, 1981.

 0038-531X/82/5304-0734$07.50 © 1983 Plenum Publishing Corporation

Declassified and Approved For Release 2013/03/04 : CIA-RDP10-02196R000300010004-7

Declassified and Approved For Release 2013/03/04 : CIA-RDP10-02196R000300010004-7

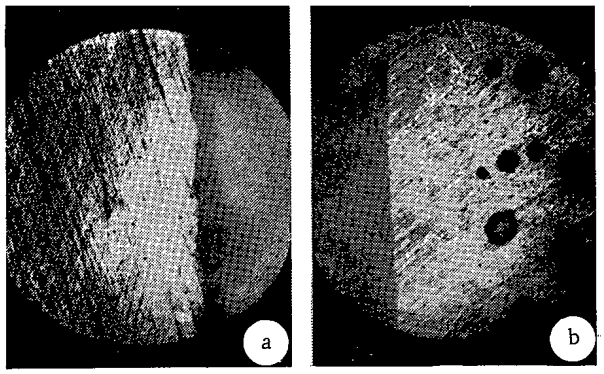

Fig. 1. Section of a polyethylene sample: a) before irradiation; b) after irradiation, × 50.

$$\left.\frac{dn(x)}{dx}\right|_{x=\delta}=0. \tag{4}$$

Solving Eq. (2), taking account of (3) and (4), we obtain

$$\delta=\sqrt{\frac{2DS\sigma_{\text{rec}}}{\nu}}. \tag{5}$$

We list certain physical characteristics of polyethylene 15902-020 [5, 6]:

Density	918 ± 1 kg/m^3
Tensile yield stress	9.8×10^6 N/m^2
Diffusion coefficient of hydrogen	4×10^{-10} m^2/sec
Solubility constant of hydrogen	6.8×10^{18} 1/(m^3 · Pa)
Rate of gas release	4×10^{23} 1/(m^3 · sec)

Since practically only hydrogen is formed in the irradiation of PE, we substitute these characteristics into Eq. (5) and obtain $\delta \approx 0.3 \times 10^{-3}$ m, which is in satisfactory agreement with the experimental value $\delta \approx 0.4 \times 10^{-3}$ m (Fig. 1).

The PE sample irradiated was a cylinder 0.04 m in diameter and 0.1 m long, turned on a lathe from block material. The sample was irradiated in the IVV-2M reactor for 72 h under the following conditions: $\varphi(E \leqslant 0.025$ eV) = 2×10^{13} neutrons/cm^2·sec, $\varphi(E \geqslant 1.15$ MeV) = 3.7×10^{12} neutrons/cm^2·sec, $T \approx 350$°K.

LITERATURE CITED

1. F. A. Makhlis, Radiation Physics and Chemistry of Polymers [in Russian], Atomizdat, Moscow (1972).
2. T. Besmann and R. Greer, J. Polym. Sci. Polym. Phys. Ed., 13, 527 (1975).
3. A. A. Tager, Physical Chemistry of Polymers [Russian translation], Khimiya, Moscow (1978).
4. L. D. Landau and E. M. Lifshitz, Theory of Elasticity, Oxford, New York (1970).
5. GOST-16337-77, High-Pressure Polyethylene. Technical Specifications [in Russian], (1978).
6. N. N. Alekseenko et al., in: Radiation Safety and the Shielding of Nuclear Power Plants [in Russian], No. 3, Atomizdat, Moscow (1977), p. 173.

Declassified and Approved For Release 2013/03/04 : CIA-RDP10-02196R000300010004-7

Declassified and Approved For Release 2013/03/04 : CIA-RDP10-02196R000300010004-7

EFFECT OF THE GEOMETRY OF MEASUREMENT ON THE ATTENUATION OF β PARTICLES

K. M. Erokhin, V. A. Mashinin, and E. V. Skachkov

UDC 539.12...17

At present there is no analytic expression for the effective transmission coefficient of β particles — the ratio of the number of recorded β particles which have passed through a target of thickness d to the number recorded at d = 0. It was shown in [1-3] that the value of the mass absorption coefficient of β particles which enters the widely used empirical expression for the effective transmission coefficient of β particles in the form of an exponent depends on the geometry of the measurement, i.e., on the source—target and target—detector distances, the target and detector dimensions, and the parameters of the incident β-radiation collimator. This dependence was treated qualitatively in the references cited. The lack of quantitative relations between the parameters describing the geometry of measurement and the effective transmission coefficient necessitates special experiments to test the empirical expressions in a given geometry.

We have derived an expression for the effective transmission coefficient for a monodirectional beam of β particles passing through a slab target, taking account of the geometry of the measurement. A uniform beam of radius r_B is incident normally on an amorphous slab target of thickness d and transverse dimensions appreciably larger than r_B; $n(E_0)$ is the β-particle spectrum, normalized to unity, with a maximum energy E_{max}. A spherical detector of radius r_D with a 100% counting efficiency is located on the axis of the beam at a distance R from the target. Suppose $r_B \gg \lambda(E_{max}, d)$, where $\lambda(E_{max}, d)$ is the maximum transverse displacement of β particles of energy E_{max} after passing through the target of thickness d. Then it can be assumed that, as in the case of a monodirectional monoenergetic normally incident uniform beam of electrons, the current angular distribution $\Psi(\theta, E_0, d)$ of the particles passing through the target is determined by the target thickness d, the angle of deflection θ from the normal to the target surface, and the initial energy E_0 [4]. It is obvious that in this case the irradiated spot on the target surface has a radius r_B.

The number of particles which emerge from an element of the target surface and are recorded by a detector at a distance r_0 from the axis of the beam is determined by the current angular distribution $\Psi(\theta, E_0, d)\cos\theta$ and the solid angle subtended by the detector at this point. Summing the detector readings over the area of the irradiated spot and over the spectrum $n(E_0)$, we find the total number of transmitted particles recorded by the detector. Dividing this expression by the number of particles recorded at d = 0, we obtain the following expressions for the effective transmission coefficient:

$$K(d, E_{max}\alpha_0, B) = \frac{4}{\alpha_0^2}\int_0^{E_{max}} dE_0 n(E_0)\int_0^{\alpha_0}\alpha d\alpha\int_0^{\pi} d\varphi\int_0^{\theta'}\Psi(\theta, E_0, d)\cos\theta\sin\theta\, d\theta \text{ for } \alpha_0 \leqslant 1, \quad (1)$$

$$K(d, E_{max}, \alpha_0, B) = K(d, E_{max}, 1, B) + 4\int_0^{E_{max}} dE_0 n(E_0)\int_1^{\alpha_0}\alpha d\alpha\int_0^{\varphi'} d\varphi\int_0^{\theta'}\psi(\theta, E_0, d)\cos\theta\sin\theta d\theta \text{ for } \alpha_0 \geqslant 1, \quad (2)$$

where the parameters of the geometry are $\alpha_0 = r_B/r_D$; $B = r_B/R$; φ is the polar angle; $\sin\varphi' = 1/\alpha$;

$$\operatorname{tg}\theta' = B(\alpha\cos\varphi + \sqrt{1-\alpha^2\sin^2\varphi});\ \operatorname{tg}\theta'' = B(\alpha\cos\varphi - \sqrt{1-\alpha^2\sin^2\varphi}). \quad (3)$$

Translated from Atomnaya Énergiya, Vol. 53, No. 4, pp. 270-271, October, 1982. Original article submitted December 30, 1981.

 0038-531X/82/5304-0736$07.50 © 1983 Plenum Publishing Corporation

Declassified and Approved For Release 2013/03/04 : CIA-RDP10-02196R000300010004-7

Declassified and Approved For Release 2013/03/04 : CIA-RDP10-02196R000300010004-7

The presence of two expressions for $K(d, E_{max}, \alpha_0, B)$ is due first to the difference in the definitions of the number of recorded particles at $d = 0$ for $\alpha_0 \leqslant 1$ and $\alpha_0 \geqslant 1$, and second to the impossibility of describing the limits of integration by a single expression.

Analytic expressions for the function $\Psi(\theta, E_0, d)$ for arbitrary values of d, E_0, and θ have not been obtained so far. However, an analysis of the experimental angular distributions shows that for a target thickness d larger than the diffusion length $d_D(E_0)$ of electrons of energy E_0, the current angular distribution follows the law $\beta(\theta) = \cos^2\theta$ for materials with atomic number $Z \leqslant 30$, and $\beta(\theta) = (\cos\theta + 0.717)\cos\theta$ for $Z \geqslant 50$ [5]; i.e., $\Psi(\theta, E_0, d)\cos\theta = P(E_0, d)\,\beta(\theta)$, where $P(E_0, d)$ is determined from the condition

$$F(d, E_0) = 2\pi \int_0^{\pi/2} \psi(\theta, E_0, d)\cos\theta\sin\theta\, d\theta. \tag{4}$$

Here $F(d, E_0)$ is the total transmission coefficient for a normally incident beam of electrons of energy E_0 passing through a target of thickness d — the ratio of the total number of particles passing through the target to the number of particles incident on the target. Then for a thickness $d > d_D(E_{max})$ the expression for the effective coefficient takes the form

$$K(d, E_{max}, \alpha_0, B) = K(d, E_{max})\, f(\alpha_0, B), \tag{5}$$

where $K(d, E_{max})$ is the total transmission coefficient for β particles with the spectrum $n(E_0)$ passing through a target of thickness d; $f(\alpha_0, B)$ is a factor describing the effect of geometry, which for $\alpha_0 \leqslant 1$ has the form

$$f(\alpha_0, B) = \frac{2}{\pi\alpha_0^2}\,\frac{\int_0^{\alpha_0} \alpha\, d\alpha \int_0^{\pi} d\varphi \int_0^{\theta'} \beta(\theta)\sin\theta\, d\theta}{\int_0^{\pi/2} \beta(\theta)\sin\theta\, d\theta}, \tag{6}$$

and for $\alpha_0 \geqslant 1$

$$f(\alpha_0, B) = f(1, B) + \frac{2\int_1^{\alpha_0} \alpha\, d\alpha \int_0^{\varphi'} d\varphi \int_{\theta''}^{\theta'} \beta(\theta)\sin\theta\, d\theta}{\pi\int_0^{\pi/2} \beta(\theta)\sin\theta\, d\theta}. \tag{7}$$

The form of the function $\beta(\theta)$ which appears in Eqs. (6) and (7) is determined by the target material; i.e., the values of $f(\alpha_0, B)$ also depend on the target composition. It was noted in [2] that the graphs of $K(d, E_{max}, \alpha_0, B)$ vs target thickness for $d > d_D(E_{max})$ are parallel for measurements in different geometries. This is explained by the presence in Eq. (5) of the factor $f(\alpha_0, B)$ which depends on the geometry of the measurement.

The quantity $\lambda(E_{max}, d)$, which limits the applicability of the expressions derived, reaches a maximum $\lambda_{max}(E_{max}, d) \approx 0.3\, L(E_{max})$, where $L(E_{max})$ is the maximum range of electrons of energy E_{max} in the target material [6]. Thus, for electrons with $E_{max} = 2$ MeV, $\lambda_{max} = 1.2$ mm in aluminum, while in lead $\lambda_{max} = 0.4$ mm, which are appreciably smaller than the beam dimensions used in practice.

The experimental expressions were tested on an arrangement consisting of an aluminum screen which was opaque to β particles and had openings for attaching a ring with a target. By changing the inside radius of the ring the parameter α_0 was varied from 0.24 to 5.3. A

Declassified and Approved For Release 2013/03/04 : CIA-RDP10-02196R000300010004-7

Declassified and Approved For Release 2013/03/04 : CIA-RDP10-02196R000300010004-7
type BIS-M $^{90}Sr + ^{90}Y$ β-particle source with a 1.5-mm-diameter active portion was located 110 mm from the screen. Particles were recorded with an L6A semiconductor detector. By changing the detector—target distance from 3 to 70 mm the parameter B was varied from 0.09 to 2.1. Measurements were performed for two aluminum samples 1 and 1.3 mm thick, and two lead samples 0.1 and 0.14 mm thick. The effective transmission coefficient was defined as the ratio of the number of recorded particles which had passed through the target to the number of particles recorded by the detector located at the target. This was made necessary by the divergence of the incident beam. The experimental values of the coefficient $f_{exp}(\alpha_0, B)$ were found from (5) by using $K(d, E_{max})$ found in these same experiments, and the calculated values $f_{cal}(\alpha_0, B)$ were obtained from (6) and (7) by using $\beta(\theta) = \cos\theta$ for aluminum and $\beta(\theta) = (\cos\theta + 0.717)\cos\theta$ for lead. The error of the determination was 5%. The calculated and experimental values $f_{cal}(\alpha_0, B)$ and $f_{exp}(\alpha_0, B)$ are in good agreement, which indicates the correctness of the expressions derived.

LITERATURE CITED

1. L. Daddi and V. D'Angelo, Int. J. Appl. Rad. Isotopes, 14, 341 (1963).
2. I. V. Kukharenko et al., in: Radiation Technology [in Russian], No. 6, Atomizdat, Moscow (1971), p. 94.
3. H. Thümmel and G. Körmer, Isotopenpraxis, 12, 262 (1976).
4. N. P. Kalashnikov, V. S. Remizovich, and M. I. Ryazanov, Collisions of Fast Charged Particles in Solids [in Russian], Atomizdat, Moscow (1980).
5. V. F. Baranov, Dosimetry of Electron Radiation [in Russian], Atomizdat, Moscow (1974).

MECHANISM OF FORMATION OF DEPOSITS ON HEATING SURFACES COOLED BY ORGANIC COOLANTS

A. I. Gavrilin, N. G. Gataullin, B. A. Mikhailov, V. E. Fedoseev, and Yu. V. Chechetkin

UDC 621.039.534.7

When using organic liquids as coolants for nuclear reactors, deposits are formed on the surface of the fuel elements, consisting of impurities and polycondensed products of the radiation-thermal decomposition of the coolant [1-3]. Having a relatively low thermal conductivity and considerable roughness ($\lambda = 0.4$-0.8 W/(m·°K) and $\delta = 50$-150 μm [1]), the deposits impair the thermohydraulic characteristics of the fuel-element assemblies and reduce their transmission cross-section, which leads to a shortening of the operating period and a reduction of the technicoeconomic indices of nuclear power plants.

The formation of deposits in a reactor is a complex physicochemical process, which is affected by numerous factors: the chemical and factional composition of the coolant, temperature and hydraulic conditions, radiation intensity, etc. As a result, when studying the process of formation of the deposits, the role of experimental investigations increases — in particular test-rig investigations — allowing the effect of the individual thermohydraulic parameters to be distinguished. In the present paper, the results are given of test-rig investigations of the effect of the temperature of the heating surface (T) and the coolant velocity (W) on the formation of deposits.

The investigations were conducted with natural and forced coolant circulation, for which the coolant of the primary circuit of the ARBUS nuclear power plant was used — ditolylmethane($C_{15}H_{16}$), which is a compound of the diphenylmethane series [3]. In the first case, a pyrolytic capsule of stainless steel was used, similar to that used in [1], with 260 g of coolant in which the experimental section (ES) was immersed; this was a stainless steel tube with a diameter of 1.6 × 0.16 mm and a length of 7.8 cm. The ES was heated by the direct passage of an electric current through it. Experiments with forced circulation were conducted on a closed circulation test-rig with a volume of 0.3 m³. Tubes of carbon steel were used as the ES, with a diameter of 12 × 1.5 mm and a length of 1 m. The ES were connected to the

Translated from Atomnaya Énergiya, Vol. 53, No. 4, pp. 271-272, October, 1982. Original article submitted May 5, 1982.

 0038-531X/82/5304-0738$07.50 © 1983 Plenum Publishing Corporation

Declassified and Approved For Release 2013/03/04 : CIA-RDP10-02196R000300010004-7

Declassified and Approved For Release 2013/03/04 : CIA-RDP10-02196R000300010004-7

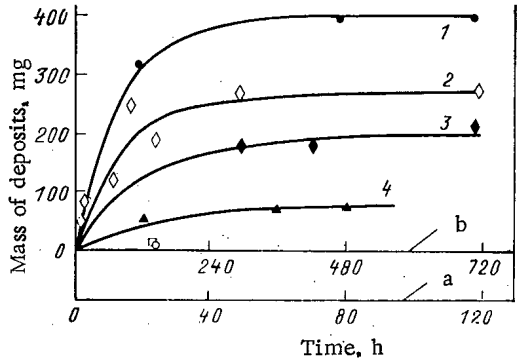

Fig. 1. Dependence of the mass of deposits (10^{-1} for natural circulation) on the time for natural (a) and forced (b) circulation: 1) $m = 400\ (1 - e^{-4.3\cdot10^{-6}\tau})$; 2) $m = 26.6\ (1 - e^{-2.2\cdot10^{-5}\tau})$; 3) $m = 19.5\ (1 - e^{-1.5\cdot10^{-5}\tau})$; 4) $m = 79\ (1 - e^{-1.7\cdot10^{-6}\tau})$; ●) experimental data for $C_{h.b.} = 6\%$; $C_{Cl} = $ mg/kg; T = 553°K; W = 2.6 m/sec; ◇) natural circulation for $C_{h.b.} = 13\%$; $C_{Cl} = 2$ mg/kg; T = 608°K; ◆) natural circulation for $C_{h.b.} = 13\%$; $C_{Cl} = 2$ mg/kg; T = 553°K; ▲) for $C_{h.b.} = 13\%$; $C_{Cl} = 2$ mg/kg; T = 553°K; W = 1.5 m/sec; ○, □) for natural circulation with T = 608°K after the experiments with $\tau = 120$ and 24 h, respectively; $C_{h.b.}$ and C_{Cl} are, respectively, the concentrations of polycondensed high-boiling products of radiation-thermal decomposition and chlorine in the coolant.

load circuit of the rectifier unit. During the experiments the coolant velocity, the pressure in the test-rig, and the power applied to the ES were maintained constant. The mass of the deposits was determined as the difference in mass of the ES samples with the deposits and after removal.

In experiments of different duration on the pyrolytic capsules, it was established that the main mass of the deposits is formed approximately in the first 40 h, after which the intensity of deposition decreases and the mass of deposits remains almost constant (Fig. 1, curves 2 and 3). The speed of arrival at the steady-state level and the amount of deposits in this case depends on the temperature of the experimental section and the difference between the temperature of the ES and the coolant. Repeated tests of the coolant with the same parameters but with a new ES do not lead to the formation of deposits. Similar results were obtained earlier in [1, 4]. It can be supposed that the steady state is determined by the conversion into deposits of a material, capable of precipitation in these conditions. With increase of the temperature of the ES, the range of compounds capable of precipitation is widened. The mass of the stationary deposits is directly proportional to $\exp(-E/kT)$, where E is a certain energy of activation, J; k is Boltzmann's constant (Fig. 2, solid curve). From the results of experiments on the arrival of the steady state with different values of T, E and the coefficient C can be determined from the condition $m_0 = CV_{exp}(-E/kT)$, where m_0 is the mass of deposits in steady-state conditions; V is the volume of coolant. In order to identify the substances responsible for the formation of the deposits, it is necessary to investigate the chemical and fractional composition of the coolant before and after the experiment.

The experiments on the circulation test-rig were conducted with a coolant velocity of 1.5-5 m/sec and a surface temperature of the ES of 423-635°K. The mass of the deposits is proportional to the temperature of the ES (see Fig. 2), and the steady-state value for prolonged (20-30 days) experiments (see Fig. 1, curves 1 and 4). In view of the volume of coolant considered in the test-rig, it is probable that a reduction of the concentration of material in these conditions cannot be the reason for the cessation of growth of the deposits. This is confirmed also by the formation of the very same amount of deposits on the new ES placed in the test-rig after the first ones. It was supposed that the state of dynamic equilibrium of the deposits is caused by the equivalence of the force of adhesion of the particles to the surface [5], attenuating in proportion to the increase of thickness of the deposits, and the force acting on a particle from the direction of the moving liquid — the

Declassified and Approved For Release 2013/03/04 : CIA-RDP10-02196R000300010004-7

Declassified and Approved For Release 2013/03/04 : CIA-RDP10-02196R000300010004-7

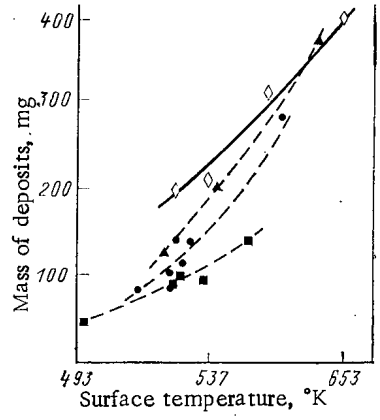

Fig. 2. Dependence of the mass of the deposits (10^{-1} for natural circulation) on the surface temperature; ——) m = 2200 $e^{-3.6 \cdot 10^{-20}/kT}$ (for natural circulation); ▲, ● and ■) experimental data for W = 1.5, 2.6 and 5 m/sec, respectively; ◇) natural circulation (capsules) for $C_{h.b.}$ = 6% and C_{Cl} = 2.5 mg/kg.

erosive force [6]. It is obvious that there will be no reduction of the cohesive forces with increase of the thickness of the deposits in a reactor where, under the action of radiation, chemical bonds are formed in the deposits. The coolant velocity will doubly affect the growth of the deposits: on the one hand to intensify the mass transfer due to diffusion and, on the other hand, to increase erosion. The ratio between these processes depends to a great extent on the effective diameter of the particles forming the deposits. The calculation of the masses of the deposits, taking account of mass transfer due to diffusion [6] and the transfer of particles due to thermo-emf [7], coincides satisfactorily with the experimental data shown in Fig. 2. The reciprocal dependence of the velocity ($\sim W^{-1.36}$) confirms the presence in the coolant of quite large particles (5-15 μm). By using a relatively pure coolant, a direct dependence is observed for the growth of the deposits on the coolant velocity ($\sim W^{0.5-1.0}$) [1, 2].

Thus, the test-rig experiments have allowed the dependence of the formation and growth of deposits on the thermohydraulic factors to be established, and the experimental results coincide satisfactorily with the calculated results, obtained on the basis of the considered mechanism of the process.

LITERATURE CITED

1. R. Sullivan and R. Keen, Film Formation on Heat Transfer Surfaces, IDO-11401, USAEC, Chap. 7 (1964).
2. J. Smee et al., Organic Coolant Summary Report, AECL-4922 (1975).
3. V. A. Tsykanov et al., Preprint Scientific-Research Institute of Nuclear Reactors 25(433), Dimitrovgrad (1980).
4. P. Benson, Development of the Pyrolytic Fouling Test for Organic Reactor Coolants, NAA-SR-7362 (1962).
5. A. D. Zimon, Adhesion of Dust and Powders [Russian translation], Khimiya, Moscow (1976).
6. R. Nijsing, Diffusional and Kinetic Phenomena Associated with Fouling, EUR 543.e (1964).
7. V. P. Brusakov, At. Energ., 30, No. 1, 10 (1971).

Declassified and Approved For Release 2013/03/04 : CIA-RDP10-02196R000300010004-7

Declassified and Approved For Release 2013/03/04 : CIA-RDP10-02196R000300010004-7

TEMPERATURE FIELDS OF ELECTRICITY GENERATING THERMAL EMISSION ELEMENTS IN CHANGES OF THE WIDTH OF THE GAP BETWEEN THE ELECTRODES

A. G. Tsitsin

UDC 621.362

Though a system for spacing the gap between the electrodes has been provided, during the operation of an electricity-generating thermal emission element the width of the gap can be modified by the influence of fields up to the full size of the gap and, hence, until the electrodes come in contact with each other (usually in the central cross section of an electricity-generating element). A short circuit in the electrical circuitry of the elements is then the consequence. The possibility of such a hypothetical case has been treated in service-life testing and in investigations made on electricity-generating elements after their stay in a reactor [1, 2].

We present in this work an algorithm for calculating the temperature field of coaxial electricity-generating elements. The algorithm was developed on the basis of a mathematical model of nonstationary heat conduction in complicated composite bodies [3]. The nonuniformity of the heat exchange in circumferential direction over the outside of the jacket of the electricity-generating element was disregarded. As in [4], the discrete microspacers are considered "smeared" into a continuous ring. It is therefore possible to solve the axially symmetric problem of heat conduction. It was assumed that the heat exchange in the gap between the electrodes takes place by radiation, heat conduction through a mixture of gases in the gap, and "electron cooling." The density of the thermal emission current in the gap was assumed to depend not only on the electrode temperature and the cesium pressure in the gap but also upon the width of the gap between the electrodes.

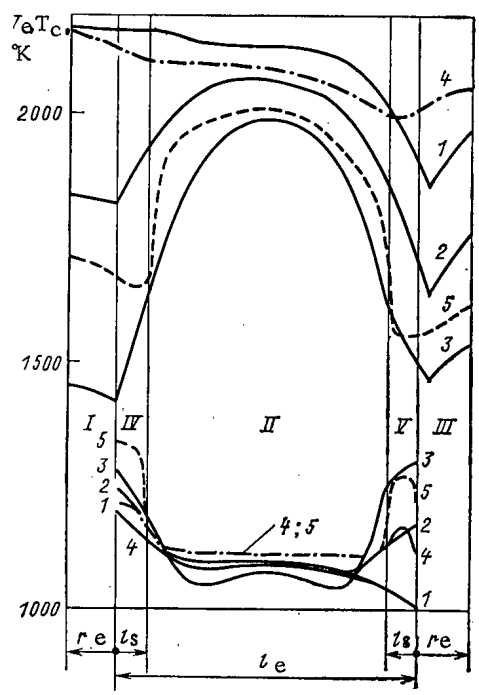

Fig. 1. Distribution of the temperature along the electrodes of an electricity-generating element (II) with spacers (IV and V) and along the end-face sections (I and III) for $q_v = 4 \cdot 10^8$ W/m³ and $\Delta = r_c - r_e = 0.00025$ m; 1) $\lambda_s^* = 0$ [4]; 2) $\lambda_s^* = 0.2$ W/m·°K [4]; 3) $\lambda_s^* = 1.0$ W/m·°K [4]; 4) $\lambda_s^* = 0$; 5) $\lambda_s^* \neq 0$ ($\delta_s = 0.0002$ m).

Translated from Atomnaya Énergiya, Vol. 53, No. 4, pp. 273-274, October, 1982. Original article submitted February 18, 1982.

0038-531X/82/5304-0741$07.50 © 1983 Plenum Publishing Corporation

Declassified and Approved For Release 2013/03/04 : CIA-RDP10-02196R000300010004-7

Declassified and Approved For Release 2013/03/04 : CIA-RDP10-02196R000300010004-7

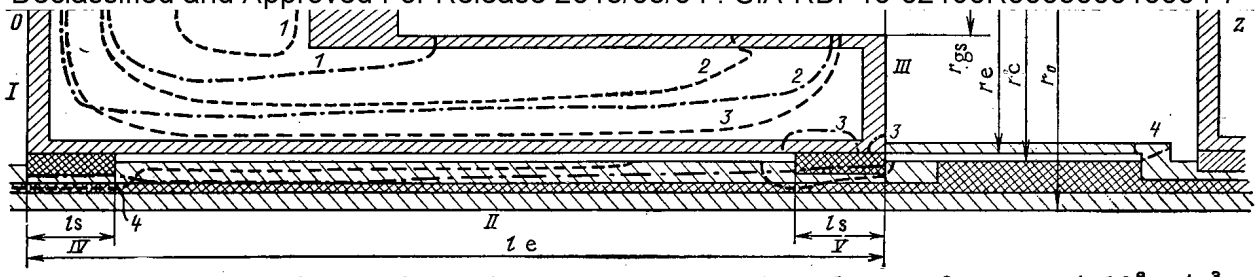

Fig. 2. Temperature field of an electricity-generating element for $q_V = 4 \cdot 10^8$ W/m³ and $\Delta = 0.00025$ m; —•—•—) $\delta_s = 0$; — — — —) $\delta_s = 0.0002$ m. Isotherms 1-4) 2700, 2400, 2200, and 1100°K, respectively.

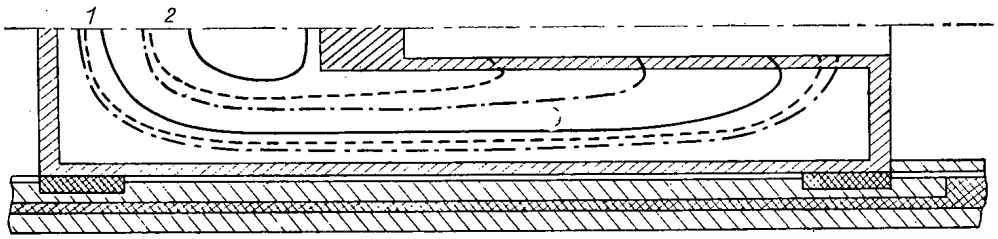

Fig. 3. Temperature field of an electricity-generating element for $q_V = 4 \cdot 10^8$ W/m³; $\delta_s = 0.0002$ m; $\Delta = 0.00035$ (——); 0.00025 (— — —); and 0.00015 (—•—•—). Isotherms 1, 2) 2200 and 2600°K, respectively.

It was of interest to compare the results of the calculation of the electrode temperature in an electricity-generating element according to the model proposed with the results according to the model of [4]. An electricity-generating element with a tungsten emitter of diameter $2r_e = 0.01$ m, length $l_e = 0.03$ m, and a microspacer of diameter $2r_s = 0.007$ m and length $l_s = 0.003$ m [4] was chosen for our studies. Figure 1 exhibits the results of temperature calculations of both the electrodes and the faces of an electricity-generating element (curves 4 and 5). It follows from a comparison of curves 1 and 4 that differences not exceeding 3% were obtained in the calculations made with the various methods when no heat leaks off through the belt of spacers the effective thermal conductivity λ_s^* of which was assumed as zero. This result of 3% can be considered a confirmation of the usefulness of the proposed algorithm. Assuming that the emitter temperature (curves 2 and 3 of Fig. 1) was attained at a width $\delta_s = 0.0002$ m of the contact zone (indentations made the spacers in the emitter body), the calculated coefficient of thermal conductivity λ_s of the beryllium oxide was 5.3 and 26.5 W/m·°K. The temperature dependence of the coefficient of thermal conductivity of the beryllium oxide was taken into consideration in the proposed model [5]. This accounts for the position of curve 5 between curves 2 and 3 (see Fig. 1), because for $T_s \approx 1650$°K the value $\lambda_s = 17$ W/m·°K is obtained. The form of curve 5 confirms the conclusion of [4] that the temperature profile along the emitter is bell-shaped. The temperature distribution corresponding to the time at which a stationary temperature field had been reached in the electricity-generating element is shown in Fig. 2, where the outflow of heat from the emitter to the collector (for $\delta_s = 0.0002$ m) through the spacers (zones IV and V) and the switching connection piece (zone III), as well as the overflow of heat over the gas-removal system, are clearly noticeable.

In [6] a mathematical formulation of the thermal resistance problem of an electricity-generating element was proposed, the element being "matched" through a boundary condition in the gap between the electrodes. But the model disregarded the heat exchange near the end faces of the electricity-generating element. The proposed improvement of the model has shown that the heat transfer from the emitter to the collector (in zones III, IV, and V) must not be disregarded (see Fig. 1). Let us analyze the influence of the size of the gap between the electrodes upon the temperature distribution in the electricity-generating element (Fig. 3). When the gap between the electrodes is reduced, the intensity of "electron cooling" of the emitter is enhanced, and vice versa. On this occasion the temperature $T(r_e, l_e/2, t)$ changes from 1895°K (at $\Delta = 0.00015$ m) to 2085°K (at $\Delta = 0.00035$ m). Thus, when this effect is disregarded in service-life considerations, a substantial error can be made in the determination of the temperature fields and the energy characteristics of an electricity-generating element.

Declassified and Approved For Release 2013/03/04 : CIA-RDP10-02196R000300010004-7

Declassified and Approved For Release 2013/03/04 : CIA-RDP10-02196R000300010004-7

LITERATURE CITED

1. E. S. Bekukhambetov et al., At. Energ., 35, No. 6, 387 (1973).
2. G. A. Batyrbekov et al., At. Energ., 40, No. 5, 382 (1976).
3. A. G. Tsitsin, Izv. Vyssh. Uchebn. Zaved., Mashinostr., No. 5, 144 (1980).
4. N. M. Rozhkova and V. V. Sinyavskii, At. Energ., 49, No. 2, 137 (1980).
5. R. A. Belyaev, Beryllium Oxide [in Russian], Atomizdat, Moscow (1980).
6. A. G. Tsitsin, Izv. Vyssh. Uchebn. Zaved., Mashinostr., No. 7, 9 (1978).

CALCULATIONS OF THE IRRADIATION CHARACTERISTICS IN REACTOR TESTS

E. S. Glushkov, N. N. Ponomarev-Stepnoi, and I. G. Timofeev

UDC 621.039.52.034.3

Reactor testing in looping channels of research reactors is one of the stages in the production of fuel elements. The conditions of operation of fuel elements in a real reactor and in the tests can differ substantially. Thus, there arises the problem of selecting conditions of fuel-element testing in looping channels and of comparing the results with specifications.

Apart from the energy parameters (heat liberation and energy delivered), the operational capacity of a fuel element in a reactor depends upon the conditions of irradiation mainly by fission products and neutrons. The interaction of the fission products is given by the rate of their production and accumulation. The number of atoms displaced under the influence of neutrons per atom of the material considered (i.e., the quantity $dp\alpha$) can serve as a measure of the irradiation by fast neutrons. The quantity characterizes the influence of neutron irradiation upon the properties of a material in a better way than the flux of neutrons with an energy above some threshold value of the activation of some threshold detector [1].

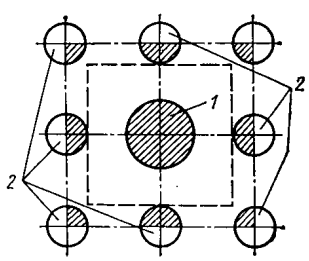

Fig. 1

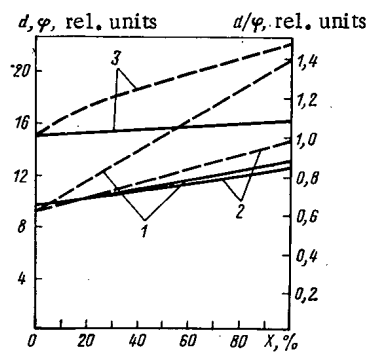

Fig. 2

Fig. 1. Scheme of an initial cell on the plane for calculating PG-100: 1) PG-100; 2) working channels of the reactor for materials testing, the channels surrounding the looping channel PG-100.

Fig. 2. Dependence of 1) d, 2) φ, and 3) the ratio thereof upon the fuel enrichment in a fuel element sphere for the shells of centrally located microfuel (— — —) and of a fuel element sphere (——).

Translated from Atomnaya Énergiya, Vol. 53, No. 4, pp. 274-275, October, 1982. Original article submitted April 16, 1982.

0038-531X/82/5304-0743$07.50 © 1983 Plenum Publishing Corporation

Declassified and Approved For Release 2013/03/04 : CIA-RDP10-02196R000300010004-7

Declassified and Approved For Release 2013/03/04 : CIA-RDP10-02196R000300010004-7

In order to determine the conditions of operation of fuel elements and other reactor design elements, we developed a method used in the form of the set of DAM programs [2] on a computer. The method makes use of the discrete ordinate technique [3] or the Monte Carlo technique [4] so that the neutron-physics parameters of looping channels in reactors with a complicated structure and a large number of strongly absorbing materials can be determined.

The set of DAM programs and the system of constants of [5] were used to compare the conditions of operation of fuel-element spheres in VTGR and in fuel-element tests in looping channels of a research reactor for materials testing [6, 7]. The results were used to calculate the power, the depth of the burnup, and the rate of generating displaced atoms with approximation formulas for the testing of fuel elements in the reactor for materials testing.

The results of investigations made under the conditions of testing fuel-element spheres of the VGR-50 reactor [8] in the looping channel PG-100 of the reactor for materials testing [9, 10] are listed in **Table 1**. Figure 1 shows the initial configuration of the cell selected for the calculations with the PG-100 in the scheme. Those portions of the operational channels of the materials' testing reactor which are included in the cell of the calculations are shaded. A cell containing one fuel-element sphere to be tested was singled out along the height of the PG-100. The fuel-element sphere was made from graphite and had dispersed in it uranium dioxide microfuel with a multilayer coating of pyrocarbon and silicon carbide. The technique of discrete ordinates was used to calculate a two-dimensional cylindrical cell of equivalent volume in the multigroup approximation.

It is difficult to guarantee full identity of the test conditions of fuel-element spheres in the PG-100 of the testing reactor and the conditions of operation in the VGR-50 reactor. With a 21% enrichment the average thermal power of a fuel-element sphere in the PG-100 is greater than the average power delivered in the fuel elements of the VGR-50 reactor. The increased fraction of heat liberation in the fuel element by the γ quanta of the materials' testing reactor must not be forgotten.

Interesting results were obtained for the dependencies of dpα and the fast neutron flux in the fuel-element jackets and in the microfuel-element jackets upon the fuel enrichment in the fuel elements tested in the PG-100 looping channel.

Figure 2 shows the dependence of the rate of generating displaced atoms d and the flux density φ of the fast neutrons upon the fuel enrichment for the shell of microfuel situated in the central portion of a fuel element and for the shell of the fuel-element proper at a fixed power in the surrounding channels. The increase observed in d and φ is related to the

TABLE 1. Conditions of Neutron Irradiation of Fuel-Element Spheres

Parameters	VGR-50	MR(PG-100)				
Thermal power (MW) of the reactor	137	30	30	30	30	30
Fuel enrichment (%) in fuel-element spheres	21	1	21	36	45	90
Av. neutron power (kW) of a fuel-element sphere	1,2	0,04	0,76	1,22	1,48	2,62
Power (kW) liberated in a fuel-element sphere by the γ quanta of materials' testing reactor	–	0,80	0,80	0,80	0,80	0,80
Av. thermal power (kW) of fuel-element sphere	1,2	0,84	1,56	2,02	2,28	3,42
Time (days) of operation with power	200	200	200	200	200	200
Initial load (g) of uranium in a fuel-element sphere	2,43	2,43	2,43	2,43	2,43	2,43
Depth of burnup (10^{-4} MW·day/ton) and dpα (displacement/atom)*	9,9 0,49 0,42	0,26 0,30 0,30	5,1 0,36 0,33	8,3 0,40 0,34	10 0,43 0,35	18 0,53 0,38
Neutron flux (10^{-20} neutrons/cm^2) at E > 0.18 *	7,4 7,4	6,1 6,1	6,5 6,5	7,0 6,7	7,2 6,8	8,3 7,4

*The first number refers to the shell of microfuel disposed in the central portion of a fuel element; the second number refers to the shell of a fuel-element sphere.

Declassified and Approved For Release 2013/03/04 : CIA-RDP10-02196R000300010004-7

Declassified and Approved For Release 2013/03/04 : CIA-RDP10-02196R000300010004-7

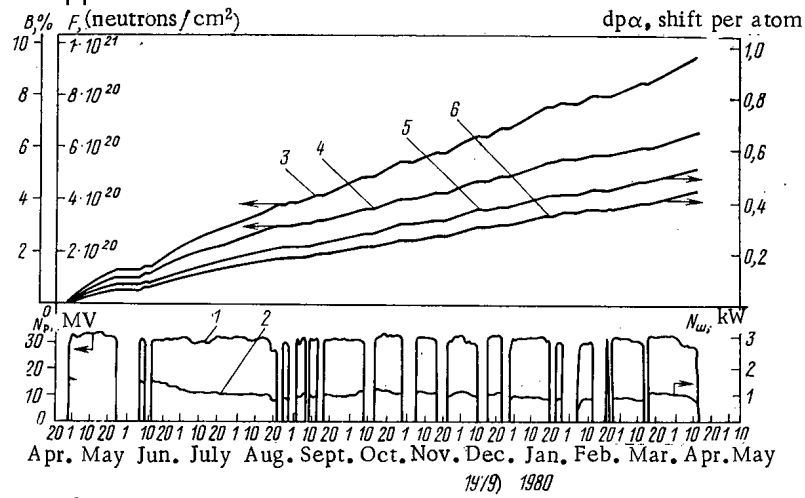

Fig. 3. Chronogram of the basic parameters of a fuel-element sphere situated in the central portion with respect to the height of the PG-100 looping channel: 1) power of the materials testing reactor; 2) neutron power in the fuel-element sphere situated in central position relative to the height of the PG-100; 3) flux of fast neutrons (with E > 0.18 MeV); 4) depth of the burnup B (%) of the fuel; 5, 6) dpα for the shells of a centrally located microfuel element and a fuel element sphere, respectively.

increased number of fission events in the fuel elements tested, because the amount of material undergoing fission in the fuel elements is increased. Under these conditions d does not change proportionately to the flux density of the fast neutrons.

The fact that the rate of generating displaced atoms and the flux density of the fast neutrons are not proportional can be explained by the fast neutrons of the materials' testing reactor, which are incident on the fuel element tested from the channels surrounding the PG-100 (neutrons of materials testing), and by the fast neutrons produced in the fuel-element proper ("intrinsic" neutrons). All these neutrons participate in the displacement of the atoms of the fuel-element materials. The "intrinsic" neutrons are characterized by a harder spectrum than the neutrons from the materials testing reactor.

The results of the calculations were used to develop a program technique which is based on approximation formulas and executed as program on the BESM-6 computer. The program technique allows the immediate calculation of invariable parameters during the testing of fuel elements in the PG-100 (Fig. 3).

LITERATURE CITED

1. N. N. Ponomarev-Stepnoi, At. Energ., 11, No. 2, 184 (1961).
2. I. G. Timofeev, Preprint IAÉ-2935, Moscow (1978).
3. A. D. Rogov, M. M. Savos'kin, and I. G. Timofeev, in: Reports on Programs and Techniques for the Design of Fast Reactors [in Russian], NIIAR, Dimitrovgrad (1975), p. 174.
4. I. G. Timofeev and A. D. Frank-Kamenetskii, Preprint IAÉ-2526, Moscow (1975).
5. V. A. Lobyntsev and I. G. Timofeev, Preprint IAÉ-2926, Moscow (1977).
6. N. N. Ponomarev-Stepnoi et al., Problems of Atomic Science and Technology, Series Atomic-Hydrogen Power Generation and Technology [in Russian], No. 2(3), 83 (1977).
7. E. S. Glushkov, N. N. Ponomarev-Stepnoi, and I. G. Timofeev, Problems of Atomic Science and Technology, Series Atomic-Hydrogen Power Generation and Technology [in Russian], No. 2(7), 114 (1980).
8. State and Chances of the Development of Work on the VTGR in the USSR [in Russian], Problems of Atomic Science and Technology, Series Atomic-Hydrogen Power Generation and Technology [in Russian], No. 1(4), 33 (1978).
9. A. S. Abramov et al., Problems of Atomic Science and Technology Series Atomic-Hydrogen Power Generation and Technology [in Russian], No. 1(6), 89 (1980).

Declassified and Approved For Release 2013/03/04 : CIA-RDP10-02196R000300010004-7

Declassified and Approved For Release 2013/03/04 : CIA-RDP10-02196R000300010004-7

10. N. I. Tikhonov et al., Problems of Atomic Science and Technology, Series Atomic-Hydrogen Power Generation and Technology [in Russian], No. 2(7), 65 (1980).

Declassified and Approved For Release 2013/03/04 : CIA-RDP10-02196R000300010004-7

Declassified and Approved For Release 2013/03/04 : CIA-RDP10-02196R000300010004-7

How To Comply With The New Copyright Law

Participation in the Copyright Clearance Center (CCC) assures you of legal photocopying at the moment of need.

Libraries everywhere have found the easy way to fill photocopy requests legally and instantly, without the need to seek permissions, from more than 3000 key publications in business, science, humanities, and social science. You can:

Fill requests for multiple copies, interlibrary loan (beyond the CONTU guidelines), and reserve desk without fear of copyright infringement.

Supply copies from CCC-registered publications simply and easily.

The Copyright Clearance Center is your one-stop place for on-the-spot clearance to photocopy for internal use.

Its flexible reporting system accepts photocopying reports and returns an itemized invoice. You send only one convenient payment. CCC distributes it to the many publishers whose works you need.

And, you need not keep any records, the CCC computer will do it for you. Register now with the CCC and you will never again have to decline a photocopy request or wonder about compliance with the law for any publication participating in the CCC.

To register or for more information, just contact:

Copyright Clearance Center
21 Congress Street
Salem, Massachusetts 01970
(617) 744-3350

a not-for-profit corporation

NAME _____ TITLE _____

ORGANIZATION _____

ADDRESS _____

CITY _____ STATE _____ ZIP _____

COUNTRY _____ TELEPHONE _____

Declassified and Approved For Release 2013/03/04 : CIA-RDP10-02196R000300010004-7

Declassified and Approved For Release 2013/03/04 : CIA-RDP10-02196R000300010004-7

CHANGING YOUR ADDRESS?

In order to receive your journal without interruption, please complete this change of address notice and forward to the Publisher, 60 days in advance, if possible.

(Please Print)

Old Address:

name

address

city

state (or country) zip code

New Address

name

address

city

state (or country) zip code

date new address effective

name of journal

THE LANGUAGE OF SCIENCE
Plenum
PUBLISHING CORPORATION

233 Spring Street, New York, New York 10013

Declassified and Approved For Release 2013/03/04 : CIA-RDP10-02196R000300010004-7

Declassified and Approved For Release 2013/03/04 : CIA-RDP10-02196R000300010004-7

MEASUREMENT TECHNIQUES
Izmeritel'naya Tekhnika
Vol. 25, 1982 (12 issues) $400

MECHANICS OF COMPOSITE MATERIALS
Mekhanika Kompozitnykh Materialov
Vol. 18, 1982 (6 issues) $330

METAL SCIENCE AND HEAT TREATMENT
Metallovedenie i Termicheskaya Obrabotka Metallov
Vol. 24, 1982 (12 issues) $420

METALLURGIST
Metallurg
Vol. 26, 1982 (12 issues) $435

PROBLEMS OF INFORMATION TRANSMISSION
Problemy Peredachi Informatsii
Vol. 18, 1982 (4 issues) $320

PROGRAMMING AND COMPUTER SOFTWARE
Programmirovanie
Vol. 8, 1982 (6 issues) $135

PROTECTION OF METALS
Zashchita Metallov
Vol. 18, 1982 (6 issues) $380

RADIOPHYSICS AND QUANTUM ELECTRONICS
Izvestiya Vysshikh Uchebnykh Zavedenii, Radiofizika
Vol. 25, 1982 (12 issues) $400

REFRACTORIES
Ogneupory
Vol. 23, 1982 (12 issues) $380

SIBERIAN MATHEMATICAL JOURNAL
Sibirskii Matematicheskii Zhurnal
Vol. 23, 1982 (6 issues) $495

SOIL MECHANICS AND FOUNDATION ENGINEERING
Osnovaniya, Fundamenty i Mekhanika Gruntov
Vol. 19, 1982 (6 issues) $380

SOLAR SYSTEM RESEARCH
Astronomicheskii Vestnik
Vol. 16, 1982 (4 issues) $275

SOVIET APPLIED MECHANICS
Prikladnaya Mekhanika
Vol. 18, 1982 (12 issues) $400

SOVIET ATOMIC ENERGY
Atomnaya Énergiya
Vols. 52–53 (12 issues) $440

SOVIET JOURNAL OF GLASS PHYSICS AND CHEMISTRY
Fizika i Khimiya Stekla
Vol. 8, 1982 (6 issues) $175

SOVIET JOURNAL OF NONDESTRUCTIVE TESTING
Defektoskopiya
Vol. 18, 1982 (12 issues) $485

SOVIET MATERIALS SCIENCE
Fiziko-khimicheskaya Mekhanika Materialov
Vol. 18, 1982 (6 issues) $345

SOVIET MICROELECTRONICS
Mikroélektronika
Vol. 11, 1982 (6 issues) $195

SOVIET MINING SCIENCE
Fiziko-tekhnicheskie Problemy Razrabotki Poleznykh Iskopaemykh
Vol. 18, 1982 (6 issues) $420

SOVIET PHYSICS JOURNAL
Izvestiya Vysshikh Uchebnykh Zavedenii, Fizika
Vol. 25, 1982 (12 issues) $400

SOVIET POWDER METALLURGY AND METAL CERAMICS
Poroshkovaya Metallurgiya
Vol. 21, 1982 (12 issues) $435

STRENGTH OF MATERIALS
Problemy Prochnosti
Vol. 14, 1982 (12 issues) $495

THEORETICAL AND MATHEMATICAL PHYSICS
Teoreticheskaya i Matematicheskaya Fizika
Vols. 50–53, 1982 (12 issues) $380

UKRAINIAN MATHEMATICAL JOURNAL
Ukrainskii Matematicheskii Zhurnal
Vol. 34, 1982 (6 issues) $380

Send for Your Free Examination Copy

Plenum Publishing Corporation, 233 Spring St., New York, N.Y. 10013
In United Kingdom: 88/90 Middlesex St., London E1 7EZ, England
Prices slightly higher outside the U.S. Prices subject to change without notice.

Declassified and Approved For Release 2013/03/04 : CIA-RDP10-02196R000300010004-7

Declassified and Approved For Release 2013/03/04 : CIA-RDP10-02196R000300010004-7

RUSSIAN JOURNALS IN THE PHYSICAL AND MATHEMATICAL SCIENCES

AVAILABLE IN ENGLISH TRANSLATION

ALGEBRA AND LOGIC
Algebra i Logika
Vol. 21, 1982 (6 issues) $270

ASTROPHYSICS
Astrofizika
Vol. 18, 1982 (4 issues) $320

AUTOMATION AND REMOTE CONTROL
Avtomatika i Telemekhanika
Vol. 43, 1982 (24 issues) issues) $495

COMBUSTION, EXPLOSION, AND SHOCK WAVES
Fizika Goreniya i Vzryva
Vol. 18, 1982 (6 issues) $345

COSMIC RESEARCH
Kosmicheskie Issledovaniya
Vol. 20, 1982 (6 issues) $425

CYBERNETICS
Kibernetika
Vol. 18, 1982 (6 issues) $345

DIFFERENTIAL EQUATIONS
Differentsial'nye Uravneniya
Vol. 18, 1982 (12 issues) $395

DOKLADY BIOPHYSICS
Doklady Akademii Nauk SSSR
Vols. 262–267, 1982 (2 issues) $145

FLUID DYNAMICS
Izvestiya Akademii Nauk SSSR, Mekhanika Zhidkosti i Gaza
Vol. 17, 1982 (6 issues) $380

FUNCTIONAL ANALYSIS AND ITS APPLICATIONS
Funktsional'nyi Analiz i Ego Prilozheniya
Vol. 16, 1982 (4 issues) $320

GLASS AND CERAMICS
Steklo i Keramika
Vol. 39, 1982 (6 issues) $460

HIGH TEMPERATURE
Teplofizika Vysokikh Temperatur
Vol. 20, 1982 (6 issues) $400

HYDROTECHNICAL CONSTRUCTION
Gidrotekhnicheskoe Stroitel'stvo
Vol. 16, 1982 (12 issues) $305

INDUSTRIAL LABORATORY
Zavodskaya Laboratoriya
Vol. 48, 1982 (12 issues) $400

INSTRUMENTS AND EXPERIMENTAL TECHNIQUES
Pribory i Tekhnika Eksperimenta
Vol. 25, 1982 (12 issues) $460

JOURNAL OF APPLIED MECHANICS AND TECHNICAL PHYSICS
Zhurnal Prikladnoi Mekhaniki i Tekhnicheskoi Fiziki
Vol. 23, 1982 (6 issues) $420

JOURNAL OF APPLIED SPECTROSCOPY
Zhurnal Prikladnoi Spektroskopii
Vols. 36–37 (12 issues) $420

JOURNAL OF ENGINEERING PHYSICS
Inzhenerno-fizicheskii Zhurnal
Vols. 42–43, 1982 (12 issues) $420

JOURNAL OF SOVIET LASER RESEARCH
A translation of articles based on the best Soviet research in the field of lasers
Vol. 3, 1982 (4 issues) $95

JOURNAL OF SOVIET MATHEMATICS
A translation of Itogi Nauki i Tekhniki and *Zapiski Nauchnykh Seminarov Leningradskogo Otdeleniya Matematicheskogo Instituta im. V. A. Steklova AN SSSR*
Vols. 18–20, 1982 (18 issues) $680

LITHOLOGY AND MINERAL RESOURCES
Litologiya i Poleznye Iskopaemye
Vol. 17, 1982 (6 issues) $420

LITHUANIAN MATHEMATICAL JOURNAL
Litovskii Matematicheskii Sbornik
Vol. 22, 1982 (4 issues) $205

MAGNETOHYDRODYNAMICS
Magnitnaya Gidrodinamika
Vol. 18, 1982 (4 issues) $325

MATHEMATICAL NOTES
Matematicheskie Zametki
Vols. 31–32, 1982 (12 issues) $400

continued on inside back cover

Declassified and Approved For Release 2013/03/04 : CIA-RDP10-02196R000300010004-7